RELATIONSHIPS BETWEEN DISSOLVED OXYGEN AND MACROALGAL DISTRIBUTION IN UPPER NEWPORT BAY

Technical Report 494
October 2006

Nikolay Nezlin
Krista Kamer
Eric D. Stein
Amanda Carr
Jim Hyde

Southern California Coastal Water Research Project

RELATIONSHIPS BETWEEN DISSOLVED OXYGEN AND MACROALGAL DISTRIBUTION IN UPPER NEWPORT BAY

FINAL REPORT

Nikolay Nezlin[1], Krista Kamer[2], Eric D. Stein[1], Amanda Carr[3] and Jim Hyde[4]

[1]Southern California Coastal Water Research Project
7171 Fenwick Lane
Westminster, CA 92683

[2]Moss Landing Marine Laboratories
7544 Sandholdt Road
Moss Landing, CA 95039

[3]Resources and Development Management Department, County of Orange
300 North Flower Street
Santa Ana, CA 92703-5000

[4]Irvine Ranch Water District
15600 Sand Canyon Ave.
Irvine, CA 92618-3102

October 31 2006

Technical Report #494

PROJECT OVERVIEW AND EXECUTIVE SUMMARY

Newport Bay is the second largest estuarine embayment in southern California and provides a suite of regionally significant ecological and recreational values. The upper bay is a State ecological reserve and provides critical natural habitat for terrestrial and aquatic species, including several Federally-listed threatened or endangered species. The lower bay provides significant recreational opportunities to the southern California community and is one of the largest pleasure craft harbors in the United States. The bay also provides significant spawning and nursery habitats for commercial and non-commercial fish species.

Like many estuaries in urban environments, Upper Newport Bay (UNB) is subject to a range of anthropogenic stressors. Over time, the nutrient regime in the watershed has changed with the steady conversion of agricultural lands to urban development. In 1983 agricultural land uses accounted for 22% of the Newport Bay watershed, while urban uses accounted for 48% (Flow Science, 2006). By 2000, agricultural uses had declined to 7% of the watershed (U.S. EPA, 2002). Historical excessive nutrient inputs lead to extensive macroalgal blooms throughout Newport Bay from the 1970s to the 1990s. While there were a number of sources of nutrient input, tailwaters from the irrigation of agricultural crops and from several commercial nurseries in the watershed were the predominant source (SARWQCB, 1998).

In response to concerns over impaired beneficial uses in the bay, a Total Maximum Daily Load (TMDL) for nitrogen (N) and phosphorus (P) for the Newport Bay/San Diego Creek Watershed was adopted in 1998. Additionally, implementation of best management practices (BMPs) such as water recycling and irrigation management to reduce water use by commercial nurseries has greatly reduced agricultural discharges of waste (SARWQCB 2006). Municipal activities to reduce nutrient loadings from urbanized land uses through implementation of the Drainage Area Management Plan have included extensive public education campaigns against over-irrigation and misuse of fertilizers, fertilizer management BMP requirements on development and significant redevelopment projects, illicit discharge and illegal connection investigations, and the implementation of model integrated pest management, pesticide and fertilizer guidelines. These guidelines have resulted in significant decreases in the amounts of nutrients applied to publicly managed lands.

The reduction in nutrient loading to UNB, changes in the magnitude of algal blooms and the potential impact of algal blooms on beneficial uses of the bay are tracked through the Newport Bay Nutrient TMDL Regional Monitoring Program. Previous studies associated with this program have suggested that the dissolved oxygen (DO) depressions in Newport Bay were most likely associated with high algal biomass. Periodic DO depressions occurred when algal biomass was 2.2 - 2.5 kg m^{-2} (Horne, 1998; EPA, 1998). Densities of 1.5 kg m^{-2} were not associated with low DO, indicating that such densities are not a threat to the aquatic life beneficial use (Horne, 1997; EPA, 1998). Since 1996, when the average density of macroalgae in UNB was 1.8 kg m^{-2} (Horne, 1997), there has been an overall decrease in algal biomass, but the Bay is still susceptible to large blooms when a flux of nutrients enters the bay, either from watershed inputs or in-bay activities such as dredging. Such blooms occurred in 1999 (dredging of the bay likely resulting in a release of nutrients from sediment), in 2004 (unknown cause of localized increase at one sampling site) and in 2005 (record rainfall resulting in increased inputs to UNB combined with the in-operation of Irvine Ranch Water District's San Joaquin Marsh[1]).

Management decisions for UNB require an understanding of factors that control the trophic condition of the bay. However, there are several technical challenges that affect the ability to monitor and assess the trophic condition of Newport Bay and thereby to assess progress toward meeting the goals of the TMDL. First, it is difficult to synoptically evaluate the abundance of macroalgae throughout the bay. Second, the spatial and temporal extent of seasonal hypoxia in the bay is unknown. Third, the relationship between macroalgal abundance and DO, and hence its utility as an indicator of eutrophication, is unknown. This study has two primary goals. The first goal is to explore the application of false color infrared (CIR) aerial photography as an alternative or complement to ground-based methods to assess macroalgal abundance. The second goal is to investigate the relationship between patterns in DO and other physical and chemical parameters and macroalgal abundance. The specific questions this study intends to answer are:

- Can macroalgal distribution be accurately assessed by CIR aerial photography?
- What is the extent of macroalgal cover over the course of the summer-autumn season?
- How do system-wide estimates of macroalgal cover based on ground measures and aerial photography compare to one another?
- What are the spatial and temporal patterns of hypoxia/anoxia in UNB?
- Are frequency and intensity of hypoxia related to macroalgal abundance?
- What other environmental factors influence hypoxia and observed variations of macroalgal abundance?

The study approach consisted of two investigations. First, water column DO, temperature, salinity, depth, and pH were continuously monitored in surface and bottom waters at three sites in UNB (Figure ES-1). Irvine Ranch Water District (IRWD) deployed two YSI 6600 Extended Deployment System (EDS) sondes at each station: one sonde collected data 0.5 m from the surface and the other collected data 0.5 m from the bottom. Data were collected at 30-minute intervals beginning June 15 and ending December 28, 2005.

Second, intertidal macroalgal distribution was surveyed with high-resolution CIR aerial photography during daytime low tides on three occasions: July 26, September 17 and October 31, 2005. Images were collected by SkyView Aerial Photography, Inc. To provide a data set to interpret the aerial images and assess accuracy, macroalgal abundance was measured on the ground by Southern California Coastal Water Research Project (SCCWRP) and Moss Landing Marine Laboratories (MLML) personnel during each overflight. The percent cover of macroalgae was measured with a quadrat at ~30 random locations throughout UNB.

The study resulted in the following general conclusions. Detailed methods, results, and conclusions are summarized in the technical chapters following this summary:

[1] The San Joaquin Marsh is typically used to denitrify urban runoff in San Diego Creek before it is discharged into UNB.

1. Color infrared photography provided a good tool for evaluation of macroalgal abundance on exposed, intertidal mudflats.

Remote sensing by CIR aerial photography was a successful technique for mapping intertidal macroalgal distribution in UNB. Two classes of macroalgae were distinguishable based on the image analysis: *Ceramium* spp. and *Ulva* spp. The overall accuracy of classification (i.e., the percentage of pixels classified correctly) was very high (~97% on July 26, ~91% on September 17, and ~97% on October 31, 2005), and estimates of algal cover from both ground-based measures and aerial photo-interpretation were comparable. However, aerial image analysis tended to detect a greater proportion of areas not covered by macroalgal mats than ground surveys did. There were two possible reasons for this: a limited number of endmembers used in image classification; and irregular distribution of macroalgae within the intertidal zone, with most of the macroalgae concentrated along the water's edge where ground samples were collected, resulting in a data set that did not accurately represent the true distribution of macroalgae and bare substrate within the system. Data extrapolated from the ground surveys likely overestimates macroalgal abundance, while estimates from aerial imagery are likely conservative. Aerial photo-interpretation was not able to provide any information on the thickness of macroalgal mats and, therefore, not appropriate for estimating biomass.

2. Overall algal extent was high and exhibited clear spatial and temporal patterns.

The area of UNB covered by macroalgae significantly increased from July to September and decreased in October (Figure ES-2). Based on aerial image analysis, the overall portion of the intertidal zone covered by *Ceramium* spp. and/or *Ulva* spp. was 45% in July, 91% in September, and 70% in October. In general, there was a longitudinal gradient in macroalgal abundance with more algae near the head of the estuary and less in downstream areas. Macroalgal composition of the seaward regions was dominated by *Ceramium* spp. until October, when *Ulva* spp. replaced *Ceramium* spp. in the lower estuary. In contrast, *Ulva* spp. was the dominant algae at the head of the estuary throughout the study period.

3. Hypoxic events primarily occurred in late summer-early fall, following algal blooms, and were associated with particular physical conditions.

Results of the time series analysis support an emerging conceptual model of bottom water hypoxia resulting from a combination of increased primary productivity (and subsequent oxygen demand associated with macroalgal blooms) and vertical stratification of the water column (i.e., increased residence time of bottom waters; Figure ES-3). Specific instances of hypoxia tended to occur during nighttime low tides in the late summer-early fall, particularly during neap tidal series. Temperature and salinity data indicate that there was vertical stratification at these times as well. The long-term trends of DO concentration were especially pronounced in the bottom layer and also correlated with water column stratification resulting from solar heating of surface waters and freshwater discharge decreasing surface salinity (Figure ES-4). There was a time lag between initial observations of macroalgal proliferation and the onset of hypoxia. This was likely associated with the time required for macroalgae to senesce and sink to the bottom. This contribution of organic material from macroalgae to sediments increased sediment oxygen demand through both biological and oxygen-consuming biogeochemical pathways. Thus, macroalgae seen growing in the intertidal zone in June and July may have contributed to bottom water hypoxia several months later.

4. Macroalgal abundance was not quantitatively related to the frequency of hypoxia.

The abundance of *Ceramium* and *Ulva* spp. as determined from aerial photography explained very little of the variability in surface and bottom water hypoxia (based on a threshold of 3.0 mg L^{-1}), though the frequency of bottom water hypoxia was generally correlated with *Ulva* spp. abundance. DO values <3.0 mg L^{-1} were considered hypoxic for the purposes of this report; this value was chosen based on a review of scientific literature (Kamer and Stein 2003). However, individual species may have higher DO requirements. A DO threshold of 5.0 mg L^{-1} may be adopted for regulatory purposes to protect designated beneficial uses in UNB. Therefore, at the request of the Santa Ana Regional Water Quality Control Board (Regional Board), DO values were compared to a 5.0 mg L^{-1} threshold as well. There were stronger relationships between macroalgal abundance and the frequency of DO measurements <5.0 mg L^{-1}. Together, *Ceramium* and *Ulva* spp. explained roughly 50% of the variability in the frequency of DO values <5.0 mg L^{-1} in surface and bottom waters. *Ulva* spp. alone explained 75% of the variability in the frequency of DO measurements <5.0 mg L^{-1} in bottom waters and 57% of the variability; however, these relationships should be used with caution. in surface waters. UNB is a relatively shallow system (average depth <1 m) with relatively short (~7 days) residence time and significant tidal range (~2 m maximum). Wind driven mixing and tidal mixing may limit the occurrence of hypoxia, even during macroalgal bloom events

Next Steps

Although this study provides valuable insight into the mechanisms that influence hypoxia in UNB, additional work is necessary to develop predictive tools relating physical factors and biological factors (e.g., macroalgal blooms) to hypoxia. Specifically, a more complete understanding of nutrient cycling and budgets should be developed for UNB. The relative roles of biological and sediment oxygen demand over inter- and intra-annual cycles should be investigated. Finally, a dynamic simulation model for nutrients should be developed for UNB. This model would allow investigation of the role hydrodynamics (e.g., freshwater input, stratification, tidal cycles) and biogeochemistry (e.g. nutrient cycling, sediment oxygen demand) on hypoxia. Such a model could also be used to evaluate the anticipated effect of potential management actions on endpoints such as hypoxia and macroalgal blooms.

Remote sensing holds promise as a management tool for assessment of coastal estuaries and lagoons. The approach developed in this study should be applied to other southern California coastal wetlands to determine the robustness of the methodology between systems and to help further refine the algorithms used to translate the image analysis to macroalgal abundance. In addition to the color infrared imaging we used, hyperspectral imaging and high resolution satellite imagery should also be explored in the future with the following considerations in mind: spatial resolution, ability to resolve macroalgal mat thickness, ability to target tidal phase, and cost.

Figure ES-1. Location of water quality measurements using Sonde 1 (S1), Sonde 2 (S2), and Sonde 3 (S3) in Upper Newport Bay.

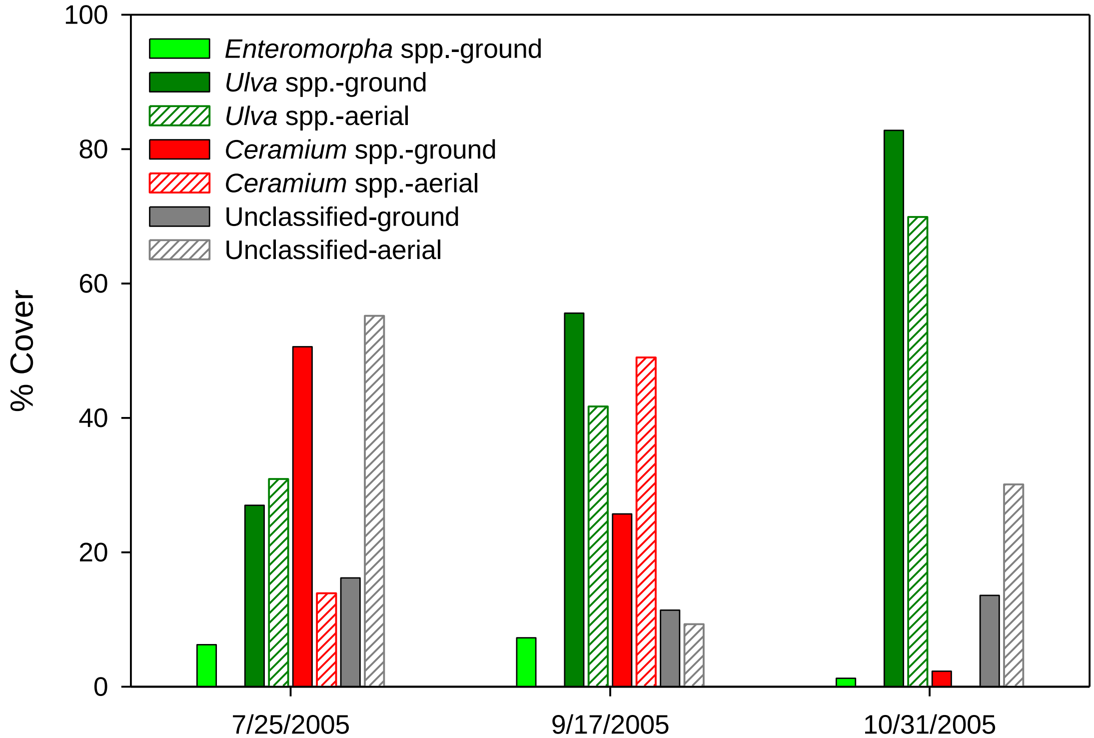

Figure ES-2. Percent cover of macroalgae and unclassified substrate in the exposed, intertidal zone of Upper Newport Bay estimated from ground-based data and aerial image analysis. Zero values indicate zero percent cover for that category.

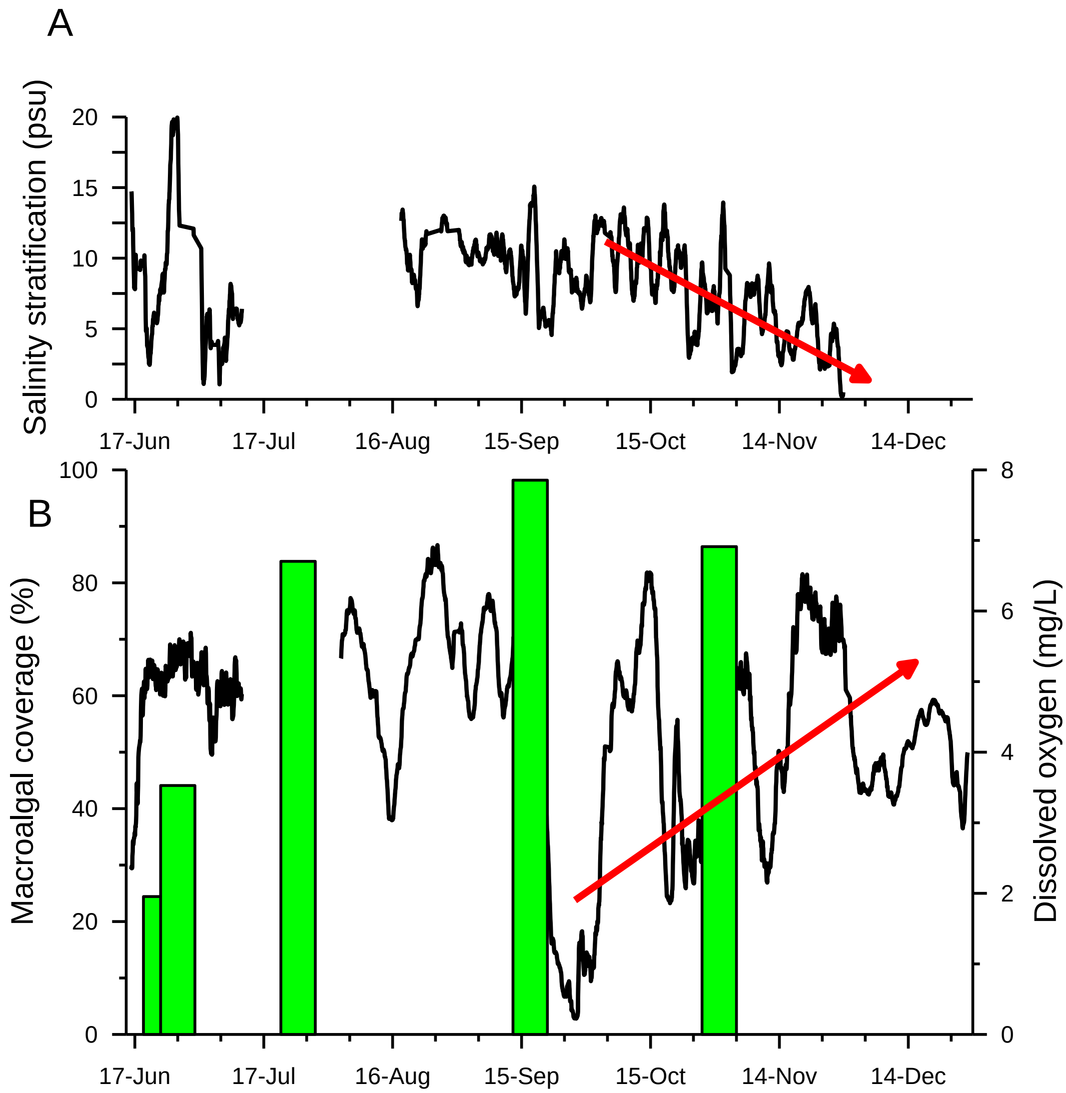

Figure ES-3. Index of stratification estimated as the difference between salinity in the bottom and surface layers (A) and total macroalgal coverage in the UNB intertidal zone (bar chart) and DO concentration in the bottom layer of the head of the estuary (S3; B). Hourly time-series of stratification index and DO were smoothed with running average with 1-day (25-points) window. Arrows show general trend of increasing bottom DO (decreasing hypoxia) from September to December (B) coincident with decreasing stratification (A).

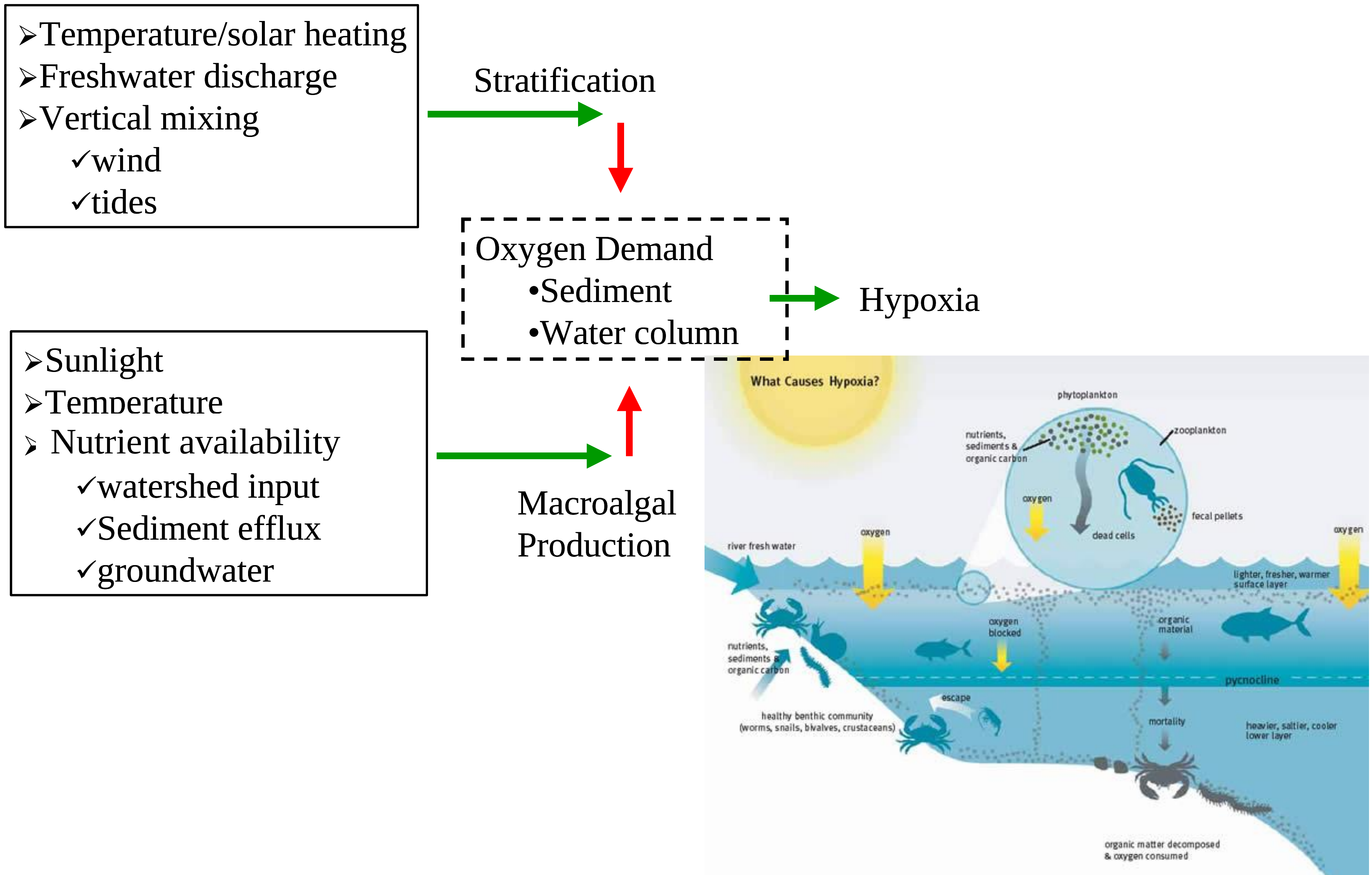

Figure ES-4. Conceptual model of factors that contribute to hypoxia in UNB.

ACKNOWLEDGEMENTS

This work was funded by the California State Water Resources Control Board through a grant to the County of Orange Resources and Development Management Department (SWRCB Agreement No. 04-192-558-0). Thanks to Doug Shibberu at the Santa Ana Regional Water Quality Control Board for project support. Thanks to David R. Young at the US Environmental Protection Agency, Western Ecology Division, for technical expertise and guidance. Thanks to Andy Aguilar, Emily Briscoe, Michelle Cordrey, Liesl Tiefenthaler, and Dawn Petschauer for their assistance in the field, often very early in the morning.

TABLE OF CONTENTS

LIST OF ACRONYMS

ASE	Air-sea exchange
BMP	Best Management Practice
CIR	Color infrared
CIMIS	California Irrigation Management Information System
CRS	Coastal Remote Sensing
DEM	Digital elevation model
DO	Dissolved oxygen
DO%s	Dissolved oxygen saturation
DQOs	Data quality objectives
EDS	Extended Deployment System
EOF	Empirical Orthogonal Functions
IfSAR	Interferometric Synthetic Aperture Radar
IRWD	Irvine Ranch Water District
MLML	Moss Landing Marine Laboratories
MNF	Minimum Noise Fraction Rotation
N	Nitrogen
NEM	Net ecosystem metabolism
OF	Oxygen flux
P	Phosphorus
PCA	Principle Component Analysis
QA	Quality assurance
QC	Quality control
RMP	Regional monitoring program
S	Water salinity
SAM	Spectral Angle Mapper
SCB	Southern California Bight
SCCWRP	Southern California Coastal Water Research Project
SDC	San Diego Creek
T	Water temperature
TMDL	Total Maximum Daily Load
UNB	Upper Newport Bay

LIST OF TABLES

LIST OF FIGURES

CHAPTER 1. APPLICATION OF COLOR INFRARED AERIAL PHOTOGRAPHY TO ASSESS MACROALGAL EXTENT

Introduction

Large blooms of opportunistic green macroalgae such as *Enteromorpha* and *Ulva* spp. occur in estuaries and coastal lagoons throughout the world (Sfriso et al., 1987; Sfriso et al., 1992; Schramm and Nienhuis, 1996; Raffaelli et al., 1999) often in response to increased nutrient loads from developed watersheds (Valiela et al., 1992; Nixon, 1995; Paerl, 1999). While these algae are natural components of estuarine systems and play integral roles in estuarine processes (Pregnall and Rudy, 1985; Kwak and Zedler, 1997; Boyer, 2002), blooms are of ecological concern because they can reduce the habitat quality of an estuary. They can deplete the water column and sediments of oxygen (Sfriso et al., 1987; Sfriso et al., 1992; Peckol and Rivers, 1995) leading to changes in species composition, shifts in community structure (Raffaelli et al., 1991; Ahern et al., 1995; Thiel and Watling, 1998), and loss of ecosystem function.

Traditional methods of assessing macroalgal distribution and abundance often involve ground-based measurements of percent cover or biomass at multiple locations in a system. Data can be extrapolated from the individual measurements to the entire system; however, the appropriateness of this relies on the degree to which the sampling locations represent the larger system. These traditional methods are limited in that they cannot provide a synoptic view of algal distribution over comparatively large areas due to the limited number of samples that can be collected and processed during each survey and often insufficient resources to sample the entire study area. In contrast to more stable terrestrial landscapes that can be sampled over longer time periods, this problem is especially crucial in variable marine environments where macroalgae may drift with the tides and change location daily and the sampling window is relatively short.

Remote sensing (i.e., aerial or satellite image analysis) provides an alternative to ground-based methods for assessment of macroalgal extent. Aerial photography provides more appropriate spatial resolution than satellite imagery for assessment of spatial patterns of aquatic vegetation along seashores, including estuaries (Lehmann and Lachavanne, 1997). Satellite observations are more cost-effective (Ferguson and Korfmacher, 1997), but the spatial resolution of satellite imagery severely limits its possible utilization for aquatic vegetation mapping. Typically, aquatic vegetation form narrow strips along water bodies (Kirkman, 1996) and are therefore barely wider than the highest resolution of most present day satellites (e.g., 20 m for SPOT and 30 m for Landsat TM). The problem is especially pronounced in southern California where estuaries are often small and the intertidal areas are limited to narrow zones or areas within the estuary.

Aerial photography is particularly well-suited for quantitative analysis of terrestrial vegetation where it is necessary to discern areas covered by different types of substrate (Campbell, 1987; Avery and Berlin, 1992; Wilkie and Finn, 1996; Jensen, 2000; Lillesand and Kiefer, 2000). For this, false color infrared (CIR) photography is an effective method, because it emphasizes the contrast between vegetated and non-vegetated substrate. In contrast to natural color photography representing three main visible color bands (i.e., blue, green, and red), CIR photography uses film to transform green, red, and nearinfrared wavebands into blue, green and red, respectively. Vegetation, in contrast to non-vegetated substrate, strongly reflects in nearinfrared; as such, in

CIR imagery different types of vegetation are easily distinguishable by red-color areas of different color tone, representing different levels of near-infrared reflectance (Avery and Berlin, 1992). Airborne imagery can be also collected using more sophisticated tools, from digital cameras to hyperspectral radiometers (see Myers and Miller, 2005); the advantage of these new technologies is high spectral resolution, the disadvantages are logistical problems and cost.

In coastal ocean sciences, aerial photography has been used for assessment of various parameters (see Hilton, 1984), including chlorophyll concentration and phytoplankton biomass in coastal waters (Harding et al., 1994; Richardson et al., 1994; Hoogenboom et al., 1998), coastal plume tracers (Carder et al., 1993), benthic substrates (Werdell and Roesler, 2003; Vahtmae et al., 2006), coral reefs (Mumby et al., 1998; Andrefouet et al., 2003; Andrefouet et al., 2004; Mumby et al., 2004), and different kinds of benthic macrophytes including kelp (Jensen et al., 1980; Deysher, 1993) and seagrass meadows (Bulthuis, 1995; Ferguson and Korfmacher, 1997; Robbins, 1997; Ward et al., 1997; Pasqualini et al., 1998; Kendrick et al., 2000). Past studies have shown that a combination of green, red and near-infrared wavebands (i.e., color-infrared or CIR) is best for identification of surface macrophytes in freshwater basins (Malthus and George, 1997).

To date, only a handful of studies have used aerial photography to identify macroalgae in marine and estuarine habitats. Several focused on deep estuaries or embayments (Bulthuis, 1995; Sheppard et al., 1995) as opposed to the shallow estuaries that form along much of the Pacific Coast. Young et al. (1998) successfully used CIR aerial photography to map macroalgae and eelgrass in Yaquina Bay, a shallow estuary in Oregon. Ground truth data were collected for several days before and after the overflights. Classification of aerial imagery was in good agreement with ground data when the density of vegetation exceeded 75% cover. However, at lower densities of macroalgae, the agreement was lower, indicating that remote sensing methods may be less sensitive to low densities of algae than traditional ground surveys (D. Young, pers. comm.).

The goal of this study was to explore the application of CIR aerial photography as an alternative to traditional, ground-based methods to analyze the changes in the abundance of macroalgae in Upper Newport Bay (UNB), a eutrophic estuary in southern California. Our specific objectives were 1) to determine if the area in UNB covered by macroalgae could be accurately assessed by aerial CIR photography; 2) to identify the best methods of imagery processing and data transformation; and 3) to compare system-wide estimates of macroalgal extent based on ground measures and aerial photography. Additionally, we analyzed spatial and temporal patterns of macroalgal abundance with special attention on the factors influencing macroalgal biomass in different parts of the estuary. Lastly, we discuss the limitations of CIR and the problems we encountered.

Methods

Site description

Newport Bay (Figure 1-1) is the second largest estuarine embayment in southern California. The main freshwater inflow is San Diego Creek, which drains 85% of the 400 km^2 watershed. The main channel of UNB is wide with extensive broad mudflats and shallow areas; however, the center of the channel is dredged to 5 m below sea level for sediment retention purposes. UNB is separated from the Pacific Ocean by the Lower Bay, which has been dredged and developed into a marina with no natural area remaining. Water residence time in UNB can be 1 week during neap tide (RMA, 2000).

UNB is a state ecological reserve and provides critical natural habitat for a number of terrestrial and aquatic threatened and endangered species that use the estuary for refuge, foraging, and breeding. UNB provides significant spawning and nursery habitats for commercial and non-commercial fish species. However, UNB is subject to anthropogenic stressors. Much of the watershed was converted from orchards and row crop farms to an urban environment; by the late 1980s, 64% of the land was used for residential and commercial purposes (Gerstenberg, 1989). Historically, high nutrient loads from the watershed have resulted in macroalgal blooms (Kamer et al., 2001; Kennison et al., 2003).

Remote sensing-data collection and analysis

High-resolution CIR aerial photography and ground-based field measurements were used to determine exposed, intertidal macroalgal distribution in UNB three times from July through October 2005. Aerial images were collected during daytime low tides (<0.70 m) with clear skies and sun angle >30° above the horizon on July 26, September 17 and October 31, 2005, by SkyView Aerial Photography, Inc. Vertical aerial photographs were taken by a forward image-motion compensating, GPS-triggered camera with a 153-mm lens. Kodak Aerochrome III Infrared film in 23 x 23 cm format was used. The images were collected from a height of ~1000 m resulting in a nominal scale of 1:6000. The frontal overlap between photographs was 60% and side overlap was 40%, in accordance with the recommendations for airborne remote sensing (Myers and Miller, 2005). Thirty-three images were collected on July 26, 36 on September 17, and 33 on October 31, 2005. All images were digitized on a high-resolution photogrammetric color scanner at a scanning resolution not less than 32 microns (800 dpi) in 24 bit color and saved in a TIFF format. The final ground sample distance (GSD) in each digital pixel was 25 cm; there were 100 pixels in each 2.5 x 2.5 m (6.25 m^2) area. Each digital image contained three wavebands, representing green (500 - 600 nm), red (600 - 750 nm), and near-infrared (750 - 1000 nm).

To provide a data set to interpret the aerial images and assess accuracy, macroalgal abundance was measured on the ground during each overflight. Percent cover of macroalgae was recorded at ~30 locations randomly distributed throughout the exposed mudflat area by placing a 1.25 x 1.25 m quadrat strung with two orthogonal sets of 5 equally spaced taut strings in the four compass sectors around a central point. The type of cover (macroalgal species, bare mud, mussels, or "other") under each intercept was recorded for a total of 100 points within a 6.25-m^2 area. The location of the central point was recorded with a sub-meter accuracy GPS. All ground sampling was conducted within the one low tide period surrounding the overflight (~5 hours); we felt this was critical since macroalgal mats can move during inundation.

The analysis of UNB imagery included three steps: (1) creation of georegistered composite images for each survey based on geometric transformations (i.e., orthorectification, georegistration and mosaicing); (2) image enhancement achieved by MNF transformation; and (3) estimation of the areas covered by macroalgae in each composite image by SAM pixel classification (MNF and SAM are described below). These steps correspond to the conventional approach used in processing of digital images (Caloz and Collet, 1997). All images were processed using ENVI software Version 4.2 (Research Systems, Inc.). Each image was orthorectified (i.e., corrected for distortions introduced by the camera geometry, look angles, and topography) and georegistered using the coordinates of recognizable landmarks (25 - 40 for each image) obtained from the "Google Earth" website. Then, all images taken during one flight were merged using ENVI "mosaic" option, thus creating one composite georegistered image of 0.25-m spatial resolution for each survey.

Next, the areas not relevant to the analysis were removed from each composite image. We clipped the areas in which elevation exceeded 32 m above the image reference level[2] using a high-resolution Digital Elevation Model (DEM) obtained from the NOAA Coastal Services Center/Coastal Remote Sensing (CRS) Program website (http://www.csc.noaa.gov/crs/). This DEM was developed from recent airborne Interferometric Synthetic Aperture Radar (IfSAR) observations and has pixel resolution ranging from 1.25 to 2.50 m. The water surface, the areas of low elevation other than intertidal zone (e.g., slips with recreational boats) and the areas covered by vascular plants (dominated in UNB by *Spartina foliosa* and *Salicornia* spp.) were removed manually by creating a mask. As all ground data we used for classification (see below) were collected in the intertidal zone rather than in water or the zone covered by vascular plants, we could not segregate these three zones using image classification methods. Instead, we used expert assessment of CIR photographs, where water was clearly distinguished by its dark color and the areas covered by vascular plants by rough texture and sharp edges.

Before classification, images were transformed in order to more clearly separate patterns from random differences in pixel coloration. The goal of this transformation was to remove noise (i.e., differences between image pixels that are not related to differences in vegetation) and make each image more consistent to achieve better classification results. All three composite CIR images (each containing three bands) were transformed by Minimum Noise Fraction Rotation (MNF) method (Green et al., 1988). The MNF transformation includes two cascaded Principal Components transformations. The first transformation, based on an estimated noise covariance matrix, decorrelates and rescales the noise in the data, resulting in a transformed image in which the noise has unit variance and no band-to-band correlations. The second step is a standard Principal Components transformation of the noise-whitened data. In general, this transformation enables a reduction of the dimensionality of the image spectrum to segregate noise in the data, which makes sense when the number of bands is substantially higher than three, such as in hyperspectral imagery. However, the analyzed images contained only three bands; as such, the dimensionality of the data was not changed, but the separability (i.e., the quantitative measure of difference) between the classes and unclassified samples dramatically improved.

The ground survey macroalgal abundance data were used to classify the images. Ground samples where one type of substrate dominated (i.e., contributed >80% of total sample area) were attributed to classes representing this data type (Tables 1-1 to 1-4). Ground samples without at least 80% cover by one substrate (e.g., 50% *Ulva* spp., 20% *Ceramium* spp., and 30% bare mud) were not used because their optical properties could not reliably be matched to a specific

[2] This is not 32 m above mean sea level (MSL), rather it is above the reference elevation provided with the digital elevation model (DEM).

substrate. Each class was then divided into two groups of equal size. The optical properties of the first group (endmember) were used for classification and the optical properties of the second group (control) were used for validation of the classification results (Tables 1-2 to 1-4). A minimum of six ground samples were needed to establish a class: three for use as endmembers for classification and three for use as controls for validation. On July 26 and September 17, two classes of endmembers were established: *Ceramium* spp. and *Ulva* spp. On October 31, there were no ground samples with >80% *Ceramium* spp. and only one endmember class was used: *Ulva* spp. In July, one ground sample had >80% *Enteromorpha* spp. cover; no other ground samples during the entire study had >80% *Enteromorpha* spp. Thus, it could not be used for classification. The number of samples characterizing other substrates (e.g., bare mud, mussels) was also insufficient for classification and the optical characteristics of these samples were very different from each other (see Results section). The separability was estimated as a Jeffries-Matusita index (Richards, 1999).

After MNF transformation, the images were processed by the method of supervised classification, i.e., each pixel was compared to endmembers that were estimated on the basis of ground data analysis. As a result of this comparison, most pixels were attributed to distinct classes associated with the endmembers. Those pixels, which appeared to be different from all endmembers were attributed to an "unclassified" group. The results of analysis (Tables 1-2 to 1-4; Figures 1-2 to 1-4) illustrate that this unclassified group appears to primarily represent un-vegetated substrate, the optical properties of which are different from the areas covered by macroalgae.

As a method of supervised classification we used the Spectral Angle Mapper (SAM) algorithm. As a measure of similarity SAM uses the angle between the endmember and each pixel spectrum vectors in the space which dimensionality results from the number of analyzed bands (in our images it is a 3-dimensional space). Smaller angles represent closer matches to the reference spectrum. We selected this method because it is relatively insensitive to topographic illumination and albedo effects (Kruse et al., 1993), which can be significant in the exposed intertidal zone.

Validation of each image was assessed using a conventional methodology including such indices as total accuracy, confusion matrix, commission error, omission error, producer accuracy, and user accuracy (Congalton and Green, 1999).

Previous studies have shown longitudinal gradients in salinity, nutrient availability and macroalgal abundance in UNB (Kamer et al., 2001; RMA, 2001; Kennison et al., 2003; Boyle et al., 2004). Thus we divided UNB into four regions starting from the mouth of San Diego Creek and proceeding downstream toward the ocean (Regions A - D; Figure 1-1). Within each individual region, we determined the area of exposed intertidal mudflat covered by different classes of substrate (*Ceramium* spp., *Ulva* spp., or unclassified) as both an absolute number and as a percentage of the area exposed from the aerial images. We also calculated mean percent cover within each region from the ground-based data and compared the results to those from the image analysis. We did this for all of UNB as a whole as well.

The tidal levels during aerial surveys ranged from 5 cm (October 31) to 60 - 70 cm (September 17 and July 26, respectively). To estimate the influence of tidal level on the spatial coverage of different substrates in UNB intertidal zone, we applied the water mask estimated for the survey when the tidal level was highest (July 26) to the image when the tidal level was lowest (October 31). This was done for UNB as a whole and for each region separately (A - D). Mosaics of the aerial images for each flight are shown in Appendix A.

Results

Aerial imagery classification

In the original aerial images, the optical characteristics of each class were very close (Figures 1-2A, 1-3A, 1-4A). The brightness of the pixels within each class or unclassified sample varied within a wide range due to illumination and terrain effects. At the same time, the brightness of all three bands was strongly correlated within each class. Also, the optical characteristics of identical classes were different between different surveys. This difference can be explained by the changes in illumination, resulting from sun angle and cloudiness. In particular, on September 17 the brightness of all three bands was significantly lower than on July 26 and October 31.

All classes within each survey (both endmembers and controls) were compared using the Jeffries-Matusita separability measure (Richards, 1999). This index ranges from 0 to 2.0 and indicates how well the selected pairs of classes are statistically separate. Values greater than 1.9 indicate that the classes have good separability (Richards, 1999). These indices were low between the endmember and the control of the same class and high between different classes (Table 1-5).

After MNF rotation, the brightness in different bands became uncorrelated, the groups became more compact, and the differences between each class became more evident (Figures 1-2B, 1-3B, 1-4B; Table 1-5). On July 26, the optical characteristics of *Ceramium* spp. and *Ulva* spp. were easily distinguished, and the respective endmember and control groups of *Ceramium* spp. and *Ulva* spp. were each very close (Table 1-5). On September 17, lowest indices of separability were between the endmember and the control of the same class (0.31 for *Ceramium* spp. and 0.17 for *Ulva* spp.). However, the separability between different classes was lower than on July 26, seemingly resulting from low brightness. On October 31, the endmember and control of *Ulva* spp. class were very close.

After MNF transform, the samples dominated by bare mud and mussels were very different from the macroalgal classes and the unclassified samples with macroalgal mixtures (Figures 1-2 to 1-4). These differences were especially evident during July 26 and October 31, 2005.

Aerial imagery validation

After all three composite images were transformed by MNF rotation and classified by SAM method using the endmembers obtained from one-half of the ground samples, the accuracy of the results was verified on the basis of the second half of the samples (Tables 1-6 to 1-8). The overall accuracy of classification (i.e., the percentage of pixels classified correctly) was very high (~97% on July 26, ~91% on September 17, and ~97% on October 31, 2005).

The “user accuracy” of *Ulva* spp. classification (i.e., the percentage of image pixels correctly classified as *Ulva* spp. when compared to ground data) was perfect (100%) in each survey. The “producer accuracy” of *Ulva* spp. (i.e., the percentage of pixels in *Ulva* spp. control sample areas that were correctly classified in the image) was also high (~99% on July 26; ~88% on September 17; ~97% on October 31). The user accuracy of *Ceramium* spp. classification was ~100% in July and ~80% in September; the producer accuracy was 95% in July and 97% in September. Decreased user accuracy of *Ceramium* spp. in September may have been due to heterogeneity of optical properties.

Macroalgal coverage of Upper Newport Bay

Based on the analysis of aerial images, the area of the exposed, intertidal mudflat area of UNB covered by macroalgae increased from July to September and decreased in October (Figure 1-5; Table 1-9). Coverage by *Ceramium* spp. and *Ulva* spp. combined was 45% in July, 91% in September, and 70% in October. Ground-based measurements of macroalgal abundance produced trends similar to those based on aerial photographs, but the absolute values were different (Figure 1-5). For example, in July more than 3.5 times as much *Ceramium* spp. was measured in the ground data (50.6 % cover) as was estimated from the aerial images (13.9 % cover). In the aerial images, 55.2% of the area was unclassified, meaning the pixels could not be assigned either *Ulva* spp. or *Ceramium* spp. classification and were probably un-vegetated substrate, whereas only 22.4% of the ground data was not *Ulva* spp. or *Ceramium* spp. The 22.4% was composed of *Enteromorpha* spp. (6.2%), bare mud (9.3%), and other substrate (6.9%).

In July, there was a longitudinal gradient in macroalgal abundance. Based on aerial image analysis, Area D, closest to the ocean, had 25% macroalgal cover, while Region A near the mouth of San Diego Creek had 60% cover (Figure 1-6; Table 1-9). Macroalgal composition of the seaward regions was dominated by *Ceramium* spp. whereas in the upstream regions, *Ulva* spp. was more prolific. In September, the cover of both *Ceramium* spp. and *Ulva* spp. increased in all regions of UNB. Combined cover of *Ceramium* spp. and *Ulva* spp. ranged from 87% in Region D to 93% in Region B; *Ceramium* spp. was the dominant alga in Regions B - D but *Ulva* spp. was dominant in Region A. By the end of October, *Ulva* spp. coverage increased dramatically in all regions of UNB except Region A, where it declined slightly from September. *Ceramium* spp. was so sparse that it was not classified in the October 31 images; its area was estimated as zero. In September and October, the differences in macroalgal abundance between the upper and the lower parts of UNB were much less than in July.

The patterns of macroalgal coverage estimated from ground-based samples and from aerial photography were similar in throughout Regions A - D, but again the absolute values were different (Figure 1-6). Percent cover of macroalgae determined from aerial image analysis was often lower than that estimated from ground surveys, with the exception of *Ceramium* spp. in September; its estimated cover from the aerial images was higher than that of the ground surveys in each region. The remote sensing also tended to detect more unclassified area (area that could not be identified as *Ceramium* spp. or *Ulva* spp.) than the ground surveys. Ground sampling detected *Enteromorpha* spp. in Regions B - D throughout the study, but as noted earlier, this alga was not abundant enough to be used as a classification in the aerial image analyses.

Maps of macroalgal distribution from the three surveys are presented in Figures 1-7 to 1-10. *Ulva* spp. always dominated Region A. In the three other regions, significant portions of the intertidal zone were un-vegetated in July. In September, much of these areas were occupied by *Ceramium* spp., which was replaced by *Ulva* spp. by the end of October.

Discussion

Remote sensing by CIR aerial photography was a successful technique for mapping intertidal macroalgal distribution in UNB (Figures 1-7 to 1-10.). The accuracy assessment indicated that the classifications generated from the aerial image analyses can be used with confidence, and estimates of algal cover were comparable based on both ground-based measures and aerial photo-interpretation. The technique is probably most effective when macroalgal mats are dense. In our study, we were able to correctly identify areas with more than 80% cover of *Ceramium* spp. or *Ulva* spp. We may not have been able to correctly identify areas with less dense macroalgae. Similar work in Yaquina Bay, OR, has shown a similar pattern of success. High agreement between aerial image analysis and ground surveys was found when vegetation exceeded 75 % cover, but agreement decreased as the vegetation became less dense (D. Young, pers.comm).

The total accuracy achieved in this study (>90%) substantially exceeds the accuracy reported for other studies focused on mapping of benthic substrates. For example, the accuracy of mapping of seagrass meadows in North Carolina was 72.6% (Ferguson and Korfmacher, 1997) and benthic substrates in Corsica was 62% to 92% (Pasqualini et al., 1997). Our results are comparable with the accuracy of mapping of coastal habitats at the Caribbean island Anguilla (91.3%; Sheppard et al., 1995) and in Yaquina Bay, OR (>90%; D. Young, pers. comm.). Unfortunately, few areal assessments of marine substrates include proper estimation of accuracy. In general, an overall accuracy of 85% is recommended as a cutoff between acceptable and unacceptable results (Congalton and Green, 1999).

The accuracy of assessment of surface substrates on the basis of remotely sensed imagery depends on proper selection of the method of image processing. This study illustrates that the MNF method (Green et al., 1988) is an effective tool to remove noise from remotely sensed images and enhance the differences between the endmembers used for classification and validation of classification results. A salient feature of this method is a decrease of the number of bands, making this method especially useful for processing of hyperspectral imagery, where the number of bands often exceeds 100. However, even when the number of bands is as small as three (as is the case in our study), MNF transformation significantly improves the images, resulting in better classification. MNF transformation is based on the Principle Component Analysis (PCA) method, different modifications of which were repeatedly used for analysis of remotely sensed imagery, including aerial photography of benthic habitats (Ferguson and Korfmacher, 1997; Pasqualini et al., 1997; Pasqualini et al., 1998).

The SAM method of assessment of similarity between pixels is recommended for the analysis of images in which brightness is highly variable but strongly correlated between bands, which can result presumably from terrain effects. The SAM method estimates similarity from the angles between the pixel vectors in multi-dimensional space, which corresponds to the ratio between the brightness values of different bands rather than the absolute brightness values. It should be noted, however, that MNF transform removes a significant part of correlation between bands, enabling usage of other methods of classification. In our study, the SAM method was also applied to original CIR images before MNF transform and provided satisfactory results, though they were not as good as the results obtained after MNF transform.

There were discrepancies between estimates of macroalgal cover from the aerial image analysis and the ground sampling, probably due to two factors. First, the number of classes used in aerial image classification was limited by the number of identifiable endmembers. Therefore, if pixels could not be classified as either *Ceramium* spp. or *Ulva* spp., then they were unclassified. These pixels however, might have represented areas with *Enteromorpha* spp., which, while found during ground surveys, was not abundant enough to be used as an endmember, or a mixture of algae and bare substrate that did not match the spectral signatures of the endmembers. This would serve to increase the proportion of unclassified area determined from the aerial images relative to the area determined by ground surveys not to contain macroalgae. One way to alleviate the discrepancies would be to collapse *Enteromorpha* spp. into *Ulva* spp., as has been recently suggested in the literature (Hayden and Waaland, 2002; Hayden et al., 2003). This action could also be justified based on the ecological similarity of these algae; they have similar nutrient uptake and growth rates (Fujita, 1985; Kamer et al., 2002).

Second, the macroalgae may have been irregularly distributed within the intertidal zone, with most of the macroalgae concentrated along the water's edge where ground samples were collected. This would have resulted in a ground data set that did not accurately represent the true distribution of macroalgae and bare substrate within the system. We suspect that most of differences observed between the two data sets are due to the unintentional ground sampling bias toward vegetated areas. The end result is that data extrapolated from the ground samples likely overestimate macroalgal abundance, while estimates from aerial imagery are likely conservative.

The observed spatial pattern of macroalgal distribution is typical of UNB. Previous studies also showed very high cover of *Enteromorpha* and *Ulva* spp. at the head of UNB and the highest *Ceramium* spp. cover at the seaward end (Kamer et al., 2001). Macroalgal abundance, particularly that of green algae, is often strongly related to nutrient availability (Sfriso et al., 1987; Hernandez et al., 1997; Schramm, 1999). Kennison et al. (2003), Boyle et al. (2004), and Sutula et al. (2006) each measured higher water column dissolved nitrogen (N) and phosphorus (P) concentrations at the head of UNB compared to further downstream, which in part could explain the persistent, high density of *Ulva* spp. in Region A. The area contained in Region A also had the highest sediment N and P concentrations and benthic nutrient efflux (Kennison et al., 2003; Sutula et al., 2006).

The dominance of *Ceramium* spp. in the seaward regions of UNB has not been seen previously, while later in the season, *Ceramium* spp were replaced by *Ulva* spp. *Ceramium* spp. has been found in UNB in high density patches (Kamer et al., 2001) but it was not present in large, homogenous mats with continuous coverage over large areas as it was in this study. Kennison et al. (2003) did not report the occurrence of *Ceramium* spp. Its increase in abundance may be due to a change in the nutrient regime of UNB that allows it to compete successfully.

One limitation of the CIR aerial photography is that it can only quantify the spatial extent of the mats and not the thickness. Therefore, only percent cover, not biomass, can be determined. Previous studies (Kamer et al., 2001; Kennison et al., 2003) have not attempted to correlate macroalgal percent cover and biomass, and we do not recommend doing so at this time either. A statistically significant, reliable relationship is unlikely because the thickness of algal mats can vary greatly (K. Kamer, pers. obs.). However, percent cover provides a reasonable metric for abundance and clearly depicts temporal and spatial changes in macroalgae throughout this study. Different remote sensing technologies, such as hyperspectral imagery, which collects data in many bands in the visible and near-infrared spectra, may provide discrimination between mats of different thicknesses, but this has yet to be investigated.

Another limitation is that CIR photography can only be used to assess the distribution of exposed vegetation, rather than submerged vegetation. When benthic plants are covered by water, even at shallow depths, their optical signatures are dramatically obscured (Sheppard et al., 1995) and CIR often does not resolve between submerged vegetation and other types of substrate because water strongly absorbs nearinfrared radiance. To successfully use CIR aerial photography to map intertidal vegetation, the lowest tide possible should be targeted in order to maximize exposure of the intertidal zone. Natural color photographs have been successfully used for visualization of submerged vegetation (Ferguson et al., 1993; Marshall and Lee, 1994; Pasqualini et al., 2001), and hyperspectral imaging may offer unique advantages for mapping subtidal vegetation as well (Dierssen et al., 2003). However, these studies were conducted in relatively clear waters. It is unknown whether or not any type of imagery could penetrate UNB's turbid waters.

We further recommend collecting all images during similar tidal phases since the amount of intertidal area exposed depends on tidal level. In southern California the tidal range can be as much as 2 m. The water level during our surveys was highest on July 26, 2005; only 60.9 ha were exposed compared to 73 ha on October 31, 2005. While we normalized our data to the total area surveyed by calculating each classification as a percentage of the whole, we were concerned that differences in macroalgal distribution with elevation affected our results. After applying the water mask from July 26 to the October 31 dataset, the percentage of the total area covered by *Ulva* spp. increased slightly from 69.9% to 72.5% (Table 1-9). While this increase is small, surveying during more similar tidal phases would have simplified our inter-survey comparisons.

Our ability to classify bare substrate (i.e., mud) was due to an insufficient number of ground samples with more than 80% bare ground. We used the data set from our random sampling for both calibration and validation. Our classification probably would have been more successful had we stratified our sampling by targeting different substrates for the endmember data set and obtained a sufficient number of samples. When the image is highly mosaic, relatively large (i.e., significantly exceeding the accuracy of georegistration) homogenous areas covered by main substrates (i.e., endmembers) should be selected. Substrates with optical properties that are expected to vary (e.g., bare substrate) should be sampled in greater number then the substrates of more consistent color (e.g., macroalgae). Finally, it is worth mentioning that the minimum number of samples recommended by Congalton and Green (1999), 50 for each class, was not achievable in this study because we prioritized completion of the ground survey within one tidal cycle. Nevertheless, the small number of samples collected in this study resulted in high classification accuracy.

Collection of ground data for each individual aerial survey is necessary because the spectral signatures of the substrates were not transportable through time. Our data (Tables 1-2 to 1-4) show that the optical signatures of different classes were not consistent among surveys. The illumination conditions of each survey varied with sun angle and azimuth and atmospheric conditions. Hyperspectral imaging offers the possibility of eliminating ground truthing for classification by creating a standardized spectral library. However, ground data collection during each survey for atmospheric correction is required in order to apply the spectral library. Additionally, current hyperspectral image collection and processing costs were prohibitively expensive within the context of this study.

We conclude that remote sensing is an accurate, effective tool for assessing estuarine, intertidal macroalgal coverage with broad applications. The spatial extent of the macroalgae measured in this study can be used as a baseline for comparison with future studies to assess changes over time. This technology can also be used to assess relative eutrophication synoptically in multiple systems. Hyperspectral imaging and high resolution satellite imagery should be explored also in the future with the following considerations in mind: spatial resolution, ability to resolve macroalgal mat thickness, ability to target tidal phase, and cost.

References

Ahern, J., Lyons, J., McClelland, J., Valiela, I., 1995. Invertebrate response to nutrient-induced changes in macrophyte assemblages in Waquoit Bay. Biological Bulletin 189, 241-242.

Andrefouet, S., Payri, C., Hochberg, E.J., Che, L.M., Atkinson, M.J., 2003. Airborne hyperspectral detection of microbial mat pigmentation in Rangiroa atoll (French Polynesia). Limnology and Oceanography 48, 426-430.

Andrefouet, S., Payri, C., Hochberg, E.J., Hu, C., Atkinson, M.J., Muller-Karger, F.E., 2004. Use of in situ and airborne reflectance for scaling-up spectral discrimination of coral reef macroalgae from species to communities. Marine Ecology - Progress Series 283, 161-177.

Avery, T.E., Berlin, G.L., 1992. Fundamentals of remote sensing and airphoto interpretation. Prentice Hall, Upper Saddle River, N.J., 472 pp.

Boyer, K.E., 2002. Linking community assemblages and ecosystem processes in temperate and tropical coastal habitats. Ph.D. thesis, University of California, Los Angeles, 157 pp.

Boyle, K.A., Kamer, K., Fong, P., 2004. Spatial and temporal patterns in sediment and water column nutrients in a eutrophic southern California estuary. Estuaries 27, 378-388.

Bulthuis, D.A., 1995. Distribution of seagrasses in a North Puget Sound estuary: Padilla Bay, Washington, USA. Aquatic Botany 50, 99-105.

Caloz, R., Collet, C., 1997. Geographic information systems (GIS) and remote sensing in aquatic botany: methodological aspects. Aquatic Botany 58, 209-228.

Campbell, J.B., 1987. Introduction to remote sensing. Guilford Press, New York, 551 pp.

Carder, K.L., Steward, R.G., Chen, R.F., Hawes, S.K., Lee, A., Davis, C.O., 1993. AVRIS calibration and application in coastal oceanic environments: tracers of soluble and particulate constituents in the Tampa Bay coastal plume. Photogrammetric Engineering and Remote Sensing 59, 339-344.

Congalton, R.G., Green, K., 1999. Assessing the accuracy of remotely sensed data: Principles and practices. Lewis Publishers, Boca Raton, 137 pp.

Deysher, L.E., 1993. Evaluation of remote-sensing techniques for monitoring giant kelp populations. Hydrobiologia 261, 307-312.

Dierssen, H.M., Zimmerman, R.C., Leathers, R.A., Downes, T.V., Davis, C.O., 2003. Ocean color remote sensing of seagrass and bathymetry in the Bahamas Banks by high-resolution airborne imagery. Limnology and Oceanography 48, 444-455.

Ferguson, R.L., Korfmacher, K., 1997. Remote sensing and GIS analysis of seagrass meadows in North Carolina, USA. Aquatic Botany 58, 241-258.

Ferguson, R.L., Wood, L.L., Graham, D.B., 1993. Monitoring spatial change in seagrass habitat with aerial photography. Photogrammetric Engineering and Remote Sensing 59, 1033-1038.

Fujita, R.M., 1985. The role of nitrogen status in regulating transient ammonium uptake and nitrogen storage by macroalgae. Journal of Experimental Marine Biology and Ecology 92, 283-301.

Gerstenberg, G., 1989. Management plan Upper Newport Bay Ecological Reserve. State of California Resource Agency, Department of Fish and Game. Newport Beach, CA, pp.

Green, A.A., Berman, M., Switzer, P., Craig, M.D., 1988. A transformation for ordering multispectral data in terms of image quality with implications for noise removal. IEEE Transactions on Geoscience and Remote Sensing 26, 65-74.

Harding, L.W., Jr., Itsweir, E.C., Esaias, W.E., 1994. Estimation of phytoplankton biomass in the Chesapeake Bay from aircraft remote sensing of chlorophyll concentrations, 1989-92. Remote Sensing of Environment 49, 41-56.

Hayden, H.S., Waaland, J.R., 2002. Phylogenetic systematics of the Ulvaceae (Ulvales, Ulvophyceae) using chloroplast and nuclear DNA sequences. Journal of Phycology 38, 1200-1212.

Hayden, H.S., Blomster, J., Maggs, C.A., Silva, P.C., Stanhope, M.J., Waaland, J.R., 2003. Linnaeus was right all along: Ulva and Enteromorpha are not distinct genera. European Journal of Phycology 38, 277-294.

Hernandez, I., Peralta, G., Perez-Llorens, J.L., Vergara, J.J., Niell, F.X., 1997. Biomass and dynamics of growth of Ulva species in Palmones River estuary. Journal of Phycology 33, 764-772.

Hilton, J., 1984. Airborne remote sensing for freshwater and estuarine monitoring. Water Research 18, 1195-1223.

Hoogenboom, H.J., Dekker, A.G., De Haa, J.F., 1998. Retrieval of chlorophyll and suspended matter in inland waters from CASI data by matrix inversion. Canadian Journal of Remote Sensing 24, 144-152.

Jensen, J.R., 2000. Remote sensing of the environment : an earth resource perspective. Prentice Hall, Upper Saddle River, N.J., 544 pp.

Jensen, J.R., Estes, J.E., Tinney, L., 1980. Remote sensing techniques for kelp surveys. Photogrammetric Engineering and Remote Sensing 46, 743-755.

Kamer, K., Boyle, K.A., Fong, P., 2001. Macroalgal bloom dynamics in a highly eutrophic southern California estuary. Estuaries 24, 623-635.

Kamer, K., Schiff, K., Kennison, R.L., Fong, P., 2002. Macroalgal nutrient dynamics in Upper Newport Bay. Southern California Coastal Water Research Project 365. Westminster, CA, 98 pp.

Kendrick, G.A., Hegge, B.J., Wyllie, A., Davidson, A., Lord, D.A., 2000. Changes in seagrass cover on Success and Parmelia Banks, Western Australia between 1965 and 1995. Estuarine, Coastal and Shelf Science 50, 341-353.

Kennison, R.L., Kamer, K., Fong, P., 2003. Nutrient dynamics and macroalgal blooms: a comparison of five southern California estuaries. Southern California Coastal Water Research Project 416. Westminster, CA, 113 pp.

Kirkman, H., 1996. Baseline and monitoring methods for seagrass meadows. Journal of Environmental Management 47, 191-201.

Kruse, F.A., Lefkoff, A.B., Boardman, J.B., Heidebrecht, K.B., Shapiro, A.T., Barloon, P.J., Goetz, A.F.H., 1993. The Spectral Image Processing System (SIPS) - Interactive Visualization and Analysis of Imaging spectrometer Data. Remote Sensing of Environment 44, 145-153.

Kwak, T.J., Zedler, J.B., 1997. Food web analysis of southern California coastal wetlands using multiple stable isotopes. Oecologia (Berlin) 110, 262-277.

Lehmann, A., Lachavanne, J.-B., 1997. Geographic information systems and remote sensing in aquatic botany. Aquatic Botany 58, 195-207.

Lillesand, T.M., Kiefer, R.W., 2000. Remote sensing and image interpretation. John Wiley & Sons, New York, 724 pp.

Malthus, T.J., George, D.G., 1997. Airborne remote sensing of macrophytes in Cefni Reservoir, Anglesey, UK. Aquatic Botany 58, 317-332.

Marshall, T.R., Lee, P.F., 1994. Mapping aquatic macrophytes through digital image analysis of aerial photographs: an assessment. Journal of Aquatic Plant Management 32, 61-66.

Mumby, P.J., Green, E.P., Clark, C.D., Edwards, A.J., 1998. Digital analysis of multispectral airborne imagery of coral reefs. Coral Reefs 17, 59-69.

Mumby, P.J., Hedley, J.D., Chisholm, J.R.M., Clark, C.D., Ripley, H., Jaubert, J., 2004. The cover of living and dead corals from airborne remote sensing. Coral Reefs 23, 171-183.

Myers, J.S., Miller, R.L., 2005. Optical airborne remote sensing. In: Miller, R.L., Del Castillo, C.E., McKee, B.A., (Eds.), Remote Sensing of Coastal Aquatic Environments. Technologies, Techniques and Applications. Springer, Dordrecht, pp. 51-67.

Nixon, S.W., 1995. Coastal marine eutrophication: A definition, social causes, and future concerns. Ophelia 41, 199-219.

Paerl, H.W., 1999. Cultural eutrophication of shallow coastal waters: coupling changing anthropogenic nutrient inputs to regional management approaches. Limnologica 29, 249-254.

Pasqualini, V., Pergent-Martini, C., Fernandez, C., Pergent, G., 1997. The use of airborne remote sensing for benthic cartography: advantages and reliability. International Journal of Remote Sensing 18, 1167-1177.

Pasqualini, V., Pergent-Martini, C., Clabaut, P., Pergent, G., 1998. Mapping of *Posidonia oceanica* using aerial photographs and side scan sonar: application off the Island of Corsica (France). Estuarine, Coastal and Shelf Science 47, 359-367.

Pasqualini, V., Pergent-Martini, C., Clabaut, P., Marteel, H., Pergent, G., 2001. Integration of aerial remote sensing, photogrammetry, and GIS technologies in seagrass mapping. Photogrammetric Engineering and Remote Sensing 67, 99-105.

Peckol, P., Rivers, J.S., 1995. Physiological responses of the opportunistic macroalgae Cladophora vagabunda (L.) van den Hoek and Gracilaria tikvahiae (McLachlan) to environmental disturbances associated with eutrophication. Journal of Experimental Marine Biology and Ecology 190, 1-16.

Pregnall, A.M., Rudy, P.P., 1985. Contribution of green macroalgal mats (Enteromorpha spp.) to seasonal production in an estuary. Marine Ecology - Progress Series 24, 167-176.

Raffaelli, D., Limia, J., Hull, S., Pont, S., 1991. Interactions between the amphipod Corophium volutator and macroalgal mats on estuarine mudflats. Journal of the Marine Biological Association of the United Kingdom 71, 899-908.

Raffaelli, D., Balls, P., Way, S., Patterson, I.J., Hohmann, S., Corp, N., 1999. Major long-term changes in the ecology of the Ythan estuary, Aberdeenshire, Scotland; How important are physical factors? Aquatic Conservation 9, 219-236.

Richards, J.A., 1999. Remote Sensing Digital Image Analysis. Springer-Verlag, Berlin, 240 pp.

Richardson, L.L., Buison, D., Lui, C.J., Ambrosia, V., 1994. The detection of algal photosynthetic accessory pigments using Airborne Visible-Infrared Imaging Spectrometer (AVRIS) spectral data. Marine Technology Society Journal 28, 10-21.

RMA, 2000. Newport Bay residence time study. # Prepared for the Irvine Company. Resource Management Associates Inc. Suisun City, CA, 20 pp.

RMA, 2001. Newport Bay Water Quality Model Development 3-D Stratified Flow Analysis. # Prepared for California State Water Resources Control Board. Resource Management Associates Inc. Suisun City, CA, 212 pp.
Robbins, B.D., 1997. Quantifying temporal change in seagrass areal coverage: the use of GIS and low resolution aerial photography. Aquatic Botany 58, 259-267.
Schramm, W., 1999. Factors influencing seaweed responses to eutrophication: Some results from EU-project EUMAC. Journal of Applied Phycology 11, 69-78.
Schramm, W., Nienhuis, P.H., (Eds.) 1996. Marine benthic vegetation: recent changes and the effects of eutrophication. Springer-Verlag, New York, 470 pp.
Sfriso, A., Marcomini, A., Pavoni, B., 1987. Relationships between macroalgal biomass and nutrient concentrations in a hypertrophic area of the Venice Lagoon. Marine Environmental Research 22, 297-312.
Sfriso, A., Pavoni, B., Marcomini, A., Orio, A.A., 1992. Macroalgae, nutrient cycles, and pollutants in the Lagoon of Venice. Estuaries 15, 517-528.
Sheppard, C.R.C., Matheson, K., Bythell, J.C., Murphy, P., Blair Myers, C., Blake, B., 1995. Habitat mapping in the Caribbean for management and conservation: use and assessment of aerial photography. Aquatic Conservation: Marine and Freshwater Ecosystems 5, 277-298.
Sutula, M., Kamer, K., Cable, J., Collis, H., Berelson, W., Mendez, J., 2006. Sediments as an internal source of nutrients to Upper Newport Bay, California. Southern California Coastal Water Research Project 482. Westminster, CA, 151 pp.
Thiel, M., Watling, L., 1998. Effects of green algal mats on infaunal colonization of a New England mud flat - long-lasting but highly localized effects. Hydrobiologia 375/376, 177-189.
Vahtmae, E., Kutser, T., Martin, G., Kotta, J., 2006. Feasibility of hyperspectral remote sensing for mapping benthic macroalgal cover in turbid coastal waters - a Baltic Sea case study. Remote Sensing of Environment 101, 342-351.
Valiela, I., Foreman, K., LaMontagne, M., Hersh, D., Costa, J., Peckol, P., DeMeo-Andreson, B., D'Avanzo, C., Babione, M., Sham, C.H., Brawley, J., Lajtha, K., 1992. Couplings of watersheds and coastal waters sources and consequences of nutrient enrichment in Waquoit Bay Massachusetts. Estuaries 15, 443-457.
Ward, D.H., Markon, C.J., Douglas, D.C., 1997. Distribution and stability of eelgrass beds at Izembek Lagoon, Alaska. Aquatic Botany 58, 229-240.
Werdell, P.J., Roesler, C.S., 2003. Remote assessment of benthic substrate composition in shallow waters using multispectral reflectance. Limnology and Oceanography 48, 557-567.
Wilkie, D.S., Finn, J.T., 1996. Remote sensing imagery for natural resources monitoring : a guide for first-time users. Columbia University Press, New York, 295 pp.
Young, D.R., Specht, D.T., Clinton, P.J., Lee, H.I., 1998. Use of color infrared aerial photography to map distributions of eelgrass and green macroalgae in a non-urbanized estuary of the Pacific northwest U.S.A., Fifth International Conference on Remote Sensing for Marine and Coastal Environments, Vol. 2. 37-45 pp.

Table 1-1. Inventory of ground-based samples with coverage by one substrate exceeding 80%.

Substrate	July 26, 2005	September 17, 2005	October 31, 2005
Bare	1	-	-
Ceramium spp.	14	6	-
Enteromorpha spp.	1	-	-
Ulva spp.	7	14	21
Other (mostly unvegetated substrate)	1	3	2
Total number of samples	*31*	*30*	*26*

Table 1-2. Centers of the classes and unclassified samples (mean ± standard deviation; original image in numerator; after MNF transform in denominator) collected on July 26, 2005.

Class or sample #	Substrates	Band 1 (near-IR)	Band 2 (red)	Band 3 (green)
Endmember (6 samples)	> 80% *Ceramium* spp.	129.7±11.6 -1.71±3.20	79.1±11.2 4.96±4.79	62.4±14.0 -12.38±3.62
Control (6 samples)	>80% *Ceramium* spp.	125.3±17.8 -0.03±4.62	76.9±12.6 4.53±4.30	60.6±14.3 -12.13±3.49
Endmember (3 samples)	>80% *Ulva* spp.	150.2±9.9 -3.84±2.70	86.9±9.7 7.12±4.19	94.6±11.5 13.00±3.40
Control (3 samples)	>80% *Ulva* spp.	144.6±13.4 -6.48±4.05	77.7±10.3 2.58±4.08	83.2±13.0 12.26±3.24
Sample 3	100% bare substrate	106.0±4.1 19.99±1.91	80.6±3.1 11.55±1.37	79.2±4.4 -0.62±3.87
Sample 4	63% bare substrate 35% *Ceramium* spp.	56.6±6.6 22.26±2.09	35.6±4.5 -6.27±1.68	24.5±6.5 -6.77±2.75
Sample 10	69% bare substrate 19% *Ceramium* spp. 11% *Enteromorpha spp.*	146.9±2.2 11.12±1.94	110.8±3.5 21.55±1.87	109.0±3.8 -2.50±2.27
Sample 21	53% *Enteromorpha spp.* 42% *Ceramium* spp. 5% *Ulva* spp.	142.3±3.3 -0.32±1.38	92.1±3.1 10.64±1.30	81.6±2.8 -7.51±2.60
Sample 24	67% *Ulva* spp. 33% *Enteromorpha spp.*	156.1±6.2 -4.77±2.82	92.4±4.6 9.20±2.18	98.6±5.4 10.99±3.33
Sample 25	88% *Enteromorpha spp.* 12% *Ulva* spp.	130.5±6.3 -2.86±2.75	73.0±2.8 1.90±1.32	68.0±6.1 0.78±5.01

Table 1-3. Centers of the classes and unclassified samples (mean ± standard deviation; original image in numerator; after MNF transform in denominator) collected on September 17, 2005.

Class or sample #	Substrates	Band 1 (near-IR)	Band 2 (red)	Band 3 (green)
Endmember (3 samples)	>80% *Ceramium* spp.	68.6±6.61 / 8.13±3.06	46.9±5.01 / 2.18±2.65	57.5±5.95 / 3.64±4.36
Control (3 samples)	>80% *Ceramium* spp.	70.3±7.42 / 6.94±3.40	48.4±4.98 / 2.40±2.05	57.5±5.37 / 5.46±2.47
Endmember (7 samples)	>80% *Ulva* spp.	77.8±12.3 / 4.20±5.33	45.1±9.1 / -0.35±4.83	65.6±10.4 / -10.13±3.54
Control (7 samples)	>80% *Ulva* spp.	75.2±9.9 / 5.23±4.41	44.0±6.6 / -0.57±3.47	63.7±8.6 / -9.12±4.90
Sample 13	97% mud with mussels 3% *Ulva* spp.	57.9±2.3 / 15.56±1.95	43.4±2.2 / 3.76±1.58	56.0±2.3 / 2.30±3.44
Sample 14	75% *Ulva* spp. 20% *Ceramium* spp. 5% *Enteromorpha spp.*	64.6±3.7 / 9.29±1.56	45.5±3.5 / 1.82±2.03	53.7±4.1 / 6.70±2.25
Sample 16	51% *Ulva* spp.; 48% *Ceramium* spp.	75.5±3.4 / 5.60±2.56	48.8±2.4 / 2.24±2.00	63.3±2.5 / -1.65±3.68
Sample 19	87% mud with mussels 13% *Ulva* spp.	67.1±3.6 / 11.58±1.78	49.3±4.2 / 5.24±2.44	61.3±3.8 / 2.81±2.87
Sample 22	55% *Ulva* spp. 40% *Ceramium* spp. 5% *Enteromorpha spp.*	73.4±2.8 / 5.60±2.36	45.8±3.3 / 0.50±2.72	60.9±3.3 / -2.80±3.07
Sample 23	56% *Enteromorpha spp.* 27% *Ceramium* spp. 17% *Ulva* spp.	70.4±2.8 / 7.02±1.79	46.8±2.1 / 1.65±1.43	58.4±2.9 / 2.09±2.56
Sample 25	56% *Enteromorpha spp.*; 17% *Ulva* spp.	80.7±4.0 / 2.01±2.42	45.2±2.5 / -1.36±1.62	66.0±3.3 / -11.10±3.07
Sample 27	57% *Enteromorpha* spp.; 28% *Ulva* spp.; 15% *Ceramium* spp.	80.2±5.8 / 0.89±2.62	47.9±3.9 / -0.54±2.14	61.9±5.3 / -2.19±3.89
Sample 29	*Ceramium* spp.; *Ulva* spp.	78.7±2.3 / 4.09±1.45	52.1±2.2 / 3.35±1.33	64.5±2.4 / 1.12±3.02
Sample 30	49% *Ulva* spp.; 47% bare substrate	78.3±2.9 / 11.93±1.63	60.6±3.1 / 12.05±1.91	77.2±3.0 / -1.62±3.19

Table 1-4. Centers of the classes and unclassified samples. Mean ± standard deviation; original image in numerator and after MNF transform in denominator; collected on October 31, 2005.

Class or sample #	**Substrates**	**Band 1 (near-IR)**	**Band 2 (red)**	**Band 3 (green)**
Endmember (10 samples)	>80% *Ulva* spp.	118.8±17.3 / 5.52±7.61	61.5±8.7 / 6.51±3.72	74.3±11.3 / -13.65±5.45
Control (10 samples)	>80% *Ulva* spp.	125.8±11.1 / 6.65±5.71	67.5±9.3 / 4.57±5.32	81.3±12.6 / -14.81±5.22
Sample 25	99% mud with mussels	98.1±9.1 / -14.55±1.89	79.5±8.2 / -12.23±2.88	83.9±9.3 / 2.97±2.62
Sample 26	100% bare substrate	61.8±6.6 / -23.38±1.55	50.7±5.6 / -4.40±2.03	53.5±7.7 / 5.19±3.84
Sample 27	90% mud with mussels 8% *Ulva* spp.	98.1±1.9 / -9.00±1.83	69.6±3.2 / -5.22±1.92	73.3±4.0 / 1.66±2.87
Sample 41	53% *Ceramium* spp. 45% *Ulva* spp.	111.5±6.3 / 2.02±2.84	67.9±3.5 / 0.86±1.88	69.6±4.5 / 1.29±4.78
Sample 44	68% *Ulva* spp. 16% *Enteromorpha spp.* 16% bare substrate	124.9±4.4 / 10.50±3.75	61.3±3.4 / 8.97±2.79	72.6±4.7 / -13.18±2.91

Table 1-5. Jeffries-Matusita measures of separability between the classes: endmembers (E) and controls (C).

2005 Survey	Image Type	Class	Endmember or Control	***Ceramium* spp.**		***Ulva* spp.**	
				E	**C**	**E**	**C**
July 26	Original	*Ceramium* spp.	E	-	0.22	1.70	2.00
			C	0.22	-	1.64	2.00
		Ulva spp.	E	1.70	1.64	-	1.24
			C	2.00	2.00	1.24	-
	MNF transformed	*Ceramium* spp.	E	-	0.31	1.48	1.92
			C	0.31	-	1.34	1.83
		Ulva spp.	E	1.48	1.34	-	0.79
			C	1.92	1.83	0.79	-
September 17	Original	*Ceramium* spp.	E	-	0.31	1.64	1.36
			C	0.31	-	1.95	1.80
		Ulva spp.	E	1.64	1.95	-	0.17
			C	1.36	1.80	0.17	-
	MNF transformed	*Ceramium* spp.	E	-	0.31	1.64	1.36
			C	0.31	-	1.95	1.80
		Ulva spp.	E	1.64	1.95	-	0.17
			C	1.36	1.80	0.17	-
October 31	Original	*Ulva* spp.	E	-	-	-	0.48
			C	-	-	0.48	-
	MNF transformed	*Ulva* spp.	E	-	-	-	0.32
			C	-	-	0.32	-

Table 1-6. Confusion matrix and classification validation for composite image taken July 26, 2005.

Confusion matrix

Class	*Ceramium* spp. (Control)	*Ulva* spp. (Control)	Total
Unclassified	18 (4.79%)	4 (1.35%)	22 (3.27%)
Ceramium spp. (Endmember)	358 (95.21%)	0	358 (53.19%)
Ulva spp. (Endmember)	0	293 (98.65%)	293 (43.54%)
Total	376 (100%)	297 (100%)	673 (100%)

Classification validation

Class	Commission Error	Omission Error	Producer Accuracy	User Accuracy
Ceramium spp.	0.00%	4.79%	95.21%	100.00%
Ulva spp.	0.00%	1.35%	98.65%	100.00%
Overall Accuracy	96.73%			

Table 1-7. Confusion matrix and classification validation for composite image taken September 17, 2005.

Confusion matrix

Class	*Ceramium* spp. (Control)	*Ulva* spp. (Control)	Total
Unclassified	8 (2.69%)	11 (1.57%)	19 (1.90%)
Ceramium spp. (Endmember)	289 (97.31%)	74 (10.54%)	363 (36.34%)
Ulva spp. (Endmember)	0	617 (87.89%)	617 (61.76%)
Total	297 (100%)	702 (100%)	999 (100%)

Classification validation

Class	Commission Error	Omission Error	Producer Accuracy	User Accuracy
Ceramium spp.	20.39%	2.69%	97.31%	79.61%
Ulva spp.	0.00%	12.11%	87.89%	100.00%
Overall Accuracy	90.69%			

Table 1-8. Confusion matrix and classification validation for composite image taken October 31, 2005.

Confusion matrix

Class	*Ulva* spp. (Control)	Total
Unclassified	29 (2.93%)	29 (2.93%)
Ulva spp. (Endmember)	961 (97.07%)	961 (97.07%)
Total	990 (100%)	990 (100%)

Classification validation

Class	Commission Error	Omission Error	Producer Accuracy	User Accuracy
Ulva spp.	0.00%	2.93%	97.07%	100.00%
Overall Accuracy	97.07%			

Table 1-9. Areas (ha/acres and %) covered by different substrates in UNB as determined from aerial image analysis.

Region	Substrate	Survey: July 26	Survey: September 17	Survey: October 31	Survey: October 31 with water mask from July 26
A	*Ceramium* spp.	0.1 / 0.2 (0.4%)	22.4 / 55.4 (13.3%)	-	-
	Ulva spp.	10.0 / 24.7 (60.1%)	13.1 / 32.4 (77.5%)	12.4 / 30.6 (66.8%)	11.1 / 27.4 (67.0%)
	Unclassified*	6.5 / 16.1 (39.5%)	1.6 / 4.0 (9.2%)	6.2 / 15.3 (33.2%)	5.5 / 13.6 (33.0%)
	Total	16.6 / 41.0 (100.0%)	16.9 / 41.8 (100.0%)	18.6 / 46.0 (100.0%)	16.6 / 41.0 (100.0%)
B	*Ceramium* spp.	3.3 / 8.2 (12.9%)	14.0 / 34.6 (54.5%)	-	-
	Ulva spp.	7.4 / 18.3 (29.3%)	9.8 / 24.2 (38.3%)	24.1 / 59.6 (76.4%)	20.2 / 49.9 (79.7%)
	Unclassified*	14.7 / 36.3 (57.8%)	1.8 / 4.4 (7.2%)	7.4 / 18.3 (23.6%)	5.1 / 12.6 (20.3%)
	Total	25.4 / 62.8 (100.0%)	25.7 / 63.5 (100.0%)	31.5 / 77.8 (100.0%)	25.4 / 62.8 (100.0%)
C	*Ceramium* spp.	3.0 / 7.4 (35.8%)	6.1 / 15.1 (71.2%)	-	-
	Ulva spp.	0.9 / 2.2 (10.8%)	1.5 / 3.7 (17.9%)	7.3 / 18.0 (73.4%)	6.6 / 16.3 (78.7%)
	Unclassified*	4.5 / 11.1 (53.4%)	0.9 / 2.2 (10.9%)	2.6 / 6.4 (26.6%)	1.8 / 4.4 (21.3%)
	Total	8.4 / 20.8 (100.0%)	8.6 / 21.3 (100.0%)	9.9 / 24.5 (100.0%)	8.3 / 20.5 (100.0%)
D	*Ceramium* spp.	2.1 / 5.2 (19.9%)	8.2 / 20.3 (73.5%)	-	-
	Ulva spp.	0.5 / 1.2 (5.1%)	1.5 / 3.7 (13.5%)	7.3 / 18.0 (55.9%)	6.3 / 15.6 (59.3%)
	Unclassified*	8.0 / 19.8 (75.0%)	1.5 / 3.7 (13.0%)	5.7 / 14.1 (44.1%)	4.3 / 10.6 (40.7%)
	Total	10.6 / 26.2 (100.0%)	11.2 / 27.7 (100.0%)	13.0 / 32.1 (100.0%)	10.6 / 26.2 (100.0%)
Total UNB	*Ceramium* spp.	8.4 / 20.8 (13.9%)	30.5 / 75.4 (49.0%)	-	-
	Ulva spp.	18.8 / 46.5 (30.9%)	26.0 / 64.2 (41.7%)	51.0 / 126.0 (69.9%)	44.1 / 109.0 (72.5%)
	Unclassified*	33.6 / 83.0 (55.2%)	5.8 / 14.3 (9.3%)	22.0 / 54.3 (30.1%)	16.7 / 41.3 (27.5%)
	Total	60.9 / 150.5 (100.0%)	62.3 / 153.9 (100.0%)	73.0 / 180.4 (100.0%)	60.9 / 150.5 (100.0%)

* probably unvegetated substrate

Table 1-10. Areas of UNB intertidal zone and environmental conditions for aerial surveys used in this study.

Survey (2005)	Region (Figure 1-1)	Exposed intertidal zone Area (ha/acres)	Intertidal zone (%)	Time of aerial survey	Tidal level (m)	Solar elevation angle	Solar azimuth
July 26	A	16.6 / 41.0	89.2%	10:25 - 10:45 a.m.	0.70	66º	57º
	B	25.4 / 62.8	80.6%				
	C	8.4 / 20.8	84.4%				
	D	10.6 / 26.2	81.7%				
	Total	60.9 / 150.5	83.5%				
September 17	A	16.9 / 41.8	90.8%	1:15 - 1:35 p.m.	0.60	53º	-35º
	B	25.7 / 63.5	81.5%				
	C	8.6 / 21.3	86.8%				
	D	11.2 / 27.7	85.7%				
	Total	62.3 / 153.9	85.3%				
October 31	A	18.6 / 46.0	100%	2:00 - 2:30 p.m.	0.05	32º	-39º
	B	31.5 / 77.8	100%				
	C	10.0 / 24.7	100%				
	D	13.0 / 32.1	100%				
	Total	73.0 / 180.4	100%				

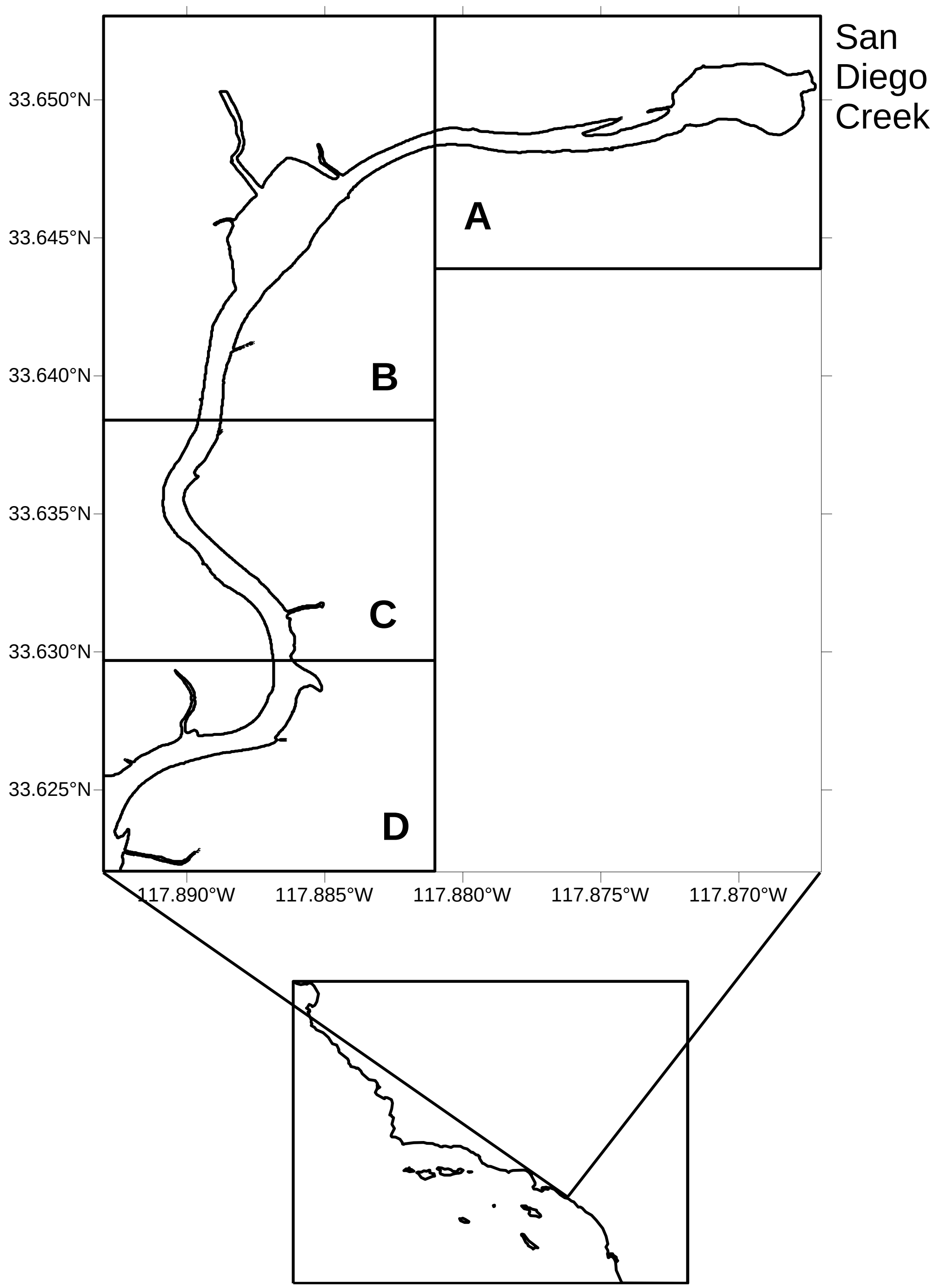

Figure 1-1. The study area of Upper Newport Bay including four regions (A - D).

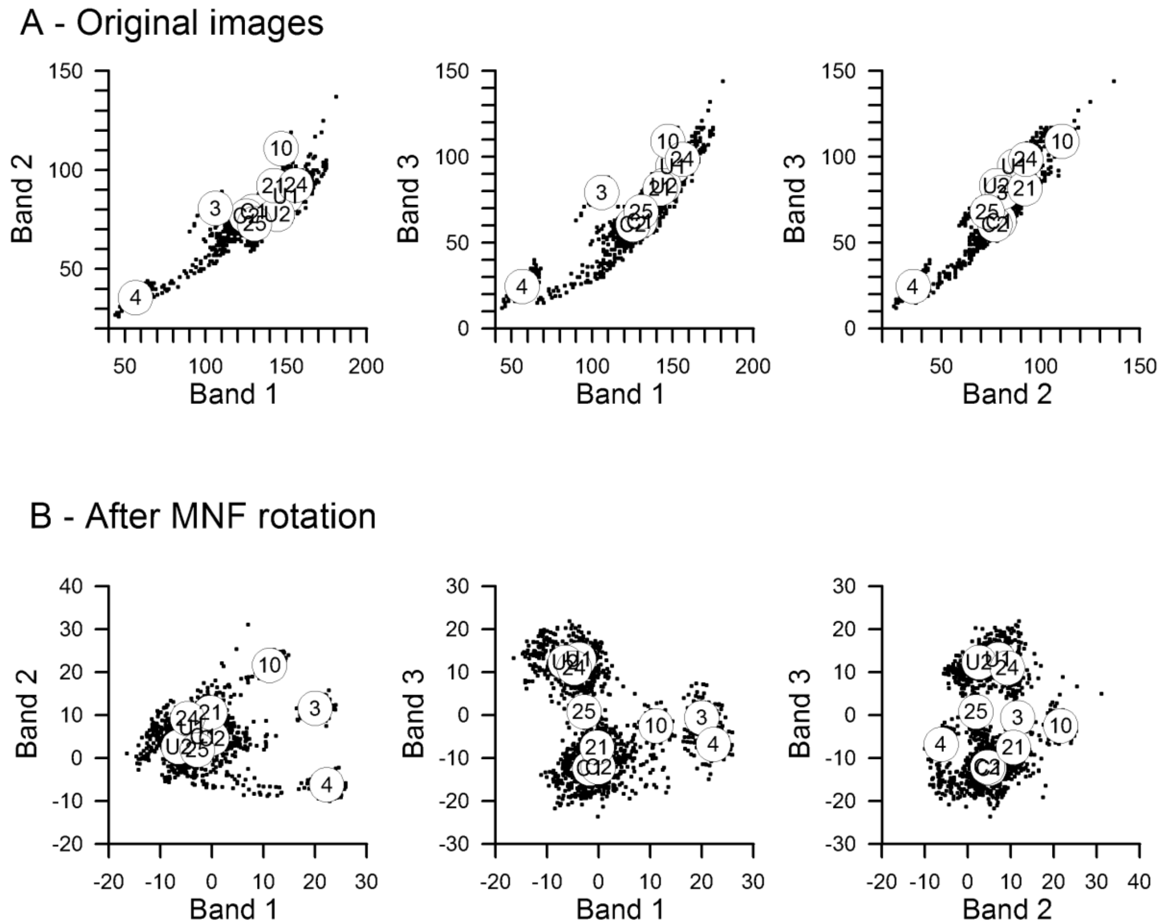

Figure 1-2. Scatterplots of pixels and locations of the means in the classes (endmembers and controls) of the UNB image taken July 26, 2005. *Ceramium* spp. Endmember (C1); *Ceramium* spp. control (C2); *Ulva* spp. endmember (U1); and *Ulva* spp. control (U2). The labels of unclassified samples are given in Table 1.

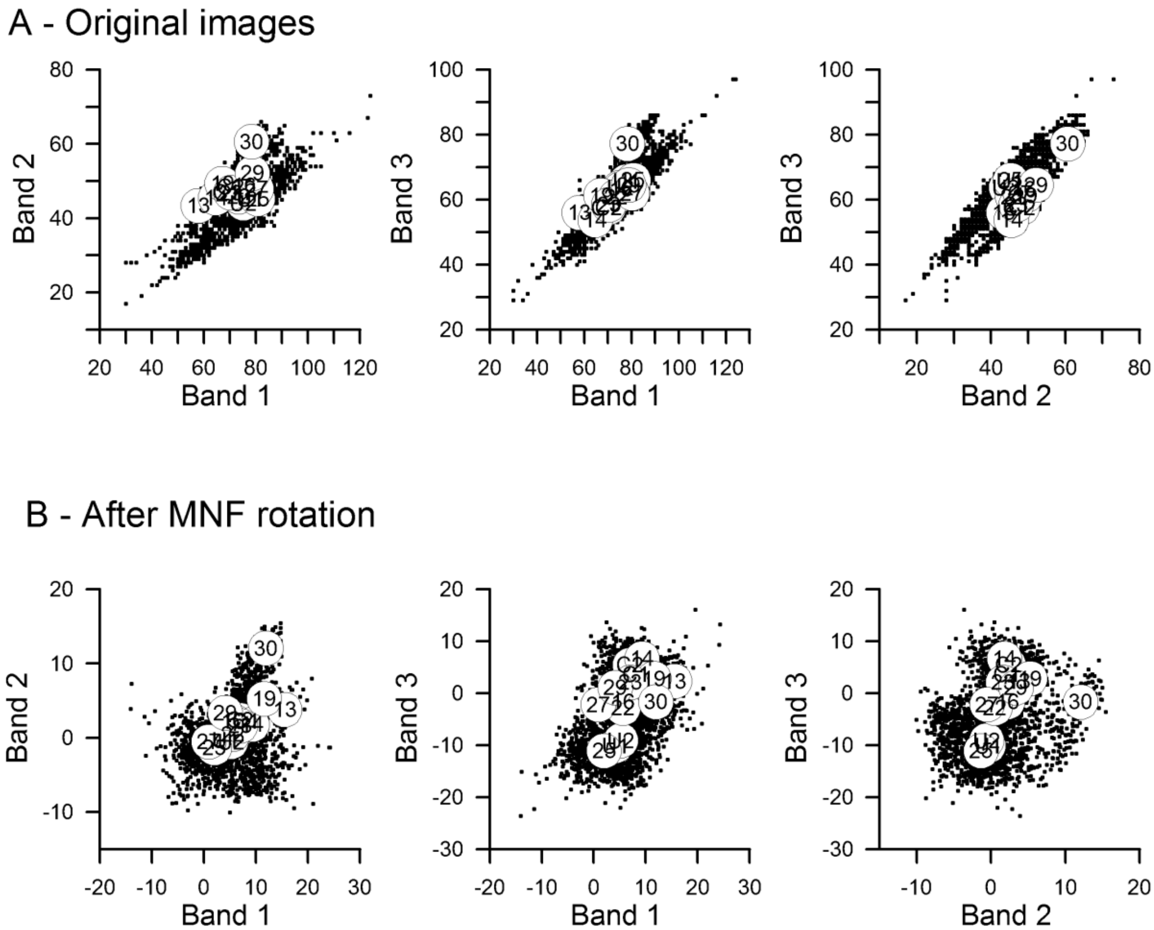

Figure 1-3. Scatterplots of pixels and locations of the means in the classes (endmembers and controls) of the UNB image taken September 17, 2005. *Ceramium* spp. Endmember (C1); *Ceramium* spp. control (C2); *Ulva* spp. endmember (U1); and *Ulva* spp. control (U2). The labels of unclassified samples are given in Table 2.

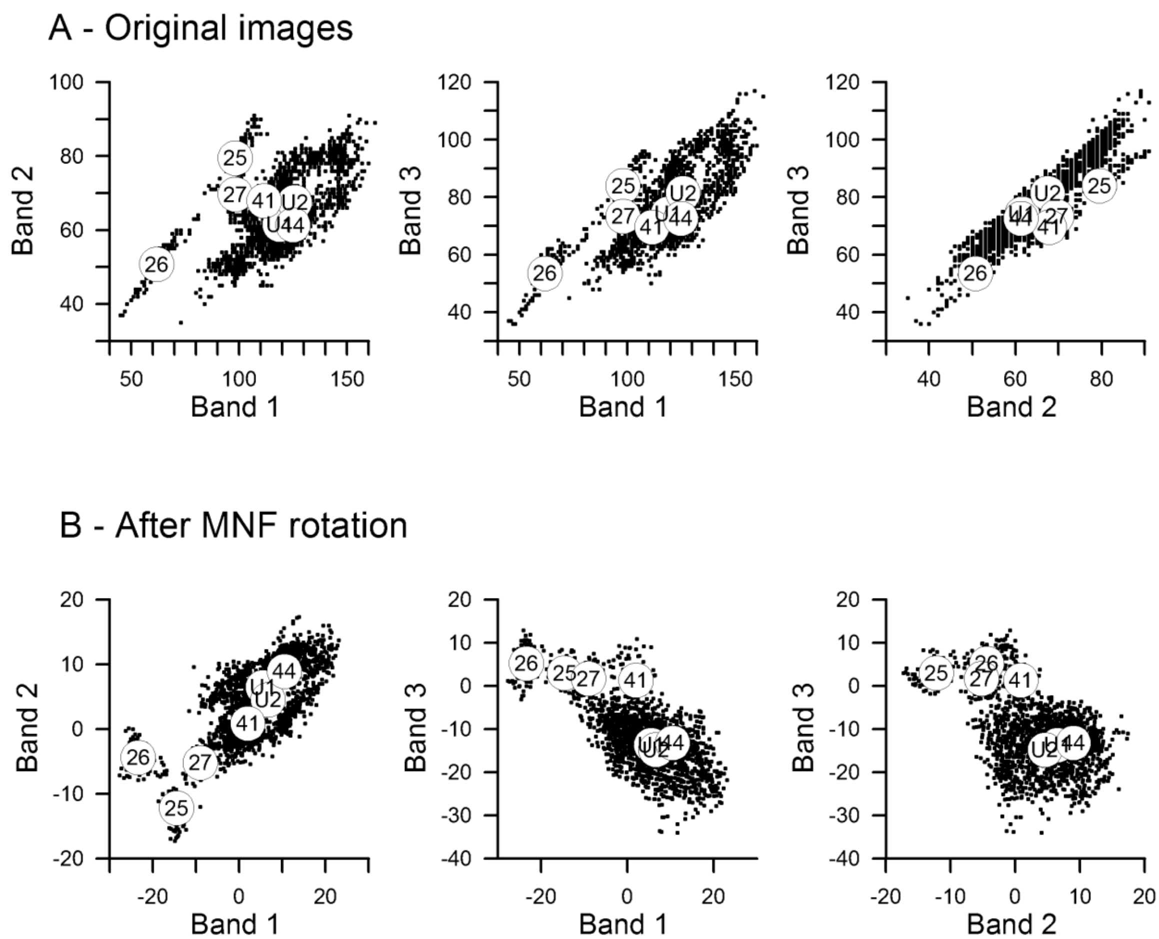

Figure 1-4. Scatterplots of pixels and locations of the means in the classes (endmembers and controls) of the UNB image taken October 31, 2005. *Ulva* spp. endmember (U1); *Ulva* spp. control (U2). The labels of unclassified samples are given in Table 3.

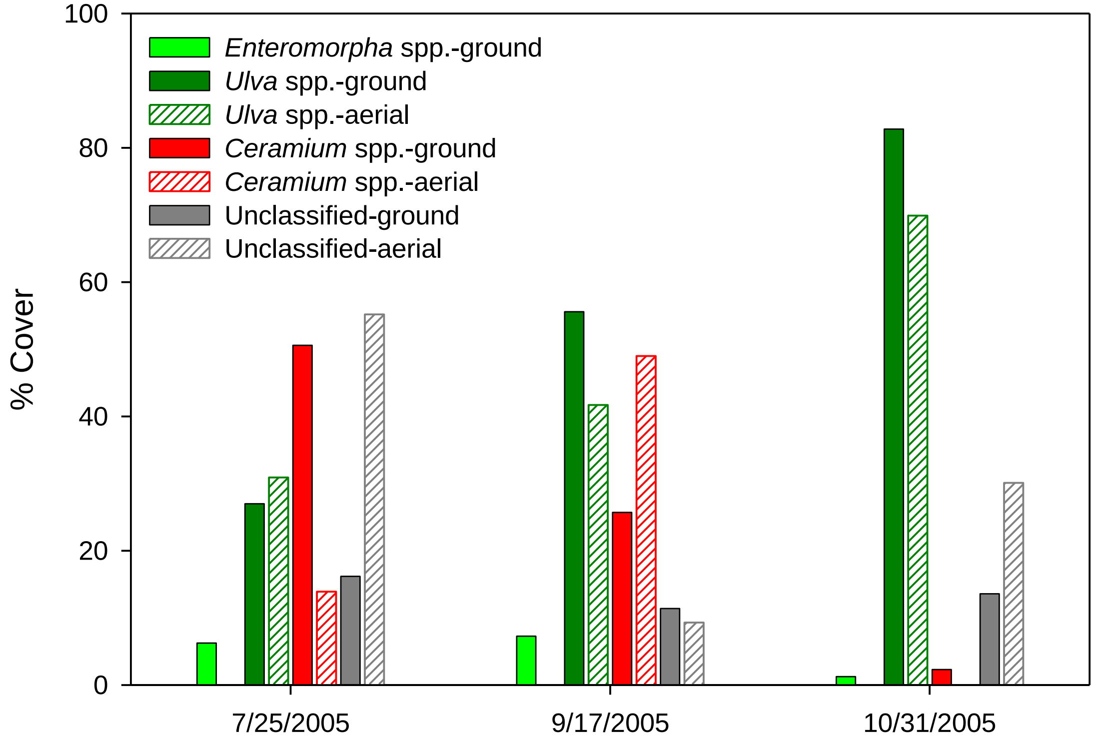

Figure 1-5. Percent cover of macroalgae and unclassified substrate in the exposed intertidal zone of Upper Newport Bay estimated from ground-based data and aerial image analysis.

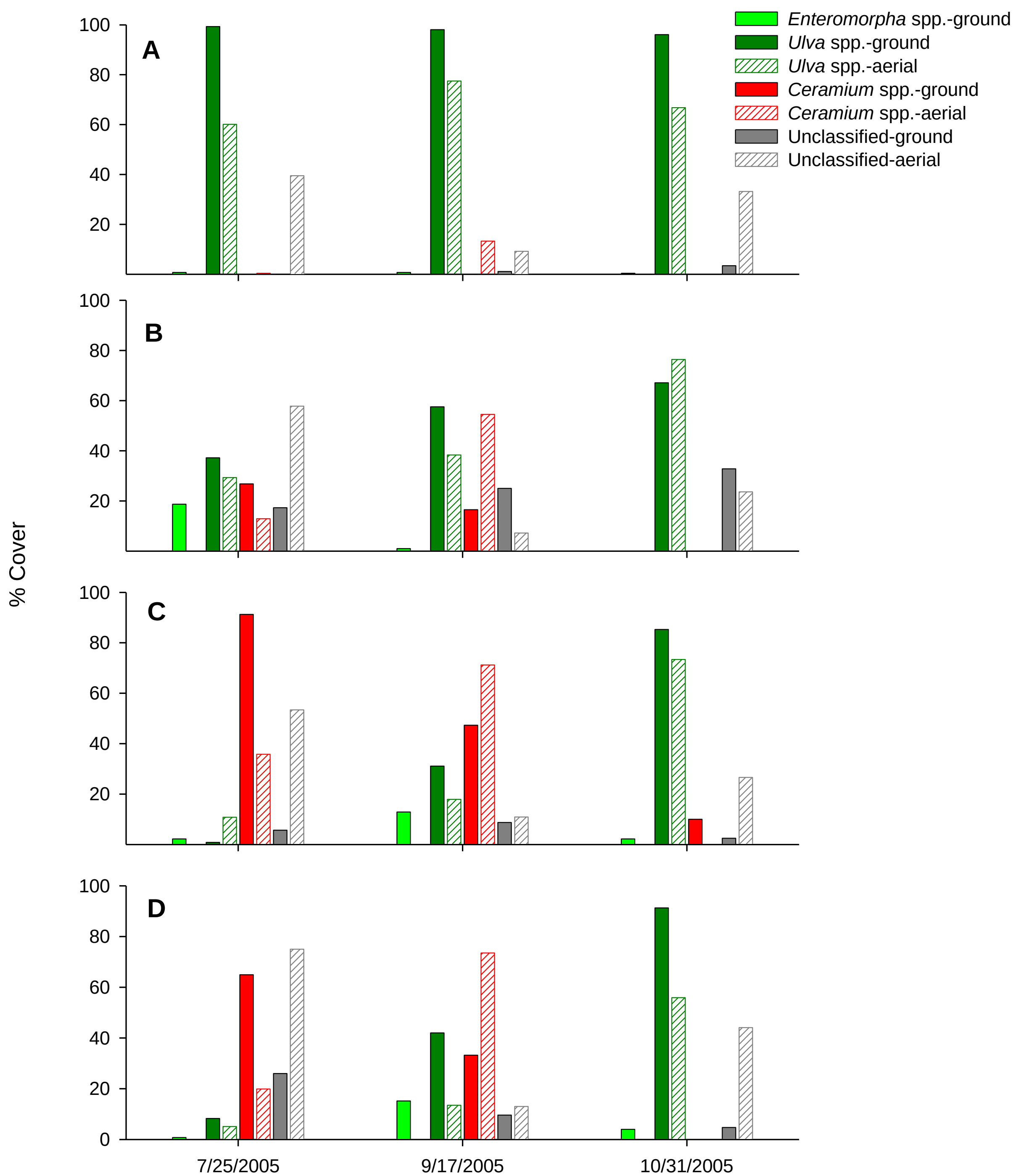

Figure 1-6. Percent cover of macroalgae and unclassified substrate in the exposed intertidal zones of different regions (A, B, C, and D as shown in Figure 1-1) of Upper Newport Bay estimated from ground-based data and aerial image analysis.

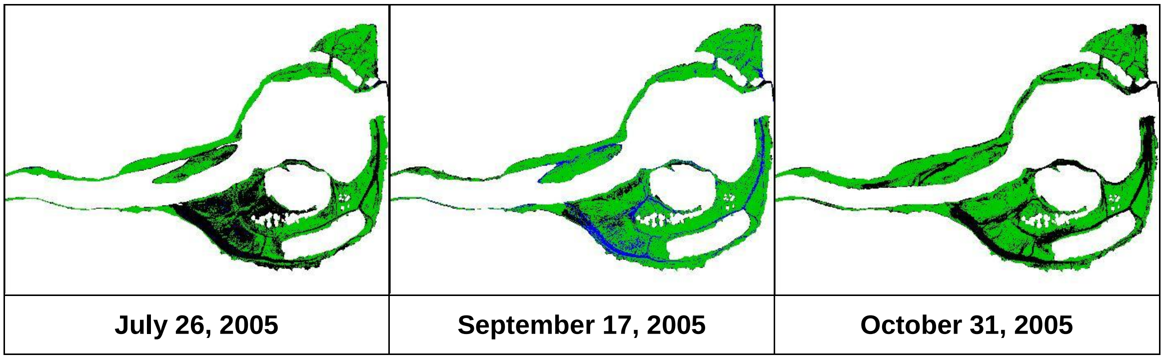

Figure 1-7. Spatial distribution of *Ceramium* spp. (blue), *Ulva* spp. (green) and bare substrate (black) in the intertidal zone of Region A (most upstream).

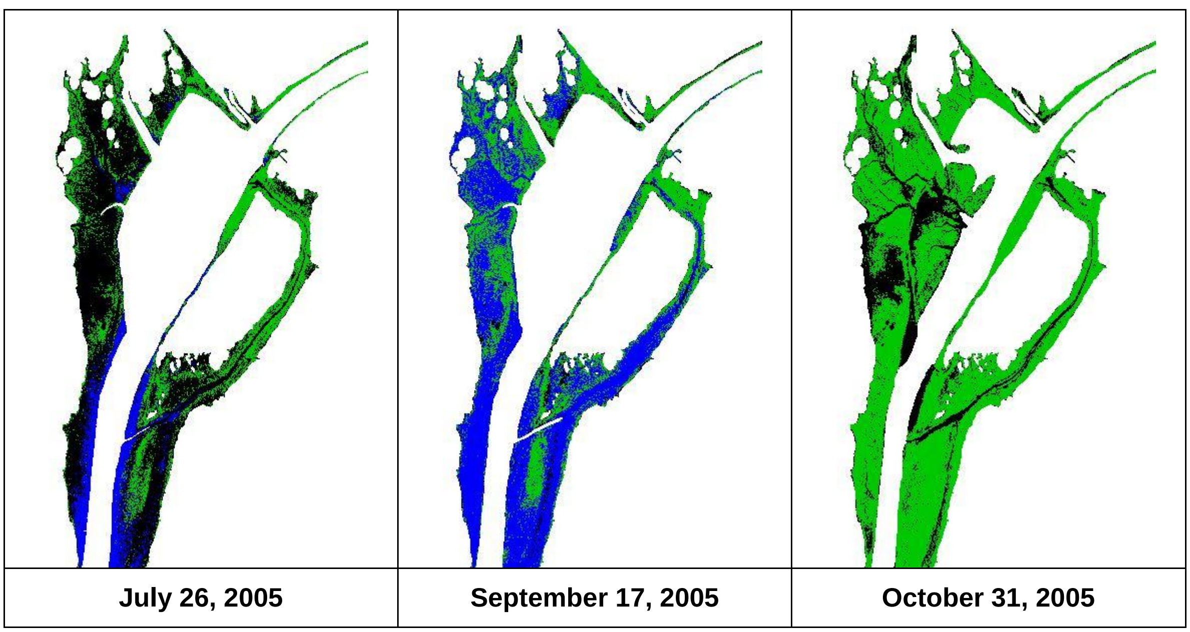

Figure 1-8. Spatial distribution of *Ceramium* spp. (blue), *Ulva* spp. (green) and unclassified substrate (black) in the intertidal zone of Region B.

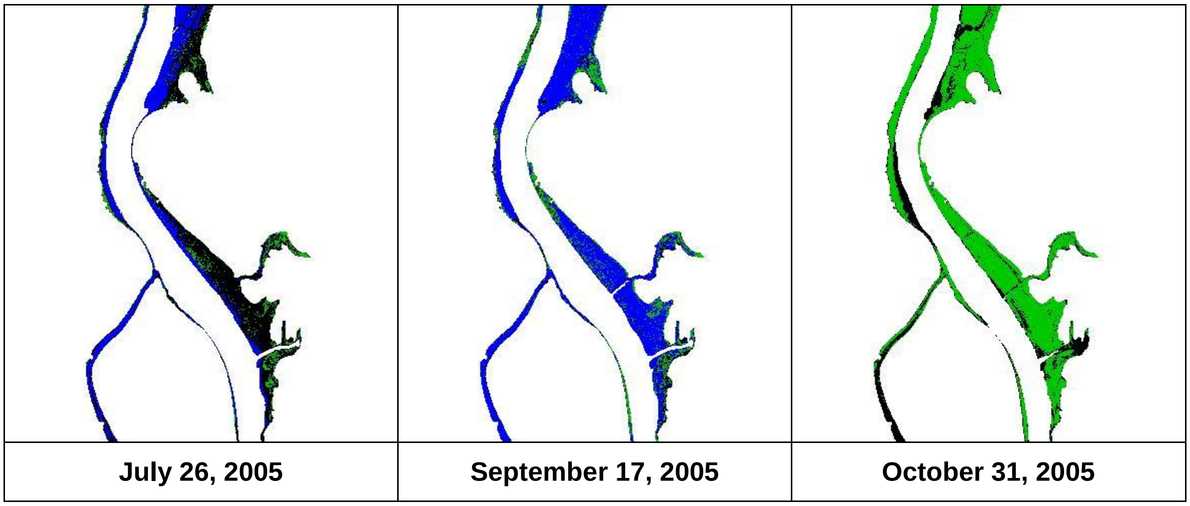

Figure 1-9. Spatial distribution of *Ceramium* spp. (blue), *Ulva* spp. (green) and unclassified substrate (black) in the intertidal zone of Region C.

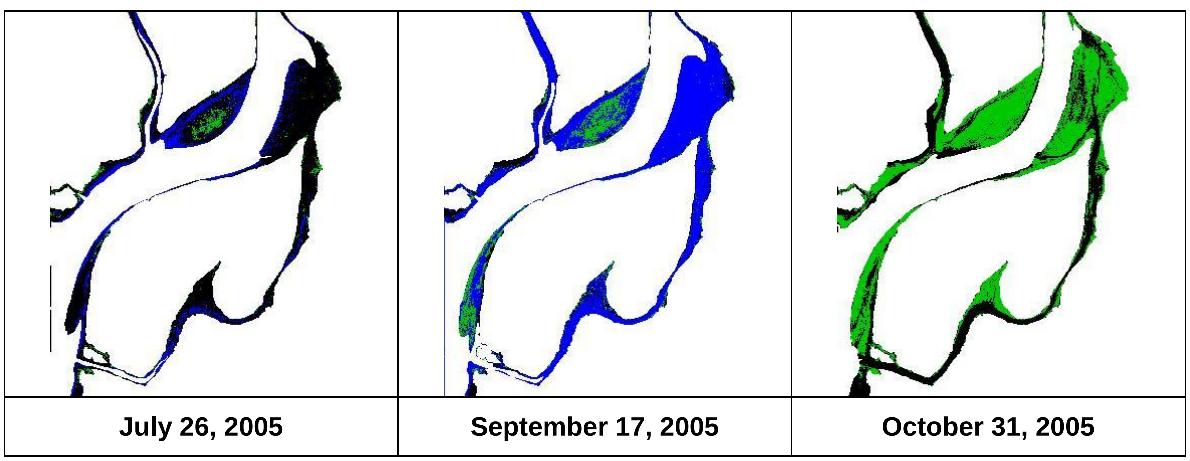

Figure 1-10. Spatial distribution of *Ceramium* spp. (blue), *Ulva* spp. (green) and unclassified substrate (black) in the intertidal zone of Region D (most downstream).

CHAPTER 2. SPATIAL AND TEMPORAL PATTERNS IN DISSOLVED OXYGEN IN RELATION TO MACROALGAL ABUNDANCE

Introduction

In response to concerns over impaired beneficial uses in Upper Newport Bay (UNB), a TMDL for nitrogen (N) and phosphorus (P) for the Newport Bay/San Diego Creek Watershed was adopted in 1998. The TMDL required the development of a regional monitoring program (RMP) for the Newport Bay watershed to assess the attainment of the goals of the Nutrient TMDL. There are several technical challenges that affect the ability to monitor and assess the trophic condition of Newport Bay and thereby to assess progress toward meeting the goals of the TMDL. First, it is difficult to synoptically evaluate the extent of macroalgae in the bay. Second, the spatial and temporal extent of seasonal hypoxia in the bay is unknown. Third, the relationship between macroalgal extent and dissolved oxygen (DO), and hence its utility as an indicator of eutrophication, is unknown. This study attempts to develop approaches and provide information to address these technical challenges. The specific questions this study aims to answer are:

- Where in UNB does hypoxia occur (site, depth)?
- When does the hypoxia occur (time of day, tidal cycle, month) and how long does it last?
- What factors influence the timing of hypoxia?
- Are frequency and intensity of hypoxia related to macroalgal biomass?

The results of this study (i.e., the combined results of the remote sensing and DO time series analysis) will assist the Santa Ana Regional Water Quality Control Board (Regional Board) in the evaluation of DO as a potential water quality management tool for UNB.

The results of this study should be viewed in light of two external factors that led to atypical conditions in UNB during the study period. First, the 2004-2005 season had near-record rainfall. Approximately 28 inches of rain fell during the wet season that preceded initiation of this study. This is more than double the long-term seasonal average and was the second highest rainfall total in the past 100 years. The high rainfall resulted in above average storm flow discharges to UNB during the storm season and increased groundwater discharges, which may have continued during the course of this study.

Second, 2004-2005 had an extended interruption of water quality treatment by the San Joaquin Marsh. The San Joaquin Marsh is a six-pond water treatment wetland covering approximately 45 acres located adjacent to San Diego Creek just above its confluence with UNB. During a typical year, inflow into the San Joaquin Marsh is continuous except for the few days associated with significant rainfall events. However, the San Joaquin Marsh was taken off line from October 25, 2004 to April 12, 2005 to remove sediment from San Diego Creek. The San Joaquin Marsh returned to continuous operation from April 12, 2005 to September 20, 2005, when it was again taken off line until December 8, 2005 to complete sediment removal. Consequently, a significant portion of N- rich San Diego Creek water passed directly into Upper Newport Bay, without undergoing N removal in the San Joaquin Marsh. The conclusions of this study will be discussed in the context of these factors.

Methods

Patterns in DO and other water quality parameters were evaluated from continuous monitoring data to characterize the surface and bottom waters during a period of intense macroalgal production in UNB. The results of this investigation were compared to measures of macroalgal coverage, as reported in Chapter 1 of this report, to determine if a relationship between intertidal macroalgal abundance and the frequency of hypoxic events exists.

Data collection

Water column DO, temperature, conductivity, salinity, depth and pH were continuously monitored in surface and bottom waters at 3 sites in UNB (Figure 2-1). IRWD deployed two YSI 6600 Extended Deployment System (EDS) sondes at each station: one sonde collected data 0.5 m from the surface and the other collected data 0.5 m from the bottom. Data were collected at 30-minute intervals beginning June 15, 2005 and ending December 28, 2005. Sondes were inspected, checked for drift, recalibrated and the data were downloaded on a bi-weekly schedule. Water density (Sigma-T) was calculated from water temperature, salinity and depth using conventional UNESCO International Equation of State, or IES80 (Pond and Pickard, 2000).

Prior to deployment, conductivity, DO and pH sensors on each sonde were calibrated and accuracy was checked by measuring standards. Standards were also measured after deployment to determine instrument drift, as follows:

$$\text{Drift} = \left(\frac{\text{Measured value of standard-known value of standard}}{\text{Known value of standard}}\right) \times 100$$

Quality control analysis

As specified in the quality assurance project plan (QAPP), data quality objectives (DQOs) were established based on drift of individual sensors during each deployment. Drift of 10% or less was acceptable and the data are considered usable without qualification. Data with drift of more than 10% and up to 20% are considered usable but qualified as estimated. If drift was 20% or more, data were rejected and should not be used in any analysis. Data were managed in batches identified by the location and date of deployment. This resulted in a unique identity for each batch of data that is applied to each record in the batch and the associated quality control (QC). All data collected from the sondes and all of the QC data were compiled into an Access database for ultimate posting and/or distribution.

In applying the QC codes of acceptable, estimated or rejected to the records for each parameter, it became apparent that there was a need for an additional DQO in order to assess the overall usability of the data. In several cases, the conductivity sensor drift was acceptable but the values reported were out of the expected range. Salinity in the southern California Bight (SCB) generally does not exceed 33.6 psu (Hickey 1993); therefore, data sets with salinity values greater than 35 psu (to allow for some evaporation and increase in salinity in the estuary) were rejected if other factors, such as large shifts in values coincident with field and laboratory calculations, indicated suspicious data. In other cases, the interdependence of the measurements was considered. For example, during some deployments the conductivity sensor drifted 20.6%, indicating the need to reject the conductivity and salinity data from that deployment. However, the DO sensor did not drift more than 10% and the drift in conductivity probably minimally affected DO measurements (the effect of conductivity on DO measurements is small relative to the effects of temperature). In other deployments, the conductivity sensor drifted 66%, which could be enough to affect the accuracy of DO measurements. To address these circumstances, we instituted another level of QC beyond what is required by the project QAPP. If conductivity drift was <30% and DO QC indicated the DO data were acceptable or estimated on their own, then the DO data were considered useable. If conductivity drift was >30% or if the salinity values were well outside of a reasonable range, then the DO data were rejected. Thus, the DQO for DO data is that the DO sensor drift must not exceed 20% and the conductivity sensor drift must not exceed 30% or conductivity values must fall within a reasonable range.

Analysis of general water quality patterns

Water temperature, salinity and DO data were analyzed for minima, maxima, and median values for each sonde location. Frequency of hypoxia was used to compare the number of hypoxic measurements among sites using the following formula:

$$\text{Frequency of hypoxia} = \left(\frac{\text{\# of hypoxic measurements}}{\text{total \# of acceptable measurements}} \right) \times 100$$

DO values <3.0 mg L^{-1} were considered hypoxic for the purposes of this report; this value was chosen based on a review of scientific literature (Kamer and Stein 2003). However, individual species may have higher DO requirements. A DO threshold of 5.0 mg L^{-1} may be adopted for regulatory purposes to protect designated beneficial uses in UNB. Therefore, at the request of the Regional Board, DO values were compared to a 5.0 mg L^{-1} threshold as well.

Frequency of hypoxia (<3.0 mg L^{-1}) and frequency of measurements <5.0 mg L^{-1} were calculated for the entire data set, each station, surface and bottom waters, and each month. To compare frequency of hypoxic measurements and measurements <5.0 mg L^{-1} between night and day, median sunrise and sunset values for each month of the study were used.

Time series analysis

To transform the data into a consistent dataset, which could be analyzed by the time-series statistical methods, we averaged the measurements obtained during each 1-hour interval (typically two measurements per hour) and attributed them to hourly intervals. The resulting dataset consisted of 24 variables (four parameters: temperature (T), salinity (S), DO and pH, at 6 stations each), and 4701 hourly observations (starting June 15, 2005 at 4 pm an ending at noon December 28, 2005).

Time series analysis requires filling gaps in the data set that occur due to sensor malfunction or data rejection through the QA process. To fill gaps in the dataset, we used the method suggested by Beckers and Rixen to fill data gaps in satellite imagery (Beckers and Rixen, 2003; Alvera-Azcarate et al., 2005). According to this method, missing data were reconstructed on the basis of their correlations with the data measured simultaneously (different parameters measured at the same location and the data measured at other locations). This was achieved by an iterative procedure. At the first step, the missing data in each column (i.e., variable) were replaced by the column mean. Then, at each iteration step, the data matrix was decomposed into factor loadings and a complete set of empirical orthogonal functions (EOF), the number of which was equal to the number of variables (i.e., 24). In accordance with the fundamentals of Principle Component Analysis (PCA) (Priesendorfer, 1988), the leading EOF modes contain maximum of variance, while the trailing EOF modes containing mostly noise. The product of factor loadings and several (significant) leading EOF modes results in a new matrix, whose principle features are similar to the initial data matrix, but with a substantial part of the noise being removed. The missing values from the initial data matrix can then be substituted by the corresponding values from the new matrix; then the resulting matrix is decomposed again and the process is repeated until converged. The number of "significant" EOF modes used in iterative process was estimated from a series of experiments with different number of significant EOF modes (from one to 24). In each experiment, 50 randomly selected points were added to the set of missing data; the mean difference (rms) between these 50 values and the corresponding newly estimated values was used as a measure of accuracy of missing data filling. According to these experiments, 15 EOF modes were used for missing data filling; the remaining 9 contained mostly noise. This allows missing values to be assigned by interpolation with surrounding data points. The result is a continuous data series that is suitable for subsequent time series analysis (i.e., PCA), wavelet transform, and time lagged cross-correlation methods.

Substituted/interpolated data should be analyzed carefully, keeping in mind that they do not represent real measurements. However, these data include the variations of the entire system under study. As such, they can be used for spectral analysis (e.g., wavelet transform), which reveals the frequencies of dominating variations, and cross-correlation analysis, which reveals time-lagged correlations between different variables measured in different locations. When applied to the water chemistry data for UNB, wavelet analysis reveals temporal (or repeating) patterns in the data. Cross-correlation diagrams allows for analysis of physical or chemical factors that may influence (or control) these patterns, including time lags that may exist between controlling factors and response variables, such as DO or salinity.

PCA and time-lagged cross-correlation are conventional statistical methods of time-series analysis, widely used in natural sciences, including meteorology and oceanography (Emery and Thomson, 2001). The analysis based on wavelet transform is a relatively new computational method for signal processing (Torrence and Compo, 1998). The wavelet transformation, in essence, takes a one-dimensional function of time and expands it into a two-dimensional space consisting of time and scale. In wavelet representation, a geophysical signal is decomposed into a sum of elementary building blocks describing its local frequency content. The wavelet analysis provides both scale and time information and allows one to separate and sort different structures on different time scales at different times. The wavelet transform software for MATLAB was produced by Aslak Grinsted (Jevrejeva et al., 2003; Grinsted et al., 2004; Moore et al., 2005).

To analyze the correlations between the measured parameters and the environmental factors, the EOFs and other indices (e.g., an index of water column stratification defined as the difference between salinity in the bottom and surface layers) were averaged to daily values. These parameters were analyzed against the following environmental factors: Mean (daily averaged) tidal level and tidal range (the daily difference between maximum and minimum tidal levels) obtained from tidal model JTides 4.5 (http://vps.arachnoid.com/JTides), freshwater discharge from San Diego Creek (SDC), solar radiation, air temperature, and wind speed measured at California Irrigation Management Information System (CIMIS) station #75 at Irvine (33º41'19"N; 117º43'14"W).

Net Ecosystem Metabolism (NEM) evaluation

To estimate the balance between primary production and respiration (net ecosystem metabolism; NEM) in different UNB regions, we used a conventional method of calculating metabolic rates from diel oxygen curve data (Odum, 1956; Odum and Hoskins, 1958). NEM is a useful indicator of trophic conditions within estuaries, such as whether autotrophic or heterotrophic sources of organic matter dominate. If NEM is positive, the system is autotrophic suggesting that internal production of organic matter dominates, while if NEM is negative, the system is heterotrophic and reliant on external sources of organic matter (Caffrey, 2003). This approach is based on the assumption that oxygen is produced during daytime due to photosynthesis of autotrophic plants (phytoplankton and macroalgae), while ecosystem respiration (i.e., uptake of oxygen by aquatic animals and plants plus biochemical oxidation of autochthonous and allochthonous organic matter) occurs continuously. NEM is calculated by subtracting aerobic respiration rates from photosynthesis rates for all components contained in a defined body of water, taking into account the diffusive oxygen flux (OF), calculated from oxygen saturation (DO%s). The water body is assumed to be homogenous, i.e., having the same metabolic history; in the areas where physical processes such as advection and diffusion dominate over biological processes, metabolic rates may be either underestimated or overestimated (Kemp and Boynton, 1980).

First, the diffusion, or air-sea exchange (ASE), was estimated as follows:

$$\text{ASE} = \left(\frac{1 - (\text{DO\%(t1)} + \text{DO\%(t2)}}{200} \right) \times 0.5 \times \text{dt}$$

where DO%(t1) and DO%(t2) are oxygen saturations (in %) for times t1 and t2 and dt is a time interval (1 hour in this study). We used a constant air-sea exchange coefficient of 0.5 g O_2 m^{-2} hour (Caffrey, 2003), which is a good assumption at wind speeds 0 – 5 m s^{-1} (Russell et al., 2006). Then, OF (g O_2 m^{-2}) was estimated for each hourly time period as OF = (DO(t2) – DO(t1)) x water depth – ASE. To calculate daily NEM, the hourly OF were summed over 24-hour periods starting from midnight. This simple model is based on oxygen production/consumption and diffusion; the model does not take into account horizontal and vertical oxygen heterogeneity and advection resulting from tidal mixing. This NEM model does not account for difference between the environmental conditions in different locations, especially in the surface and bottom layers that resulted in high variability of daily NEM estimations. The obtained NEM variations reflected horizontal and/or vertical transport of oxygen-rich or oxygen-poor water, rather than changes in local oxygen production/consumption balance. To make the resulting NEM values more consistent, they were smoothed using a running 7-day average.

Analysis of relationship between macroalgal abundance and hypoxia

We regressed the frequency of hypoxia in surface and bottom waters, separately, against macroalgal abundance to determine if there is a significant correlation. We used macroalgal abundance, as determined from each of the three the aerial surveys as described in Chapter 1 of this report, in each region of the estuary where the sondes were located. Macroalgal abundance from Region B was not used since there was no sonde in that region. We explored relationships using the combined abundance of *Ceramium* and *Ulva* spp as well as *Ulva* spp. alone. To determine the frequency of hypoxia, we selected time periods surrounding the aerial surveys and calculated the number of DO measurements <3.0 mg L^{-1} as a percentage of the total number of acceptable measurements for that period. We used the 24-hour period surrounding the aerial surveys (from 12:00 a.m. to 11:59 p.m. the day of the survey) and a 7-day period (from 3 days before the survey to 3 days after; Table 2-1).

Results

Summary of water quality QA analysis

There was a total of 1143 deployment days for all six monitoring locations (surface and bottom at 3 sites). There were 903 days when all data (depth, T, S, DO, pH) were useable and 978 days of useable DO data (Table 2-2). Because the sondes operated unattended between deployment and data retrieval, the following external factors likely influenced the quality of the data:

- Periodic luxuriant bryozoan growth on the sensors (potentially causing high variability in the data; Figure 2-2)
- Apparent incidental and short term sensor biofouling (such as an invertebrate resting on the sensor electrodes temporarily)
- Water leaking into the battery case
- Failure of the sonde to record data
- Vandalism

Internal factors, namely instrument drift, and probe failure, can also affect the quality of the data. Data that did not meet the DQOs or were compromised possibly due to the factors listed here, as well as other factors not identified, were considered "not useable".

There were four deployments during which the sondes made measurements but did not log data. Three of these deployments were at S1 Bottom from June 22 to August 2; thus, we do not have bottom water quality data from S1 for a 6-week period (Table 2-3). The sonde at S3 Surface did not log from November 30 to December 14. Data are also missing from S3 Surface from June 23 to July 12 because the sonde was turned upside down; we suspect this was an act of vandalism.

Data were rejected if the drift of the instrument over the deployment period was 20% or greater. This happened numerous times with DO and conductivity/salinity data; all pH data were acceptable. Additionally, salinity data were rejected if values exceeded 35 psu *and* if other factors, such as large shifts in values coincident with field and laboratory calculations, indicated suspicious data. Salinity affects DO measurements; an overestimate of salinity will cause an underestimate of DO. Thus, DO data were also rejected when the conductivity instrument drifted more than 30% or when salinity values were well outside a reasonable range, even if QA of the conductivity sensor indicated no significant drift.

There were several occasions in which persistent, significant drift in conductivity resulted in rejection of data for more than one sequential deployment. At S1 Surface, conductivity drift was unacceptable, resulting in rejection of salinity data, for three deployments spanning August 31 to October 20, a period of over eight weeks. Drift in conductivity of over 40% also resulted in rejection of DO data from this location for the October 5 to October 20 deployment. At S3 Bottom, unacceptable drift in conductivity and salinity values that were above a reasonable range resulted in the rejection of salinity and DO data over two deployments from July 13 to August 2. Lastly, unacceptable drift in the conductivity sensor at S3 Surface persisted over four deployments from June 15 to August 2. The S3 Surface sonde was overturned from June 23 to July 12, as noted above. Conductivity drift from July 13 to August 2 was sufficiently high that DO data were rejected as well. Other instances in which conductivity or DO data were rejected were limited to a single deployment.

Per the QAPP, we established a data completeness goal of 90 % for this project. For the DO data, 86% was successfully collected and deemed acceptable by the QA process. Overall, 79% of the data for all the parameters was successfully collected. Although we did not meet the data completeness goal established in the QAPP, we believe the data set is sufficient to analyze overall spatial and temporal trends. However, data gaps may constrain our analysis of the lower estuary during October (due to rejection of Surface and Bottom data from S1) and the upper estuary in December (due to failure of S3 and rejection of surface data). Furthermore, the ability to analyze relationships between DO and macroalgae is somewhat limited for the July overflight due to failure of the S1 bottom sonde to log. Data completeness is sufficient to analyze DO-macroalgae relationships for the September and October overflights.

Summary of water quality measurements

Individual temperatures ranged from 11.9°C to 27.2°C (Table 2-4). Median temperatures for each station were more closely grouped between 19°C and 23°C. Individual salinity values ranged from 4.1% at the head of UNB to 35.7 ‰ toward the mouth of the estuary (Table 2-5). Median salinities ranged from 23.4% at the head to 31.9% at the mouth. Individual DO measurements ranged from 0 to 23.9 mg L^{-1} (Table 2-6). Median DO ranged from 5.4 to 8.9 mg L^{-1}. The percent of hypoxic values at each station ranged from 1.2% at S2 Surface to 18.3% at S3 Bottom.

Overall, six percent (6%) of the acceptable DO measurements were hypoxic (<3.0 mg L^{-1}), and 25.5% were <5.0 mg L^{-1} (Table 2-7). Hypoxia occurred most frequently at S3 (11.6% of the time) and least frequently at S2 (2.8% of the time). Hypoxia occurred more in bottom waters (10.0%) than surface waters (1.57%). At S3, the bottom waters were hypoxic 18.3% of the time. Hypoxia often occurred more frequently at night than during the day. Hypoxia was most frequent in September (14.5%), followed by October (11.9%). Hypoxia occurred substantially less in each of the other months (<3.0%).

Hypoxia occurred more frequently at night in every month except June (Table 2-8), however the frequency of measurements <5.0 mg L^{-1} was often greater in the daytime than at night. Hypoxia occurred roughly 10% of the time or more during the day and at night in September and October. In other months, hypoxia was far less common (<3.0% of the time) during day and night time.

Specific instances of hypoxia tended to occur during nighttime low tides in the late summer-early fall, particularly during neap tidal series (see Appendices B and C). For example, hypoxic events in August and September were associated with low-low neap tides, which occurred around midnight. Nighttime hypoxia was sometimes accompanied by daytime supersaturation of DO; a good example of this is S3 in October.

Temperature and salinity data indicate that there was vertical stratification at these times as well. Increased freshwater inflow from San Diego Creek may have contributed to vertical stratification. Precipitation in October was closely followed by a decrease in surface salinity throughout UNB.

More detailed observations and plots of the time series of water quality data are provided in Appendix B and C, respectively.

Time series analysis of factors influencing DO dynamics in UNB

Four leading EOF modes explained 75% of variability of the reconstructed data matrix including four parameters (T, S, DO, and pH) at two depths and three locations (Table 2-9). These modes can be associated with natural processes in the UNB estuary. The remaining EOF modes explained minor variations and were not included in subsequent analysis.

The first EOF mode (38% of variability) primarily explained temperature variations in UNB. High factor loadings included temperature measures from all three sondes in the surface and bottom layers (Table 2-9). The temporal component of the first EOF mode was dominated by diurnal (1-day period) and especially semi-diurnal, i.e., tidal (~0.5-day period) frequencies (Figure 2-3B). The time series of EOF-1 showed an increase from the start of observations in June to the end of July and then gradually decreased to the end of December (Figure 2-3A), which agreed with seasonal variations of air and water temperature typical of the southern California climatic zone. The first EOF mode was highly correlated with air temperature (r = 0.732: time lag five days; Table 2-10) and solar radiation (r = 0.720: time lag 9 days; Table 2-10). As such, we speculate that EOF-1 reflects the variations of water temperature over the entire UNB area resulting from seasonal and diurnal oscillations of solar radiation flux and modulated by tidal mixing.

The second EOF mode (14% of variability) was associated with stratification of the head of UNB estuary. High factor loadings included T, S, and DO measured at S3 Surface, near the head of UNB (Table 2-9). All three factor loadings had similar signs, indicating a single source of warm, fresh water (possibly SDC) with a high DO concentration flowing into the surface layer at the head of estuary. The correlation between EOF-2 and SDC discharge was significant (Table 2-10), although the coefficient was small (+0.223) and the time lag was long (17 days). Another factor influencing EOF-2 was daily mean tidal level (-0.263: time lag 10 days; Table 2-10). The negative sign of this correlation indicates that the relative contribution of SDC dry-season discharge (relatively constant at 0.2 to 0.4 $m^3 s^{-1}$) to water column stratification in the head of UNB depends on the mean water level. At low water levels this contribution is greater as compared to periods with higher water levels. The wavelet power spectrum of EOF-2 contained no diurnal or semidiurnal maxima (Figure 2-4B), indicating that diurnal and tidal variations exerted insignificant influence on this process. Significant maxima of wavelet power spectrum had time periods from one week to one month; these periods changed after freshwater discharge peaked in mid-September and mid-October, supporting the idea that EOF-2 is regulated by a quasi-constant discharge from SDC typical to dry season.

The third EOF mode (12% of variability) was associated with the down-estuary (i.e., seaward) surface flow from the head of UNB. High-factor loadings included T measured by S3 and S measured by all three sondes in the surface layer (Table 2-9). The signs of factor loadings indicated that a decrease of surface temperature at the head of estuary coincided with an increase in surface salinity at the same location and a decrease in surface salinity further down-estuary. These coefficients indicated a down-estuary surface flow of fresh water. This process was modulated by diurnal and tidal variations, the peaks of which were most pronounced at wavelet power spectrum (Figure 2-5B) during spring tide periods. The time series of EOF-3 (Figure 2-5A) was positively correlated with SDC discharge (r = 0.369: time lag one day; Table 2-10). Small negative correlations among EOF-3, solar radiation and air temperature looked like a result of correlation between meteorological parameters; typically, decreases in solar radiation and air temperature due to clouds and rainstorms occur simultaneously and stimulate SDC discharge and downstream flow in UNB. A small negative correlation between EOF-2 and tidal range (-0.292: time lag two days), indicating that in UNB intensive tidal mixing hindered rather than enhanced surface flow down-estuary.

The fourth EOF mode (10% of variability) explained vertical mixing in UNB, especially at the head of the estuary. High factor loadings included T and S measured by S3 in the surface layer; DO measured at the same location in the bottom layer; and surface salinity measured by S2 and S1, located mid-estuary and the lower end of UNB, respectively (Table 2-9). As such, high values of EOF-4 indicated vertical mixing (ventilation) at the head of estuary, resulting in a decrease of surface T, increase of surface S and bottom DO, and increase of S lower in the estuary. This process was slightly modulated by diurnal and tidal oscillations evident on wavelet power spectrum (Figure 2-6B); other significant maxima at the wavelet diagram had long-scale (>10-day) periods. Two maxima (four-day and eight-day periods) on the wavelet diagram occurred in mid-September and mid-October after dramatic increases in SDC discharge. EOF-4 was negatively correlated with SDC discharge (-0.411: time lag one day; Table 2-10), which increased stratification and decreased vertical mixing. Also, EOF-4 was positively correlated with wind speed (+0.246: time lag one day), which stimulated water column mixing. Positive correlations between EOF-4 and solar radiation and air temperature may appear counterintuitive at first. However, wind speed was positively correlated with solar radiation and air temperature (r = +0.303 and +0.409, respectively) with zero time lag. This was probably due to the Santa Ana winds, which are typical of southern California in the fall, and they bring warm and dry air from inland to the coast. The correlation between EOF-4 and tidal range was positive (+0.275), indicating the role of tidal flows in water column mixing; however, the time lag (16 days) appeared too long to consider tidal range as a factor directly correlated with the intensity of vertical mixing in UNB.

Correlation between stratification and DO concentrations

To analyze correlations between DO, stratification, and environmental factors, we averaged the time series of T, S, Sigma T, and DO over daily (24-hour) intervals. The goal of this averaging was to remove diurnal and tidal variability, which exerted a substantial influence on physical and chemical parameters in UNB (e.g., diurnal and tidal variations played a dominant role in almost all processes, represented by EOF modes). When two variables oscillate with similar frequencies (e.g., diurnal or tidal), the correlation coefficient between them is high and significant, indicating nothing but a similarity of dominating frequencies. Daily averaged time series avoid this problem.

We focused on water column stratification as a major factor regulating DO concentration because pronounced stratification increases bottom water residence time and prevents its ventilation, which can result in hypoxia. Stratification can be measured by the difference between surface and bottom temperature and/or salinity. Also, high correlations with zero time lag between T, S, Sigma T, and DO in the surface and bottom layers indicate low stratification; in contrast, low or negative correlations indicate that the water column is stratified and the surface and bottom layers fluctuate independently.

Correlations between surface and bottom T and S showed that in UNB haline stratification dominates over thermal. In the head of estuary (S3), all correlations were lower and the time lags were longer than in other regions, indicating more pronounced stratification of water column. In the mid-estuary and at the mouth of estuary, T in the surface and bottom layers were highly correlated with zero time lag (Table 2-11), indicating that thermal stratification was low. At the head of estuary (S3), the correlation between surface and bottom T was much lower (+0.34) with time lag of six days bottom T leading surface. The correlation between surface and bottom S was low at the UNB mouth and negative at the head and mid-estuary, indicating pronounced haline stratification. For S, all three diagrams of correlation vs. time lag had two maxima, indicating that periodic (possibly tidal) oscillations played an important role in salinity variations. The correlation between Sigma-T in the surface and bottom layers decreased from the mouth to the head of the estuary. At the mouth of estuary, the correlation between DO in the surface and bottom layers was high (+0.51) with a one-day time lag between surface and bottom. In the mid-estuary and at the head of estuary, the correlations between DO in the surface and bottom layers were insignificant, indicating high stratification.

We used the difference between surface and bottom Sigma-T (Figure 2-7) as an index of water column stratification. The stratification index was highest in the upstream UNB region and gradually decreased downstream, resulting from freshwater discharge from SDC and vertical mixing in the downstream regions.

Stratification was negatively correlated with bottom water DO at S1 and S2 (Table 2-12), supporting the hypothesis that stratification plays an important role in development of bottom water hypoxia. At the head of estuary, however, the correlation between bottom water DO and stratification was much lower. Stratification in that region was higher and bottom water DO concentrations lower than in other regions; as such, minor variations of stratification had no influence on DO in the bottom layer. Bottom hypoxia developed under the influence of factors other than just an increase in stratification. These factors were possibly related to SDC freshwater discharge and macroalgae growth, both contributing organic matter to this UNB region, which can oxidize in the bottom layer, resulting in hypoxia.

Stratification and surface layer DO were negatively correlated at S1 and S2; however, the correlation was very low (-0.199). At S3, the correlation between stratification and surface DO was positive. We speculate that high stratification retains oxygen produced in the upper layer (by macroalgae and phytoplankton photosynthesis) and prevents it from being used for oxidation of organic matter in the bottom layer. This process is more typical of the stratified upper region of UNB than the lower portions of the estuary.

Environmental factors, including SDC discharge, daily mean water level, tidal range, and to a lesser extent, wind, modulated stratification in UNB (Table 2-13). SDC discharge was positively correlated with the stratification at S1 and S2, but not at S3 where stratification was always high and minor variations were seemingly modulated by other factors. Wind stress could increase mixing and decrease stratification; however, this influence was weak and observed at S1 only. Positive correlation between the mean tidal level and stratification could be explained by enhanced inflow of saline ocean water to UNB bottom layer during high tides; this process was more pronounced at S1 than S3. Different signs of correlation between the tidal range and stratification illustrate different effects of horizontal and vertical tidal mixing. At S1 and S2, vertical tidal mixing exerted negative influence on haline stratification, while at S3 horizontal tidal mixing dominated over vertical. From this we conclude that strong spring tides transported a larger volume of saline ocean water to that area, but in the absence of vertical mixing this water remained in the bottom layer enhancing haline stratification.

Hypoxic events in UNB

Lowest DO concentrations were observed in the bottom layer at S3, near the mouth of SDC (Figure 2-8A), and seemingly resulted from a combination of three environmental factors: increased freshwater discharge (Figure 2-9B), low solar radiation (Figure 2-9A), and sluggish bottom water ventilation due to neap tidal phase (Figure 2-9C). Freshwater discharge from SDC contains organic matter, which oxidizes in bottom waters, causing a decrease in DO. This organic matter originates in the watershed and the emergent salt marshes of UNB. After rainstorms these marshes are often flooded, and the water that drains off them is rich in organic matter. Freshwater input also enhances haline stratification and prevents ventilation of bottom waters. Low solar radiation results in decrease of photosynthesis of phytoplankton and macroalgae and lower oxygen production. At the same time, insolation of water surface can enhance thermal stratification and decrease bottom ventilation. Tides are a principle source of ventilation of near-bottom water in estuaries; as such, during the period of neap tides the residence time of bottom water increases, which can result in hypoxia.

DO concentrations in the surface layer were typically higher than in the bottom layer, especially in the head of estuary. In the following analysis, we consider hypoxia events defined as daily average DO $\leq$3 mg L^{-1}or any hourly average (during the 24-hour period) $\leq$ 1 mg L^{-1}. The first hypoxic event (DO about 2.5 mg L^{-1}) was observed in mid-June, during the start of our observations. During that time, freshwater discharge from SDC was low, but extremely low solar radiation coincided with neap tides and could have been a trigger. The second hypoxic event was observed only at S1 Surface (bottom data were absent) in the beginning of July (Julian day 184. During this period, the daily average DO was about 3.2 mg L^{-1}, but there were several instances where the hourly average DO was less than 1 mg L^{-1}). This hypoxia cannot be explained by neap tide or low insolation. However, during that period, stratification in mid-estuary was higher than normal (Figure 2-7); as such, insufficient ventilation of the bottom layer may have produced hypoxic waters, which were transported down-estuary and detected by S1. However, this observation should be viewed with caution. Although all data for S1 in the month of July met our established data quality objectives and QC standards, the sonde experienced severe biofouling that may have affected the validity of the measurements. Furthermore the DO pattern observed at this sonde was not consistent with the observations of S1 and S2.

The next hypoxic event occurred at the head of UNB in mid-August (Julian day 227; DO was about 3.1 mg L^{-1}). The cause of this hypoxia was similar to the hypoxia event in mid-June. This event coincided with low solar radiation (Figure 2-9A) and the end of neap tide period (Figure 2-9C).

The most pronounced period of hypoxia started on September 20 (Julian day 263). Over two weeks, the daily average DO concentrations measured at S3 Bottom were <1 mg L^{-1}. DO concentrations also decreased at S1 and S2 (Figure 2-8A). This hypoxic event may have resulted from an increase in freshwater discharge from SDC (by 1.7 $m^3\ s^{-1}$) associated with a rain event (Figure 2-9B). Precipitation was relatively insignificant (0.1 cm during the two-day rainstorm starting September 19), but on September 20 the San Joaquin Marsh water treatment wetland facility stopped operations and untreated water flowed directly to UNB. Subsequent settling and oxidation of organic matter associated with the freshwater discharge, may have been a contributing factor in the hypoxia, which propagated down the estuary as a result of horizontal tidal mixing. At the same time, the upper layer at the head of the estuary was not affected by hypoxia because freshwater discharge and salinity gradient (20 - 25 psu in the upper layer vs. 30 - 33 psu near the bottom) stratified the water column and isolated the surface layer from the bottom.

Before the beginning of hypoxia in the head of UNB bottom layer, two brief periods of hypoxia were measured at S1 surface, both coinciding with nighttime ebb tides on September 15 and 16. The hypoxia may have originated upstream of S1 as a result of strong thermal and haline stratification, which were observed in mid-September. Strong ebb tidal flow transported these waters to the surface and down-estuary. This short hypoxia event is similar to more pronounced hypoxia observed in early July, which was also related to strong stratification rather than low insolation, SDC discharge or neap tide.

The next hypoxic event occurred in mid-October (starting from Julian Day 290) and followed heavy rain, when precipitation was 1.5 cm and freshwater discharge from SDC exceeded 3.3 m^3 /s (vs. normal 0.2 - 0.4 $m^3\ s^{-1}$). Hypoxia affected bottom waters at all three monitoring locations and the surface waters at S1 and S2. Surface waters at S3 were isolated from the bottom layer by haline stratification and DO concentration was even higher than normal, which could be explained by active algal growth stimulated by discharged nutrients. Solar radiation was low, which seemingly decreased photosynthesis in the bottom layer and enhanced hypoxia. Tidal range was high, resulting in intensive horizontal mixing and propagation of hypoxic waters lower in the estuary, where they affected both surface and bottom layers.

The last hypoxic event at S3 was observed in mid-November (Julian Day 314). This event slightly affected both surface and bottom layers at S1 and S2 (Figure 2-8). This hypoxia was preceded by a small rainstorm (precipitation 0.5 cm; SDC discharge 0.86 $m^3\ s^{-1}$) and accompanied by several days of low solar radiation (Figure 2-9A). Tidal range was high (Figure 2-9C), stimulating horizontal mixing and propagation of hypoxic waters down-estuary.

For all aforementioned events, hypoxic waters were transported down-estuary over several tidal cycles as a result of ebb tidal flows. During the development of hypoxia resulting from freshwater discharge on September 20, DO concentration at S3 Surface was significantly higher than in the bottom layer and lower in the estuary (Figure 2-10). Both ebb tides on September 20 transported this oxygen-rich water downstream, resulting in an increase in DO at S2 surface. However, the next ebb tide on the morning of September 21 transported hypoxic waters to the surface waters at S1 and S2, and bottom water DO at these locations also decreased (from 5 to 3 mg L^{-1}). The next ebb tide on the evening of September 21 resulted in a decrease in DO in the bottom waters at all three monitoring locations and in the upper layer of S1. At the same time, this ebb tidal flow transported oxygen-rich surface water from the head of the estuary to S2. The next ebb tide on the morning of September 22 transported hypoxic water to S2 surface and S1. During the next several days, DO was >3 mg L^{-1} in surface waters while hypoxia continued in the bottom layer.

NEM

The NEM indices averaged over the period of observations (June - October) characterized UNB as a heterotrophic estuary. Oxygen production exceeded respiration only in the upper layer at S3 (Table 2-14). At the same time, respiration significantly exceeded primary production in the bottom layer at S3. Downstream, NEM indices decreased in the upper layer and increased near the bottom, which can be explained by more intensive vertical mixing, more intensive near-bottom photosynthesis resulting from higher water transparency, and the fact that allochthonous organic matter discharged from SDC was accumulated and oxidized at the head of the estuary.

Hypoxia events can be detected in the NEM timeseries as low values (Figure 2-11). Also, periods of high DO generally correspond to high NEM. For example, at S3 surface, the NEM index was especially high in August and during the first half of September, which can be associated with macroalgal bloom observed during that period.

The analysis of correlations between NEM index and environmental factors resulted in higher and more obvious correlations (Table 2-15), as compared with DO. Solar radiation was significantly correlated with NEM almost everywhere. NEM (i.e., oxygen production) in the bottom layer was better correlated with solar radiation as compared with the surface layer. The water column in UNB is characterized by high water turbidity and shallow euphotic depth; as such, photosynthesis in the bottom layer (at 3 - 5 m depth) is more sensitive to the incident solar radiation. SDC discharge and haline stratification were negatively correlated with NEM index in both surface and bottom layers; high variability in time lags indicates a high level of spatial heterogeneity. Positive correlation between NEM and air temperature may appear counterintuitive. Indeed, we expect that higher temperatures increase organic matter oxidation rate and decrease DO. Also, higher temperatures decrease oxygen solubility and its flux from the atmosphere. However, the seasonal trend in air temperature could be correlated with the seasonal trend in primary production, because the maximum biomass of macroalgae in UNB was observed during the warmest period (i.e., August - September) and decreased later.

Relationship between macroalgal abundance and hypoxia

Only one hypoxic measurement was recorded in the analysis of the 24-hour periods surrounding the aerial surveys, (October 31, S3 bottom: 2.08 mg L^{-1}). Thus, there was no relationship between macroalgal abundance and hypoxia when using the 24-hour data sets.

Analysis of the 7-day time period data resulted in more hypoxic measurements, allowing us to investigate correlations between macroalgal abundance and frequency of hypoxia (Figure 2-12). When the combined abundance of *Ceramium* and *Ulva* spp. was used, macroalgal abundance explained <1% of the variability in bottom water hypoxia and 14% of the variability in surface water hypoxia. Neither of these relationships was significant (i.e., no significant regression). When analyzed separately, *Ulva* spp. abundance explained 1% of the variability in surface hypoxia and 37% of the variability in bottom water hypoxia. Although the frequency of hypoxia was generally correlated with *Ulva* spp. abundance, the regressions were not significant and this relationship should be used with caution.

When a DO threshold of 5.0 mg L^{-1} was used, macroalgal biomass better explained the variability in the frequency of measurements <5.0 mg L^{-1}. The combined abundance of *Ceramium* and *Ulva* spp. explained roughly 50% of the variability in the frequency of DO values <5.0 mg L^{-1} in surface and bottom waters (Figure 2-13). The relationship was significant for surface water DO ($p = 0.037$) but not for bottom water DO ($p = 0.069$). *Ulva* spp. alone explained 75% of the variability in the frequency of DO measurements <5.0 mg L^{-1} in bottom waters and 57% of the variability in the frequency of DO measurements <5.0 mg L^{-1} in surface waters. The relationship was significant for both bottom ($p = 0.012$) and surface waters ($p = 0.029$).

Discussion

Hypoxia (DO <3 mg L^{-1}) occurred in less than 6% of all measurements in UNB during the period of our study, and almost always in the bottom layer. At S1 and S2 surface layer DO was seldom much higher than 5 mg L^{-1}. Only at S3 was surface water DO significantly higher, typically ranging from 7 - 10 mg L^{-1}. This may have been due to the greater abundance of macroalgae at the head of UNB, where the intertidal zone is larger, than further down-estuary. Oxygen produced by photosynthesis at the head of UNB enriches surface waters; organic matter sinks to the bottom layer where oxygen is consumed. Downstream, in the mid-estuary and mouth regions, vertical mixing decreases the difference between DO concentrations in surface and bottom layers.

Hypoxia in UNB generally occurred during nighttime low tides in the late summer-early fall, particularly during neap tidal series. In several instances, differences in temperature and salinity between surface and bottom waters indicated that strong vertical stratification was also a factor. Stratification of the water column is promoted by warmer, fresher, less dense water overlying colder, saltier, denser bottom water. These two layers of water can remain separate with very little mixing occurring between them, which increases the residence time of the bottom water. When this happens, oxygen in the bottom layer cannot be replenished. If there is significant benthic oxygen demand due to biological or biogeochemical processes, then bottom water hypoxia will occur. We saw evidence of vertical stratification during neap tide series, which exchange less water between the estuary and the ocean, resulting in less mixing and less flushing. This process may be amplified by freshwater input from the watershed which has the combined effect of increasing stratification and increasing organic matter, which in turn increases oxygen demand. Strong winds and strong tides can break up the stratification and initiate mixing between the two layers, thus replenishing oxygen in the bottom waters. Without sufficient mixing to replenish oxygen in bottom waters, hypoxia is more likely to occur.

In UNB, the spatial distribution of DO production/consumption is extremely heterogeneous, resulting in ebb tidal flows transporting downstream waters that are sometimes rich and sometimes poor in oxygen. As such, a combination of horizontal and vertical tidal mixing results in complex and unpredictable pattern of DO dynamics. As an example, most, but not all hypoxia events started in the head of the estuary. A pronounced hypoxia in the beginning of July was observed only in the UNB mouth region, where during nighttime ebb tides DO dropped to almost zero. A similar pattern was observed in mid-September, a few days before the start of most pronounced hypoxia resulting from SDC discharge. These observations illustrate that UNB does not fit the primitive scheme of tide-oxygen dynamics. In small well-mixed estuaries, DO increases by afternoon and decreases by dawn (D'Avanzo and Kremer, 1994). Diurnal DO variability is often modulated by tides, when high tide covering intertidal zone with macroalgae during daytime enriches water with oxygen and during nighttime decreases DO concentration.

In the late summer-early fall when hypoxia was most frequent, macroalgae were most abundant. Macroalgae produce oxygen via photosynthesis but as aerobic organisms, they also consume oxygen during respiration. When they consume more oxygen than they produce, they create a net oxygen sink. At night, no light is available for photosynthesis so no oxygen is produced, only consumed. In many instances hypoxia occurred in UNB during nighttime low tides, when oxygen consumption by macroalgae would have been maximal and the volume of water in the bay would have been lowest. AHA (1998) also found that hypoxia occurred during nighttime low tides when macroalgae were abundant. Hypoxia can also occur during the day when thick mats shade themselves, preventing light from reaching the lower layers. This can also create net consumption of oxygen. Macroalgae initially proliferated in July and reached maximum abundance in September 2005, the month when hypoxia was most frequent. Time series analysis suggests that hypoxia may be more frequent once *Ulva* spp. reaches a certain threshold of abundance, but additional sampling would be required to establish such a relationship. In November and December 2005, macroalgae were sparse (RDMD data) and hypoxia was infrequent. It is unknown the degree to which hypoxia would occur in the absence of algae.

Macroalgae also create an oxygen demand when they senesce and sink to the bottom where they are decomposed by bacteria. We observed a time lag between macroalgal proliferation and onset of hypoxia. Though significant macroalgal production occurred in UNB in June and July, significant hypoxia was not seen until September. Sufficient macroalgae may have to grow, senesce, and sink to the bottom before bottom water hypoxia is widespread. Lastly, the contribution of organic material from macroalgae to sediments would increase sediment oxygen demand through both biological and oxygen-consuming biogeochemical pathways. Thus, macroalgae seen growing in the intertidal zone in June and July may contribute to bottom water hypoxia several months later.

Results of this study support an emerging conceptual model of the relationship between macroalgae, stratification, and hypoxia in UNB (Figure 2-14). The macroalgal blooms that probably create a significant bottom water oxygen demand and the vertical stratification of the water column that increases the residence time of bottom waters and decreases ventilation are each controlled by a series of other physical and chemical factors. A secondary mechanism may be an increases susceptibility to hypoxia created by higher primary productivity and respiration associated with macroalgal blooms. Under such condtions, a minor external influence (e.g., low solar radiation, neap tide, turbid water, enhanced stratification, etc.) could result in dramatic disturbance of oxygen balance and hypoxia. Macroalgal blooms are controlled in part by nutrient availability (from the watershed, estuarine sediments, or ground water), available light, and temperature. Vertical stratification is likely controlled by solar heating, freshwater discharge (and subsequent surface flow down the estuary), and vertical mixing due to the wind and tides. Stratification of the water column is promoted by warmer, fresher, less dense water overlying colder, saltier, denser bottom water. These two layers of water can remain separate with very little mixing occurring between them, which increases the residence time of the bottom water. When this happens, oxygen in the bottom layer cannot be replenished. If there is significant benthic oxygen demand due to biological or biogeochemical processes, then bottom water hypoxia will occur. We saw evidence of vertical stratification during neap tide series, which exchange less water between the estuary and the ocean, resulting in less mixing and less flushing. Strong winds and strong tides can break up the stratification and initiate mixing between the two layers, thus replenishing oxygen in the bottom waters.

The supersaturation of DO seen following rainfall in September and October could have resulted from a number of factors or a combination thereof. One mechanism could have been increased primary productivity by either macroalgae or phytoplankton following the rain. Alternatively, vertical stratification due to temperature and salinity gradients could have isolated the surface layer, allowing the O_2 produced by primary producers to accumulate rather than be distributed throughout a well-mixed water column. Lastly, well-oxygenated water coming into UNB from the watershed could have been responsible.

The results of this study are consistent with results of earlier studies of UNB. The Irvine Ranch Water District (IRWD) collected data from 1997 - 2000, and 7.7% of values were <3.0 mg L^{-1} (Kamer and Stein, 2003). The IRWD data also indicated these general patterns:

- hypoxia occurred more frequently at the head of the estuary compared to down stream;
- hypoxia was more common at night than during the day;
- hypoxia occurred more frequently in the summer months than during winter months;
- hypoxia was associated with low tides; and
- DO decreased with increasing depth.

Other southern California estuaries show similar patterns of the onset of hypoxia with reduced tidal flushing. Kennison et al. (2003) measured DO in five southern California estuaries from November 2001 through December 2002: UNB, Carpinteria Salt Marsh Reserve, Mugu Lagoon, Los Penasquitos Lagoon (LPL), and Tijuana River Estuary (TJ). No values <3 mg L^{-1} were measured though macroalgae were abundant at times. However, all DO measurements were taken during the daytime in well-flushed intertidal areas and would not reflect hypoxic events that occurred at nighttime or in deeper waters. In Mission Bay, data collected July to October

2002 showed hypoxia only at a sampling station at the back of Mission Bay near Tecolote Creek that has reduced circulation during periods of low tidal flushing.

Data from the Pacific Estuarine Research Laboratory (PERL) indicate that LPL, which has some macroalgae, experiences hypoxia when the mouth of the lagoon closes and tidal circulation ceases (see Kamer and Stein, 2003 for review). When this happens, bottom water DO is often <1.0 mg L^{-1}. When the lagoon is open, hypoxia occurs on a diel cycle; during low tides after dark in the summer, DO is often <3.0 mg L^{-1}. Daily tidal flushing temporarily alleviates the hypoxia. LPL also experiences vertical stratification, leading to DO concentrations that decrease with depth. Average DO concentrations in LPL are generally higher in winter than summer.

PERL also found that DO is also often higher in the winter than the summer in TJ, and regular tidal flushing prevents persistent hypoxia (see Kamer and Stein, 2003 for review). Hypoxia occurs during neap tide series when tidal flushing is reduced. Tidal flushing relieves daily hypoxia, which occurs primarily during nighttime low tides in summer months when macroalgae are abundant. In 1998, a large *Ulva* spp. bloom was associated with hypoxia.

It is unknown how the frequency of hypoxia in UNB, from 6% of the time overall to 18% of the time at the bottom of S3, compares to other estuaries in southern California because comparable time series data is unavailable. In other larger, deeper systems associated with the east coast of the United States (e.g., Long Island Sound and Chesapeake Bay) and the Dead Zone in the Gulf of Mexico, hypoxia is frequent and persistent, lasting months at a time without relief, and often attributed to eutrophication. In comparison to these systems, hypoxia in UNB was relatively limited, rarely lasting more than two weeks at a time and often occurring only at night with relief during the day. There are a number of reasons why hypoxia in UNB may be less frequent than in other eutrophic systems. UNB is a relatively shallow system (average depth <1 m) compared to eutrophic systems with chronic hypoxia problems (e.g., Chesapeake Bay; Officer et al., 1984). The average depth in Chesapeake Bay is 6.5 m and the bottom water residence time is seven months; whereas, in UNB residence time is seven days. The tidal range in the Chesapeake Bay is 1 m, and in UNB it is 2 m. Thus, the shallowness of UNB makes it susceptible to wind driven mixing in combination with the tidal range, which increases flushing (Geyer, 1997). These mechanisms probably reduce the occurrence of hypoxia, even when both primary productivity and respiration are high.

References

Alvera-Azcarate, A., Barth, A., Rixen, M., Beckers, J.-M., 2005. Reconstruction of incomplete oceanographic data sets using empirical orthogonal functions: application to the Adriatic Sea surface temperature. Ocean Modelling 9, 325-346.

Beckers, J.-M., Rixen, M., 2003. EOF calculations and data filling from incomplete oceanographic datasets. Journal of Atmospheric and Oceanic Technology 20, 1839-1856.

Breitburg, D.L., Loher, T., Pacey, C.A., Gerstein, A., 1997. Varying effects of low dissolved oxygen on trophic interactions in an estuarine food web. Ecological Monographs 67, 489-507.

Caffrey, J.M., 2003. Production, respiration and net ecosystem metabolism in U.S. estuaries. Environmental Monitoring and Assessment 81, 207-219.

Caffrey, J.M., 2004. Factors controlling net ecosystem metabolism in US estuaries. Estuaries 27, 90-101.

D'Avanzo, C., Kremer, J.N., 1994. Diel oxygen dynamics and anoxic events in an eutrophic estuary of Waquoit Bay, Massachusetts. Estuaries 17, 131-139.

Diaz, R.J., Rosenberg, R., 1995. Marine benthic hypoxia: A review of its ecological effects and the behavioural responses of benthic macrofauna. Oceanography and Marine Biology 33.

Emery, W.J., Thomson, R.E., 2001. Data analysis methods in physical oceanography. Elsevier, Amsterdam, 638 pp.

Geyer, W.R., 1997. Influence of wind on dynamics and flushing of shallow estuaries. Estuarine, Coastal and Shelf Science 44, 713-722.

Grinsted, A., Moore, J.C., Jevrejeva, S., 2004. Application of the cross wavelet transform and wavelet coherence to geophysical time series. Nonlinear Processes in Geophysics 11, 561-566.

Hickey, B.M., 1993. Physical oceanography. In: Dailey, M.D., Reish, D.J., Anderson, J.W., (Eds.), Ecology of the Southern California Bight. University of California Press, Berkeley, pp. 19-70.

Jevrejeva, S., Moore, J.C., Grinsted, A., 2003. Influence of the Arctic Oscillation and El-Nino-Southern Oscillation (ENSO) on ice conditions in the Baltic Sea: The wavelet approach. Journal of Geophysical Research 108, 4677.

Kamer, K. and E. Stein. 2003. *Dissolved Oxygen Concentration as a Potential Indicator of Water Quality in Newport Bay: A Review of Scientific Research, Historical Data, and Criteria Development*. Southern California Coastal Water Research Project Technical Report #411.

Kemp, W.M., Boynton, W.R., 1980. Influence of biological and physical processes on dissolved oxygen dynamics in an estuarine system: Implications for measurement of community metabolism. Estuarine and Coastal Marine Science 11, 407-431.

Kennison, R.L., Kamer, K., Fong, P., 2003. Nutrient dynamics and macroalgal blooms: a comparison of five southern California estuaries. Southern California Coastal Water Research Project 416. Westminster, CA, 113 pp.

Moore, J.C., Grinsted, A., Jevrejeva, S., 2005. New tools for analyzing time series relationships and trends. EOS 86, 226,232.

Odum, H.T., 1956. Primary production in flowing waters. Limnology and Oceanography 1, 102-117.

Odum, H.T., Hoskins, C.M., 1958. Comparative studies on the metabolism of marine waters. Publications of the Institute of Marine Science, Texas 5, 16-46.

Officer, C.B., Biggs, R.B., Taft, J.L., Cronin, L.E., Tyler, M.A., Boynton, W.R., 1984. Chesapeake Bay anoxia - origin, development, and significance. Science 223, 22-27.

Pond, S., Pickard, G.L., 2000. Introductory dynamical oceanography. 2nd ed. Butterworth-Heinemann, Oxford, 329 pp

Priesendorfer, R.W., 1988. Principle Component Analysis in Meteorology and Oceanography. Elsevier Science, New York, NY, 425 pp.

Russell, M.J., Montagna, P.A., Kalke, R.D., 2006. The effect of freshwater inflow on net ecosystem metabolism in Lavaca Bay, Texas. Estuarine, Coastal and Shelf Science 68, 231-244.

Torrence, C., Compo, G.P., 1998. A practical guide to wavelet analysis. Bulletin of the American Meteorological Society 79, 61-78.

Valiela I., McClelland J., Hauxwell J., Behr P.J., Hersh D., Foreman K. 1997. Macroalgal blooms in shallow estuaries: Controls and ecophysiological and ecosystem consequences . Limnology and Oceanography 42(5): 1105-1118.

Table 2-1. Time-frames used in regressions of hypoxia frequency per 24 hours or 7 days versus macroalgal coverage.

Date of aerial survey	24 hours		7 days	
	Start 12:00 a.m.	**End 11:59 p.m.**	**Start 12:00 a.m.**	**End 11:59 p.m.**
July 26, 2005	July 26, 2005	July 26, 2005	July 23, 2005	July 29, 2005
September 17 2005	September 17, 2005	September 17, 2005	September 14, 2005	September 20, 2005
October 31 2005	October 31, 2005	October 31, 2005	October 28, 2005	November 3, 2005

Table 2-2. Summary of sonde data for total deployment days, data rejected or not recorded, and percent completeness.

Site	Total deployment days	Days data rejected or not recorded (DO)	Days data rejected not recorded (all parameters)	Days useable data recorded (DO)	Days useable data recorded (all parameters)	% completeness (DO)	% completeness (all parameters)
S1B	192	55	55	137	137	71	71
S1S	190	28	62	162	128	85	67
S2B	191	0	14	191	177	100	93
S2S	190	14	14	176	176	93	93
S3B	190	20	20	170	170	89	89
S3S	190	48	75	142	115	75	61
TOTAL	**1143**	**165**	**240**	**978**	**903**	**86**	**79**

B = Bottom
S = Surface

Table 2-3. Gaps in dissolved oxygen data.

Location		Calendar Days with Missing/Rejected Dissolved Oxygen Data						
		JUN	JUL	AUG	SEP	OCT	NOV	DEC
S1	Surface			17 - 30		5 - 20		
	Bottom	22 - 30	1 - 31	1 - 2		5 - 20		
S2	Surface							14 - 28
	Bottom							
S3	Surface	23 - 30	1-31	1-2			30	1-28
	Bottom		13-31	1-2				

Table 2-4. Summary of temperature data.

Location		Temperature (°C)			
		n	Min	Max	Median
S1	Top	9102	12.47	26.97	20.66
	Bottom	7271	13.77	25.14	19.18
S2	Top	9104	11.93	27.79	21.50
	Bottom	9106	13.74	26.50	20.35
S3	Top	7506	12.40	29.60	22.71
	Bottom	9069	14.27	27.23	21.55

n = # of measuments

Table 2-5. Summary of salinity data.

Location		Salinity (%)			
		n	Min	Max	Median
S1	Top	5496	19.67	35.14	31.44
	Bottom	6552	24.92	35.70	31.86
S2	Top	7854	11.18	35.83	29.47
	Bottom	6863	25.33	34.48	31.63
S3	Top	5512	4.14	32.02	23.38
	Bottom	8106	17.84	35.88	31.81

n = # of measuments

Table 2-6. Summary of dissolved oxygen data. n = # of measurements; D = Day; N = Night.

		Dissolved Oxygen (mg L^{-1})					
Location		n	Min	Max	Median	% <3 mg L^{-1}	% <5 mg L^{-1}
S1	Top	7213	0.06 (D)	13.55	6.48	1.16	9.64
	Bottom	6552	1.26 (N)	11.71	6.10	7.83	21.52
S2	Top	7934	0.11 (D)	16.67	6.83	1.15	11.10
	Bottom	9106	0.52 (N)	11.11	5.38	4.20	33.93
S3	Top	5872	0.08 (N)	23.50	8.94	2.30	9.79
	Bottom	8106	0.00 (N)	23.99	4.61	18.30	58.78

Table 2-7. Frequency of hypoxic measurements (<3.0 mg L^{-1}) for each station, surface versus bottom waters, and each month of the study. Frequency of measurements (<5.0 mg L^{-1}) also shown.

Data set	**# of acceptable measurements DO**	**# of measurements <3.0** mg L^{-1}	**% of measurements <3.0** mg L^{-1}	**# of measurements <5.0** mg L^{-1}	**% of measurements <5.0** mg L^{-1}
Total	44783	2688	6.00	11416	25.49
S1	13765	597	4.33	2105	15.29
S2	17040	473	2.78	3971	23.30
S3	13978	1618	11.58	5340	38.20
Surface	21019	310	1.47	2151	10.23
Bottom	23764	2378	10.00	9265	38.99
June	3608	92	2.55	893	24.75
July	3808	64	1.68	827	21.72
August	7558	115	1.52	868	11.48
September	8636	1253	14.51	2730	31.61
October	7189	853	11.87	3333	46.36
November	8078	206	2.55	1039	12.86
December	5906	105	1.78	1726	29.22

able 2-8. Frequency of hypoxia (<3.0 mg L^{-1}) and dissolved oxygen measurements (<5.0 mg L^{-1}) during the day and at night for each month of the study.

Month	Median sunrise	Median sunset	Time shift	Daytime					Nighttime				
				n	# <3.0	% <3.0	# <5.0	% <5.0	n	# <3.0	% <3.0	# <5.0	% <5.0
June	5:43 a.m.	8:03 p.m.	DST	2157	60	2.78	522	24.20	1451	32	2.21	371	25.57
July	5:52 a.m.	8:01 p.m.	DST	2227	27	1.21	546	24.52	1581	37	2.34	281	17.77
Aug	6:14 a.m.	7:37 p.m.	DST	4258	58	1.36	507	11.91	3300	57	1.73	361	10.94
Sept	6:36 a.m.	6:58 p.m.	DST	4316	572	13.25	1387	32.14	4320	681	15.76	1343	31.09
Oct	6:58 a.m.	6:21 p.m.	DST	3441	343	9.97	1669	48.50	3748	510	13.61	1664	44.40
Nov	6:25 a.m.	4:52 p.m.	PST	3535	73	2.07	537	15.19	4543	133	2.93	502	11.05
Dec	6:48 a.m.	4:48 p.m.	PST	2448	16	0.65	703	28.72	3458	89	2.57	1023	29.58

Table 2-9. Factor loadings[*] of six leading EOF modes. The loadings for which absolute value exceeds 0.2 are shaded.

Parameter	Sonde	EOF-1 39.0% (39.0%)	EOF-2 14.1% (53.1%)	EOF-3 11.9% (65.0%)	EOF-4 9.9% (74.9%)
		Percent of variability			
T	S1B	0.3382	-0.0838	-0.0658	0.0555
T	S1T	0.4408	-0.0852	-0.0510	0.0950
T	S2B	0.3953	-0.0672	-0.0776	0.0799
T	S2T	0.4816	-0.0925	-0.0697	0.1349
T	S3B	0.4316	-0.0582	-0.0604	0.1306
T	S3T	0.2003	0.4514	-0.3796	-0.6932
S	S1B	-0.0546	-0.0090	-0.1277	0.0820
S	S1T	-0.1260	0.1102	-0.4209	0.3917
S	S2B	0.0116	0.0096	-0.0594	0.0416
S	S2T	-0.1882	0.1319	-0.6105	0.2745
S	S3B	-0.0340	0.0056	-0.1962	0.0431
S	S3T	0.1071	0.7979	0.4059	0.3785
DO	S1B	-0.0238	0.1045	-0.0830	0.0665
DO	S1T	0.0244	0.0239	-0.0398	-0.0007
DO	S2B	0.0125	0.0476	-0.1476	0.0672
DO	S2T	0.0217	0.0165	-0.0250	0.0477
DO	S3B	0.0245	0.0362	-0.1441	0.2088
DO	S3T	0.0838	0.2881	-0.0948	-0.1686
PH	S1B	0.0006	0.0003	-0.0071	0.0025
PH	S1T	0.0061	0.0070	-0.0068	-0.0038
PH	S2B	0.0018	0.0054	-0.0132	0.0061
PH	S2T	0.0088	0.0059	-0.0070	0.0018
PH	S3B	0.0054	0.0084	-0.0215	0.0081
PH	S3T	0.0144	0.0237	-0.0067	-0.0069

[*]Factor loadings are coefficients representing the contributions of measured parameters to the resulting EOF modes.

Table 2-10. Maximum time-lagged correlations* between daily averaged EOFs and environmental factors. The time lag (days; d) of maximum correlation is given in parenthesis; positive time lags indicate that environmental factor is leading the EOF.

	EOF1	EOF2	EOF3	EOF4
SDC discharge	-	+0.223 (+17 d)	+0.369 (+1 d)	-0.411 (+1)
Solar Radiation	+0.720 (+9 d)	-	-0.286 (+1 d)	+0.343 (+1 d)
Air temperature	+0.732 (+5 d)	-	-0.219 (+8 d)	+0.288 (+1 d)
Wind speed	-	-	-	+0.246 (+1 d)
Tide range	-	-	-0.292 (+2 d)	+0.275 (+16 d)
Mean tide	+0.535 (0 d)	-0.263 (+10 d)	-	-

*Maximum time-lagged correlations were estimated calculating correlation coefficients with time lags from –30 to +30 days. The maximum of the resulting coefficients and its time lag are presented in the table.

Table 2-11. Maximum time-lagged correlations between T, S, Sigma-T, and DO in the surface and bottom layers at three stations. The time lag (days; d) of maximum correlation is given in parenthesis; positive time lags indicate that surface time series is leading the bottom time series.

Sonde #	T	S	Sigma-T	DO
1	+0.962 (0 d)	+0.261 (0 d) +0.396 (+12 d)	+0.477 (0 d) +0.504 (+12 d)	+0.514 (+1 d)
2	+0.983 (0 d)	-0.253 (-3 d) -0.236 (+4 d)	+0.324 (0 d) +0.337 (+10 d)	-
3	+0.340 (-6 d)	-0.243 (-14 d) -0.230 (+1 d)	-0.233 (+1 d)	-

Table 2-12. Maximum time-lagged correlations between DO concentration and stratification defined as the difference between surface and bottom S. The time lag (days; d) of maximum correlation is given in parenthesis; positive time lags indicate that stratification is leading DO.

	DO Surface	DO Bottom
S1	-0.199 (+9 d)	-0.434 (+4d)
S2	-0.372 (+7 d)	-0.354 (+4 d)
S3	+0.526 (+11 d)	-0.159 (0 d)

Table 2-13. Maximum time-lagged correlations between environmental factors and stratification defined as the difference between surface and bottom Sigma-T. The time lag (days; d) of maximum correlation is given in parenthesis; positive time lags indicate that environmental factor is leading the stratification index.

	SDC discharge	Wind	Tide range	Mean tide
S1	+0.279 (+1 d)	-0.198 (+1 d)	-0.211 (+2 d)	+0.432 (-1 d)
S2	+0.418 (+ 1 d)	-	-0.304 (+1 d)	+0.392 (-1 d)
S3	-	-0.165 (+1 d)	+0.191 (+3 d)	-

Table 2-14. NEM (mean ± standard error-0.05; g O_2 m^{-2} d^{-1}) averaged over the observed period (June - December 2005) in different UNB locations.

	Surface	Bottom
Sonde #1 (downstream)	-1.95 ± 0.94	-2.64 ± 0.61
Sonde #2 (midstream)	-0.83 ± 1.07	-3.70 ± 0.61
Sonde #3 (upstream)	2.13 ± 2.02	-4.47 ± 0.82

Table 2-15. Maximum time-lagged correlations between NEM (smoothed with a 7-day window) in surface and bottom layers of different UNB locations and environmental factors. The time lag (days; d) of maximum correlation is given in parenthesis; positive time lags indicate that environmental factor is leading the EOF.

	S1 (lower estuary)		**S2 (mid estuary)**		**S3 (head of estuary)**	
	Surface	Bottom	Surface	Bottom	Surface	Bottom
Solar radiation	+0.155 (+2 d)	+0.372 (0 d)	-	+0.303 (+1 d)	+0.312 (+8 d)	+0.399 (+3 d)
Air temperature	+0.257 (+3 d)	+0.210 (0 d)	+0.244 (+3 d)	+0.359 (0 d)	+0.269 (+7 d)	+0.345 (+7 d)
SDC discharge	-0.210 (-1 d)	-0.292 (+1 d)	-0.188 (-2 d)	-0.252 (+3 d)	-0.283 (-4 d)	-0.201 (+2 d)
Density stratification	-0.291 (+20 d)	-0.510 (+21 d)	-0.358 (+5 d)	-0.299 (-2 d)	-0.282 (+28 d)	-0.263 (+7 d)
Haline stratification	-0.307 (+20 d)	-0.541 (+20 d)	-0.358 (+5 d)	-0.317 (-2 d)	-0.270 (+28 d)	-0.253 (+7 d)

Figure 2-1. Location of water quality measurements in Upper Newport Bay. Two sondes were deployed at each station, one 0.5 m from the surface and one 0.5 m off the bottom.

Figure 2-2. Sonde retrieved from UNB showing biofouling of sensors by bryozoans and other biota.

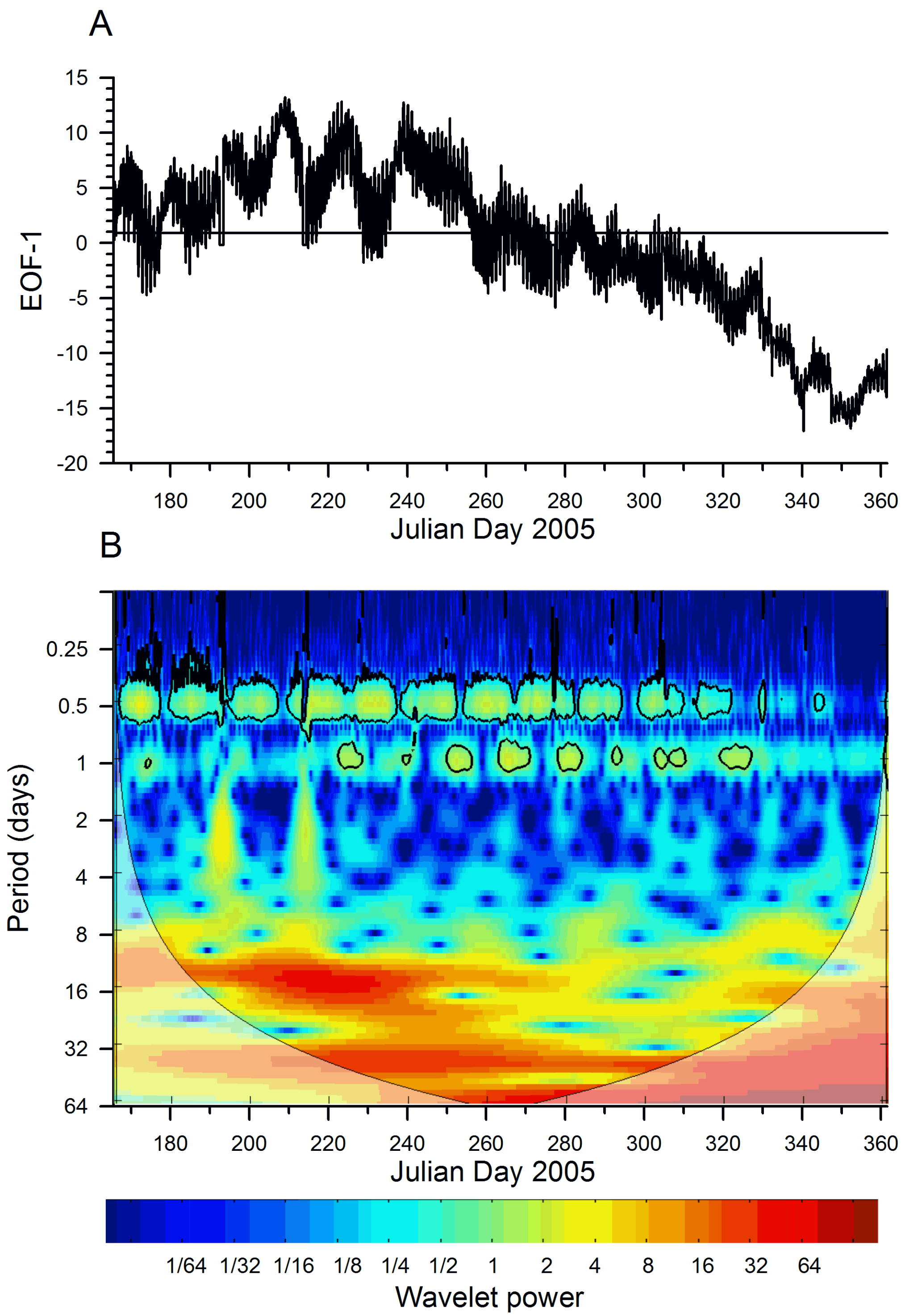

Figure 2-3. Time series (A) and wavelet transform power (B) of EOF-1 (39.0% of total variability).

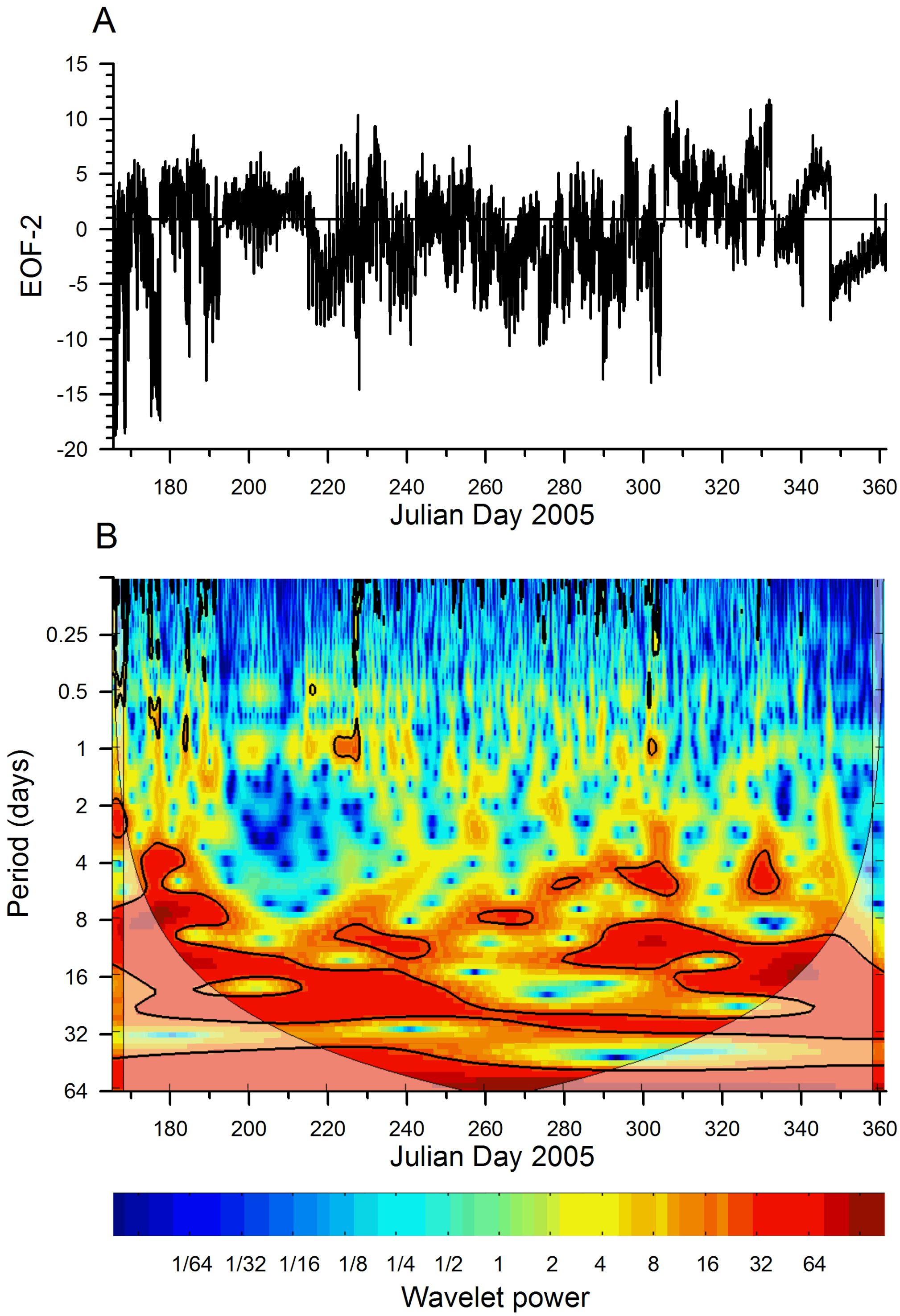

Figure 2-4. Time series (A) and wavelet transform power (B) of EOF-2 (14.1% of total variability).

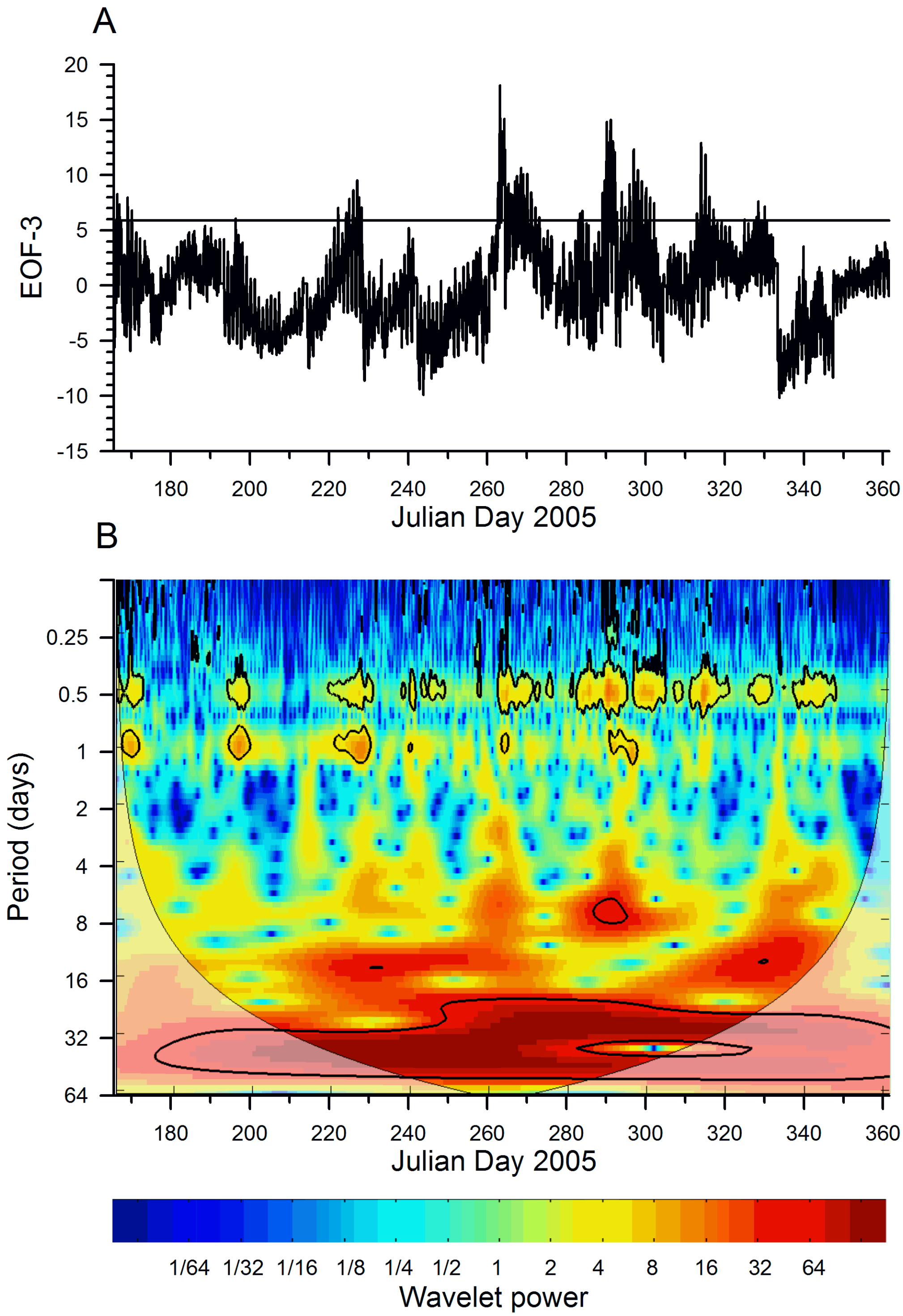

Figure 2-5. Time series (A) and wavelet transform power (B) of EOF-3 (11.9% of total variability).

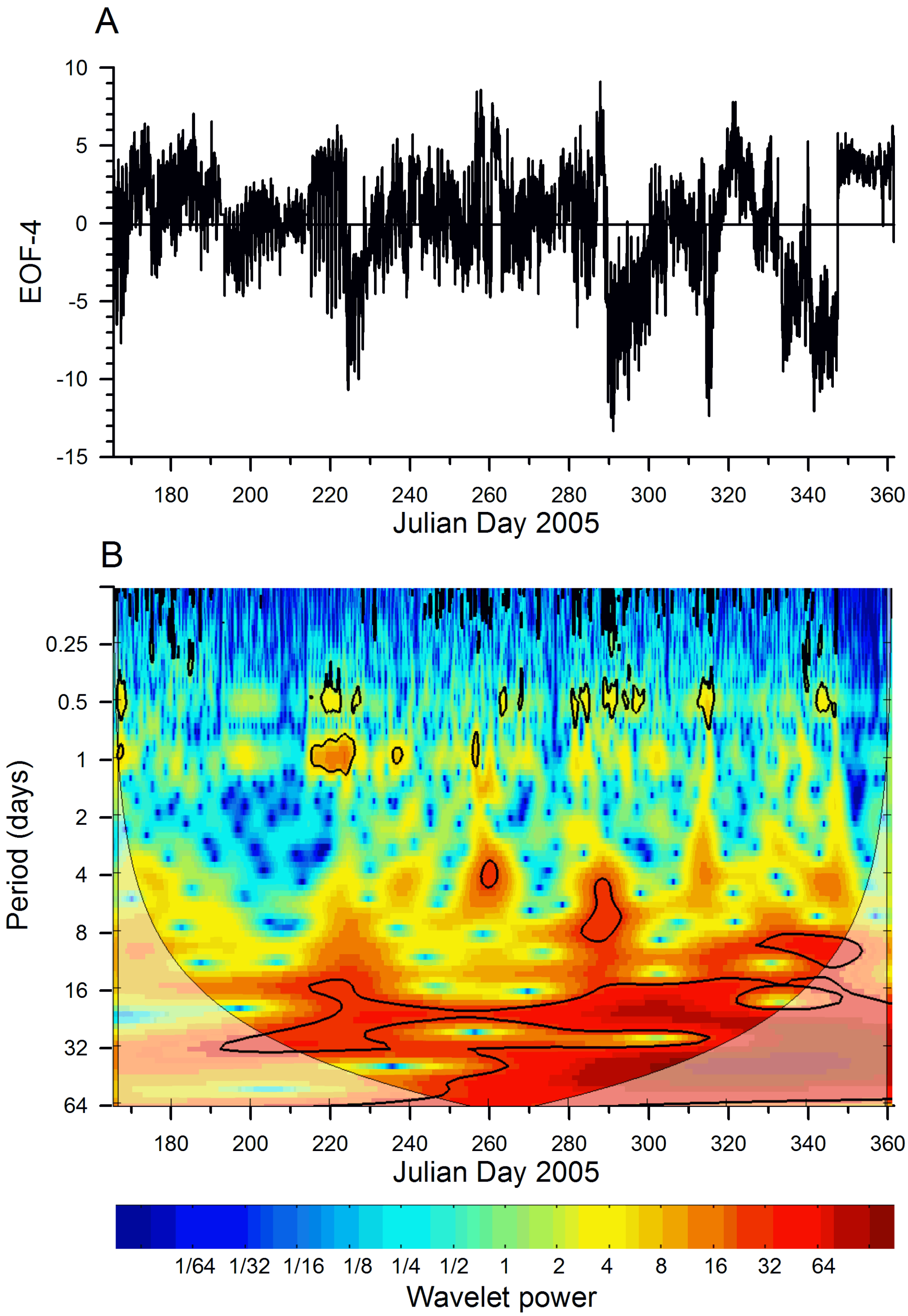

Figure 2-6. Time series (A) and wavelet transform power (B) of EOF-4 (9.9% of total variability).

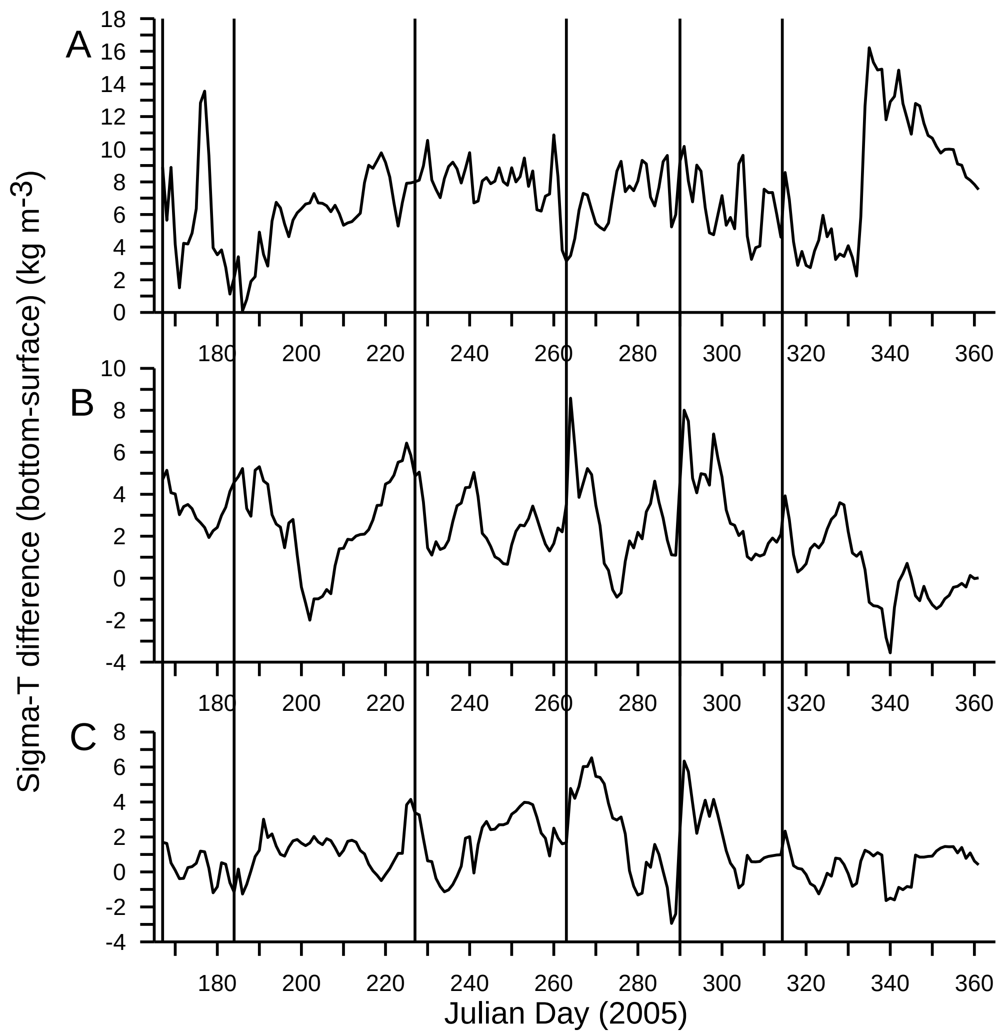

Figure 2-7. Stratification index (the difference between bottom and surface Sigma-T) in three locations in UNB. S3 is at the head of estuary (A); S2 is mid-estuary (B); S1 is at the lower end of Upper Newport Bay (C) Vertical lines indicate the beginning of six hypoxia events (see Figure 2-8). See Figure 2-1 for S1, S2, and S3 locations.

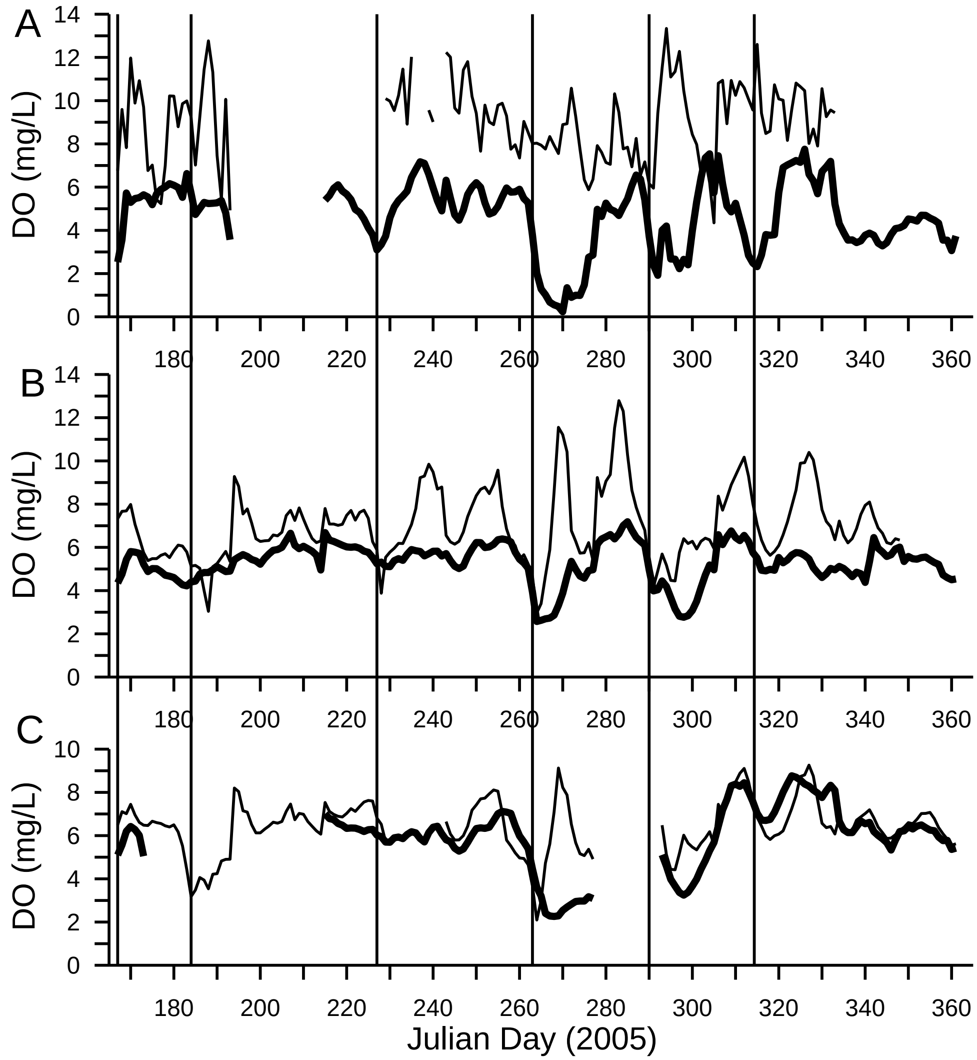

Figure 2-8. Dissolved oxygen (DO) in surface (thin line) and bottom (thick line) layers of three locations in UNB. S3 is at the head of estuary (A); S2 is mid-estuary (B); S1 is at the lower end of Upper Newport Bay (C). Vertical lines indicate the beginning of six hypoxia events. See Figure 2-1 for S1, S2, and S3 locations.

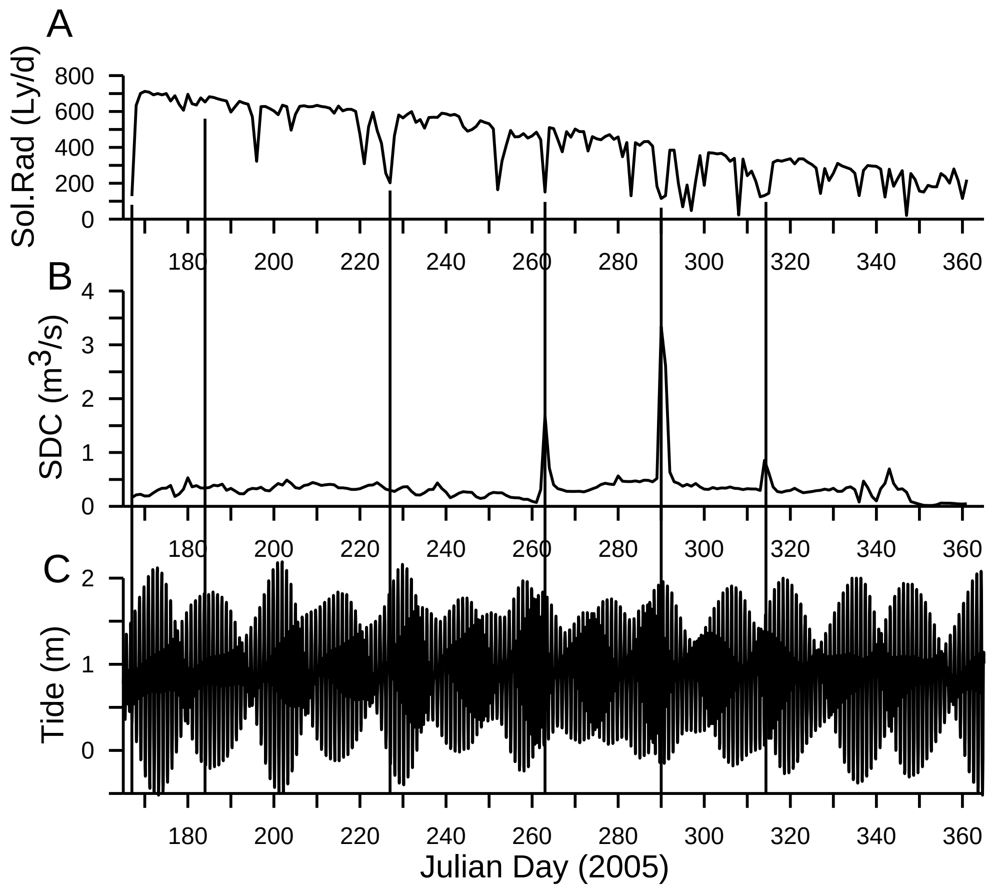

Figure 2-9. Solar radiation (A), San Diego Creek discharge (B), and tides (C) in UNB during June - December 2005. Vertical lines indicate the beginning of six hypoxia events (see Figure 2-8). See Figure 2-1 for S1, S2, and S3 locations.

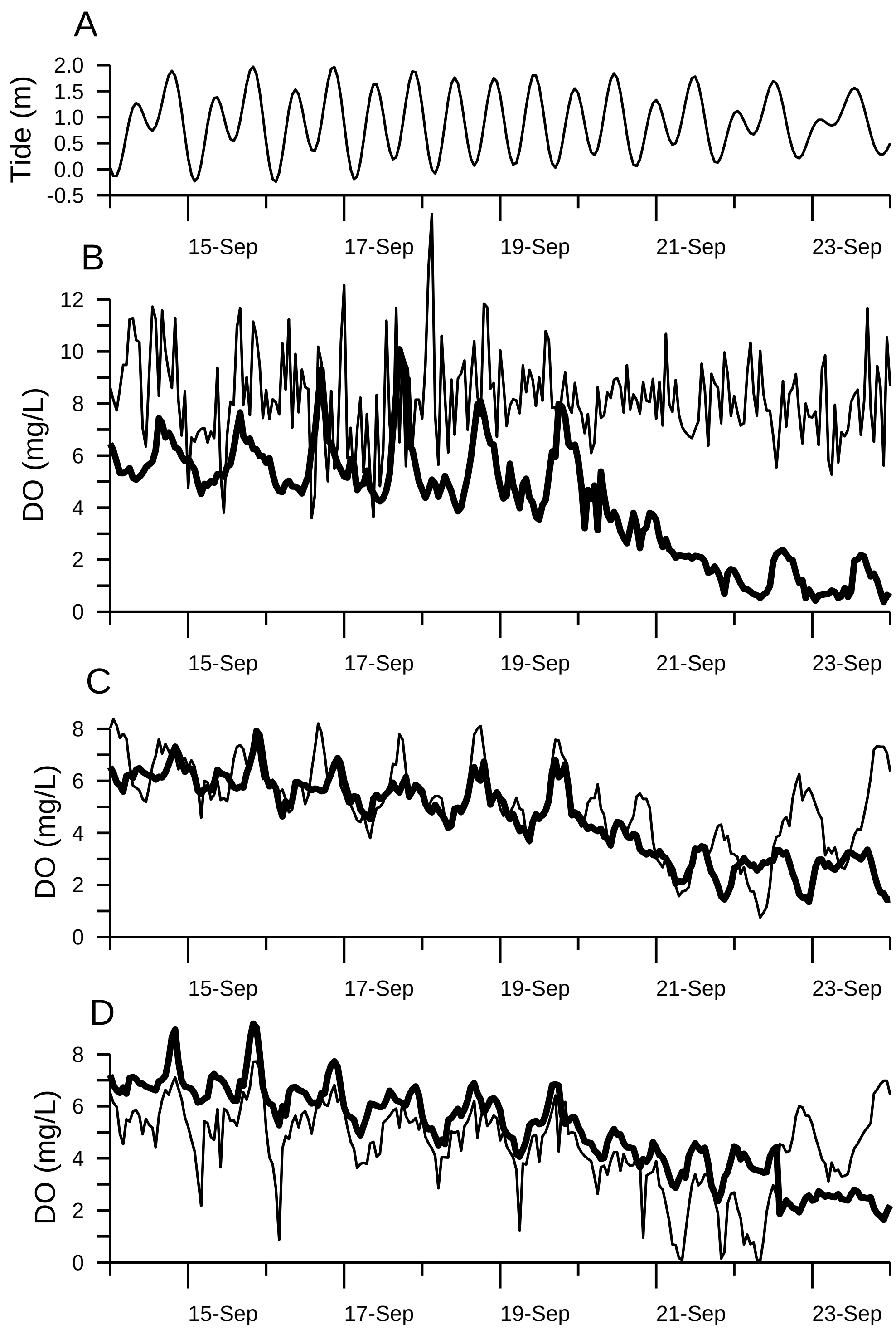

Figure 2-10. Tides (A) and DO concentrations in surface (thin line) and bottom (thick line) layers of three locations in UNB during the development of hypoxia on September 20 - 24. S3 is at the head of estuary (B); S2 is mid-estuary (C); S1 is at the lower end of Upper Newport Bay (D). See Figure 2-1 for S1, S2, and S3 locations.

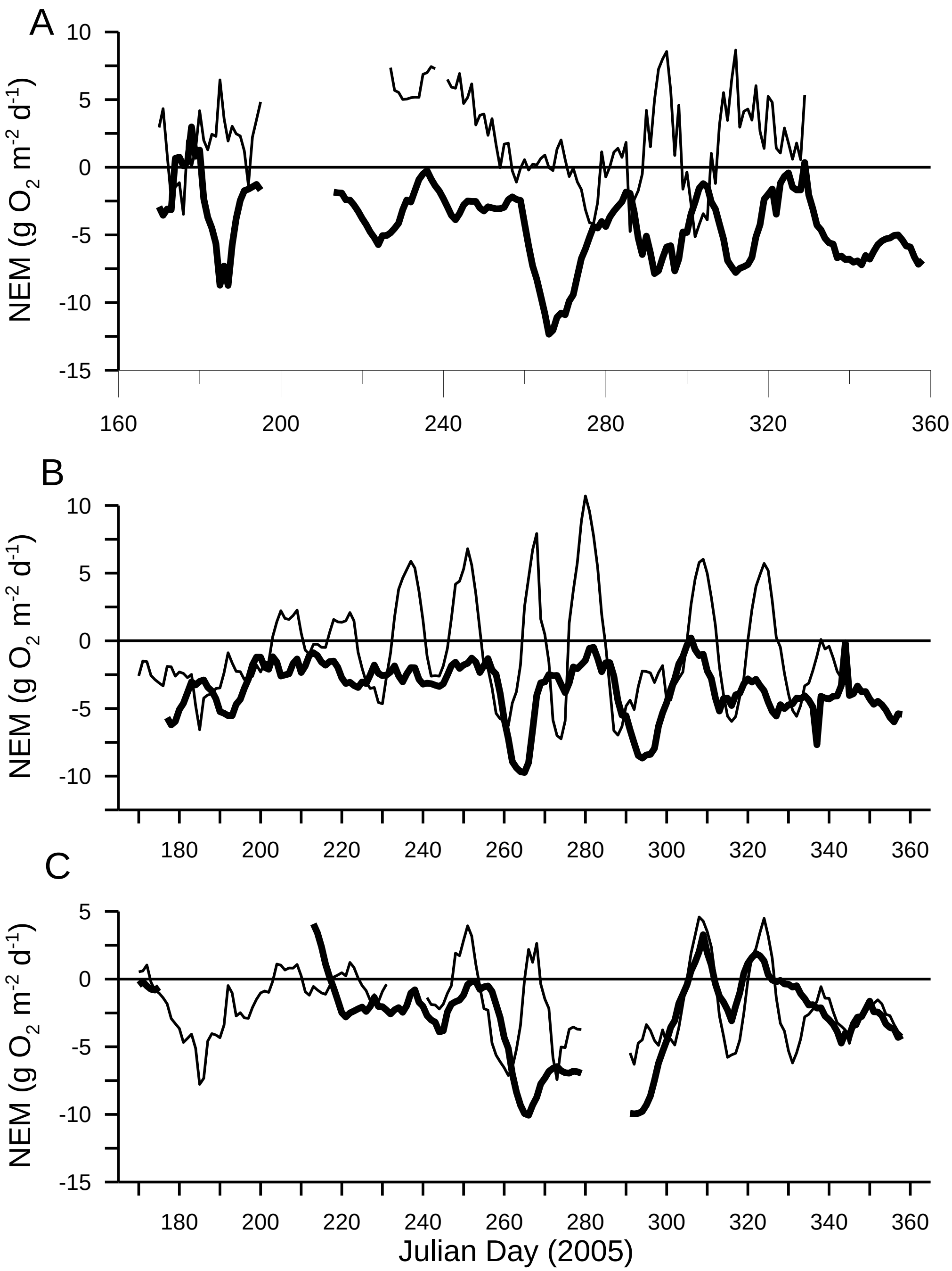

Figure 2-11. Net ecosystem metabolism (NEM, g O_2 m^{-2} d^{-1}) in surface (thin line) and bottom (thick line) layers of three locations in UNB: S3 is at the head of estuary (A); S2 is mid-estuary (B); andS1 is at the lower end of Upper Newport Bay (C). **See Figure 2-1.**

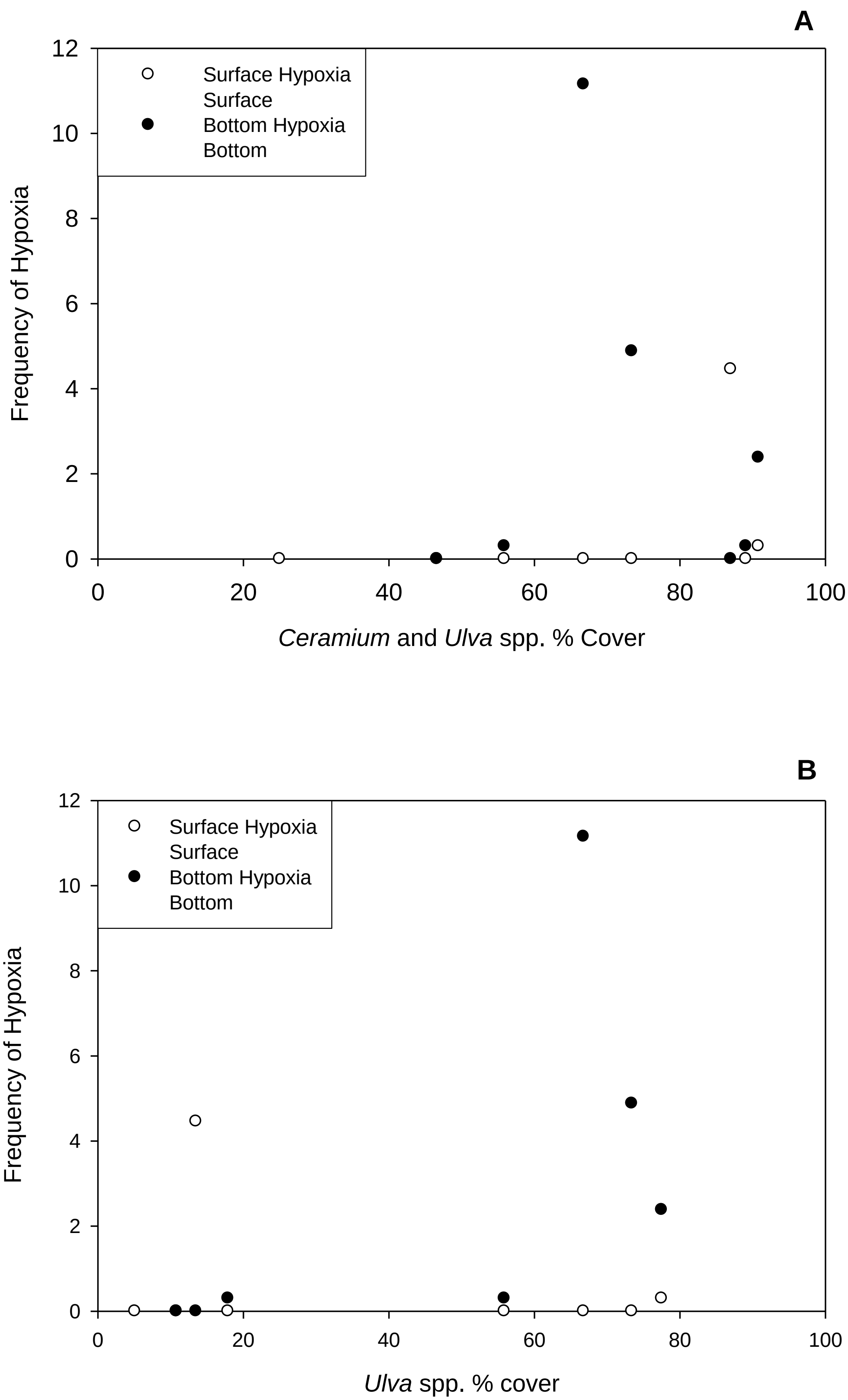

Figure 2-12. Frequency of hypoxia (DO <3.0 mg L^{-1}) over 7-day period versus *Ceramium* and *Ulva* spp. abundance (A) and versus *Ulva* spp. abundance (B).

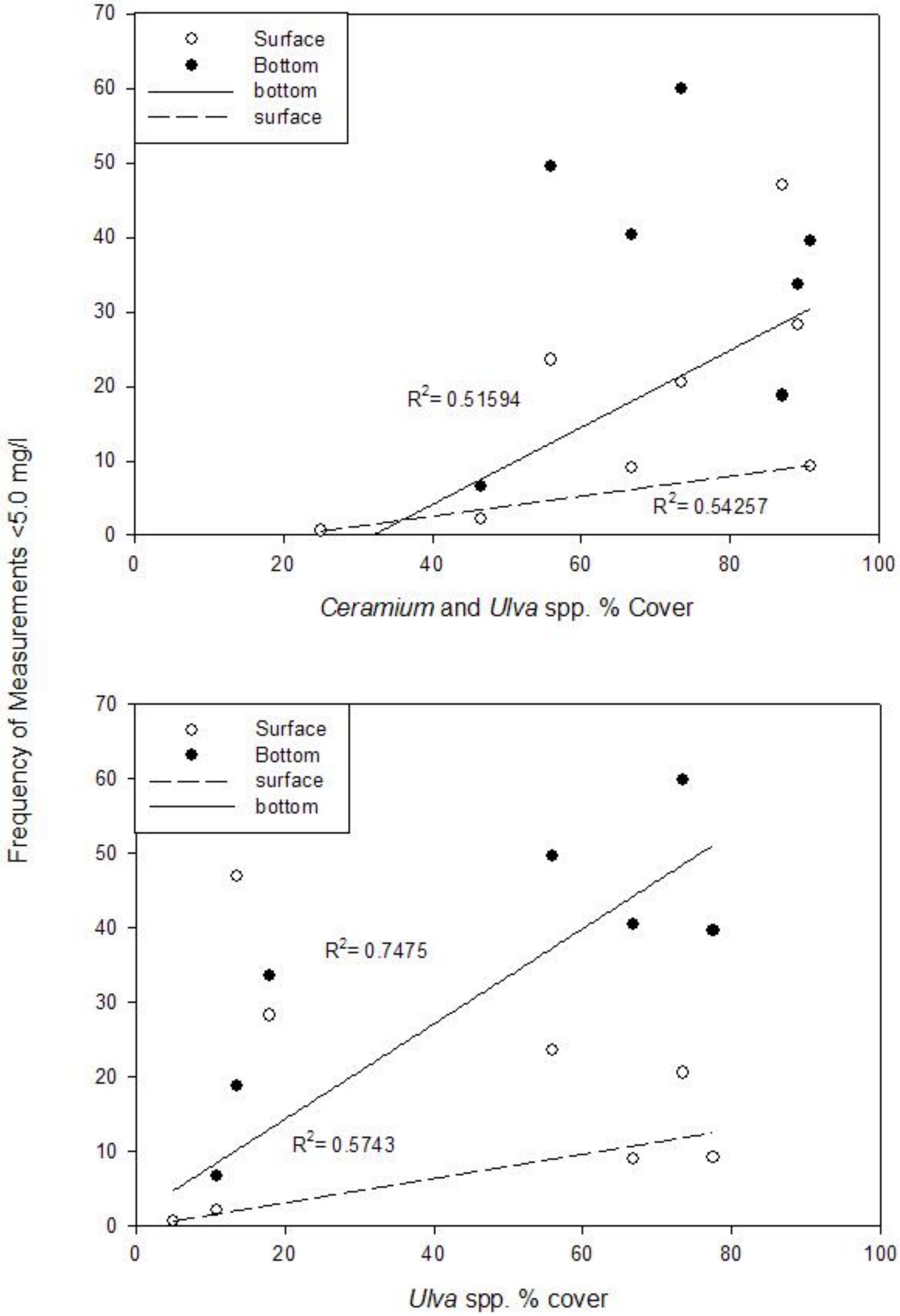

Figure 2-13. Frequency of DO measurements (<5.0 mg L^{-1}) over 7-day period versus *Ceramium* and *Ulva* spp. abundance (A) and versus *Ulva* spp. abundance (B).

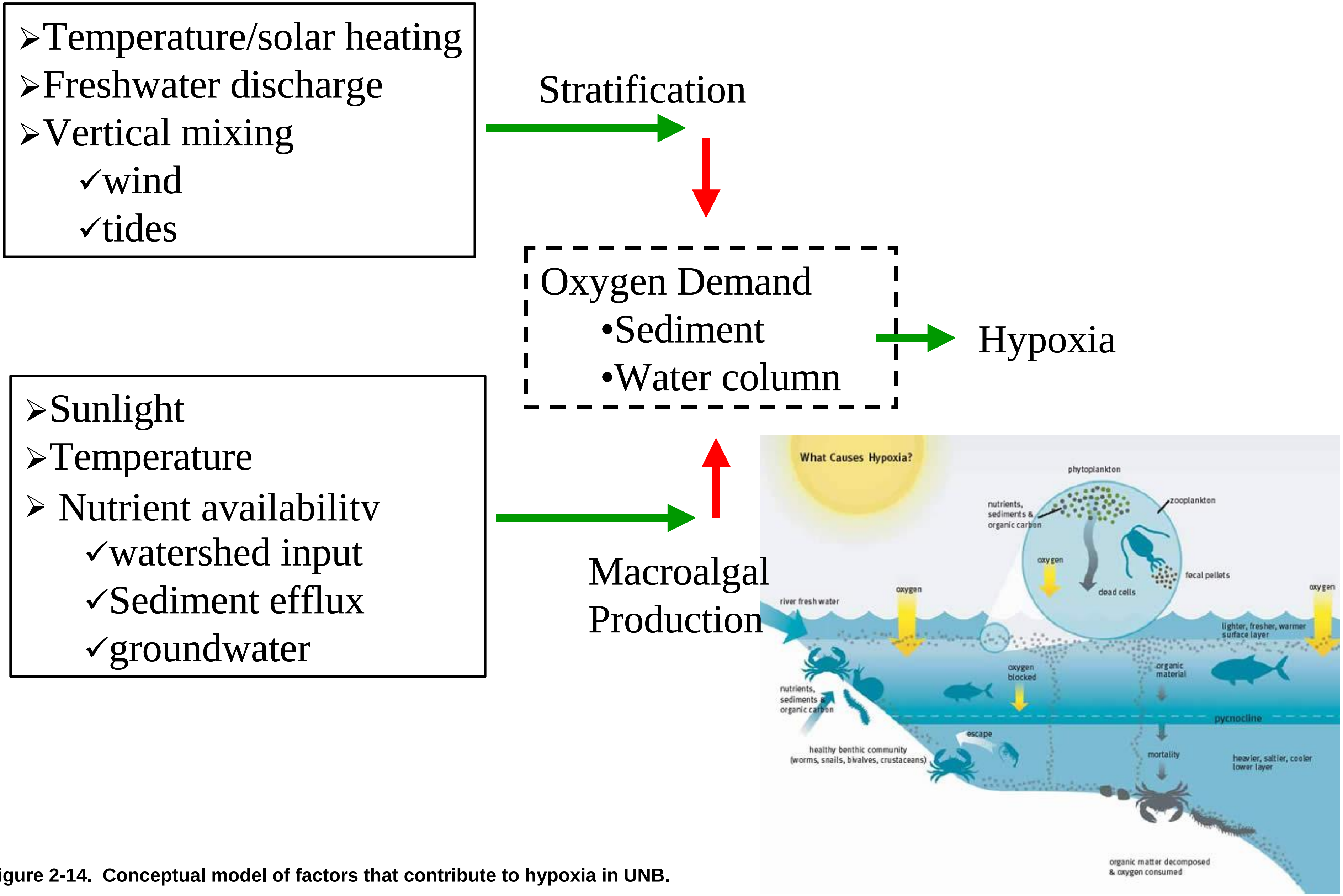

Figure 2-14. Conceptual model of factors that contribute to hypoxia in UNB.

APPENDIX A – REMOTE SENSING IMAGES

ftp://ftp.sccwrp.org/pub/download/DOCUMENTS/TechnicalReports/494_Appendix_A.pdf

APPENDIX B – INVENTORY AND EVALUATION OF WATER QUALITY DATA

ftp://ftp.sccwrp.org/pub/download/DOCUMENTS/TechnicalReports/494_Appendix_B.pdf

APPENDIX C – TIME SERIES PLOTS OF WATER QUALITY PARAMETERS

ftp://ftp.sccwrp.org/pub/download/DOCUMENTS/TechnicalReports/494_Appendix_C.pdf